Εθνικό Μετσόβιο Πολυτεχνείο
Σχολή Μηχανολόγων Μηχανικών
Τομέας Μηχανολογικών Κατασκευών & Αυτομάτου Ελέγχου

Study of Protein Kinase D on the secretory pathway of triple negative breast cancer

Διδακτορική Διατριβή

Γαλή Μαρία Αλεξία

ΠΤΥΧΙΟΥΧΟΥ ΒΙΟΛΟΓΙΑΣ ΑΠΘ

Αθήνα

24 ΜΑΙΟΥ 2023

Εθνικό Μετσόβιο Πολυτεχνείο
Σχολή Μηχανολόγων Μηχανικών
Τομέας Μηχανολογικών Κατασκευών & Αυτομάτου Ελέγχου

Study of Protein Kinase D on the secretory pathway of triple negative breast cancer

Διδακτορική Διατριβή

Γαλή Μαρία Αλεξία

ΠΤΥΧΙΟΥΧΟΥ ΒΙΟΛΟΓΙΑΣ ΑΠΘ

ΤΡΙΜΕΛΗΣ ΣΥΜΒΟΥΛΕΥΤΙΚΗ ΕΠΙΤΡΟΠΗ:	**ΕΠΤΑΜΕΛΗΣ ΕΞΕΤΑΣΤΙΚΗ ΕΠΙΤΡΟΠΗ:**
Λεωνίδας Αλεξόπουλος, Καθ. ΕΜΠ (Επιβλέπων) Νικόλαος Χρόνης, Καθ. ΕΜΠ Αριστοτέλης Χατζηιωάννου, Ερευνητής Β' ΙΙΒΕΑΑ	Λεωνίδας Αλεξόπουλος, Καθ. ΕΜΠ (Επιβλέπων) Νικόλαος Χρόνης, Καθ. ΕΜΠ Αριστοτέλης Χατζηιωάννου, Ερευνητής Β' ΙΙΒΕΑΑ Χρήστος Μανόπουλος, Επικ. Καθ. ΕΜΠ Angelika Hausser, Αν. Καθ. Universität Stuttgart Monilola Olayioye, Καθ. Universität Stuttgart Connie Jimenez, Καθ. Amsterdam University Medical Center

Prologue

The research for this dissertation was carried out under the supervision of Professor of the Mechanical Engineering Faculty of National Technical University of Athens, Leonidas G. Alexopoulos, and supported by the European Union Horizon 2020 Innovative Training Network "Exploitation of the SECRETory pathway for cancer therapy to address European Research" (SECRET) with Project Number H2020-MSCA-ITN-2019 #859962.

During my PhD, I visited and collaborated with the following institutes/universities: The Cancer Center Amsterdam, Amsterdam University Medical Center, Netherlands (Prof. Dr. Connie R. Jimenez) and The Institute of Cell Biology and Immunology, Universität Stuttgart, Germany (apl. Prof. Dr. Angelika Hausser).

I would like to express my sincere gratitude to Professor Leonidas G. Alexopoulos for his invaluable advice, continuous support, and mentoring during my PhD study. You have allowed me to grow into a researcher who achieves her goals by standing on her own two feet. You have always encouraged my desire to gain new knowledge and develop my soft skills. Thank you for introducing me to the systems biology field and trusting me to take on this PhD project. For their invaluable support and supervision, I would also like to thank apl. Prof. Dr. Angelika Hausser and Dr. Nikos Tsolakos. Angelika, you have supported my research goals from the first day of the project and were always there whenever we required your wealth of experience in this research field. Thank you as well for guiding and supervising me during my time at the Institute of Cell Biology and Immunology, hence allowing me to gain invaluable research experience and develop new lab skills. Niko, I cannot thank you enough for the continuous support throughout the project, you have allowed me to develop my critical thinking and mentored me on the values of research. Thank you for the fruitful discussions and fun times in the lab and the office. Meeting you and Professor Alexopoulos back at the Luminex conference of 2018 was the luckiest encounter!

I would also like to thank the OncoProteomics Laboratory of Cancer Center Amsterdam, Amsterdam University Medical Center, and especially its head, Prof. Dr. Connie R. Jimenez. Thank you immensely Connie for hosting me back in 2021 in your laboratory and introducing me to the field of proteomics. This secondment offered me an incredible research experience that challenged and gratified me. Thank you to all the members of the OncoProteomics lab, especially Dr. Irene V. Bijnsdorp, Dr. Sander R. Piersma, Dr. Thang V. Pham, Dr. Alex Henneman, Dr. Richard Goeij de Haas, Dr. Frank Rolfs, Madalena Nunes Monteiro, Andrea Valles and Ayse Erözenci, who were either actively involved in my research project or provided helpful knowledge on proteomics research or were simply great to work along with in the lab! Special thank you to OncoProteomics lab member Catarina Marques with whom we also collaborated in Protavio during her secondment and shared our PhD journeys! During my second secondment, in Dr. Angelika Hausser's lab, I had the joy to collaborate with Elena Gutiérrez-Galindo, Gisela Link, Zeynep Hazal Yilmaz, Sara Suárez López, Dr. Kerstin Ruoff, Elias Stahl and Jan Alexander Schlegel, all of which contributed to my lab training and were wonderful to work with! Thank you additionally to Prof. Monilola Olayioye and Dr. Cristiana

Lungu for sharing your scientific expertise and providing helpful research suggestions during my secondment.

A big thank you is owed to Dr. Raluca Tămaș for the continuous support throughout these three years in the SECRET ITN consortium, which allowed all the PhD students to gain invaluable training and be part of such a well-organized research consortium. I will miss your kindness and professionalism! For their generosity in providing research materials for my project, I would also like to thank Prof. Tilman Brummer, Dr. Ricarda Griffin and Célia Asdih from Universitätsklinikum Freiburg. Additionally, thank you to all the rest of SECRET ITN beneficiaries and especially the PhD students, Amirabbas Parizadeh, Merih Özverin, Renata Hajdu, Eleni Skourti, Negar Parizadeh, Juan Manuel García Illarramendi, Mario Macía Guardado, Jacqueline Bersano and Lorenzo Signorini, who were an incredible group to share this experience with and made all the annual meetings as much fun as they could be! I will always cherish these memories.

Thank you to the members of the Biomedical Systems Laboratory of the Mechanical Engineering Faculty of the NTUA, Dr. Danae Zareifi, Nagia Kokkori and Dr. Christos Fotis for their support during the project. An even bigger thank you is owed to all the members of Protavio LtD between 2020 and 2023 and especially Angeliki Minia, Dr. Nikos Tsolakos, Sissy Skea, Exarchos Kanelis, Dr. Vicky Pliaka, Dr. Thanos Stamogiannos and Sophia Stamatatou for their support and help during these three years. Thank you for all the laughs in the lab and the office, your incredible sense of teamwork and providing your expertise whenever I required it.

Thank you to the members of the three-member advisory committee, Prof. Nikos Chronis and Dr. Aristotelis Chatziioannou, for their guidance and support and the members of the seven-member committee, including Ass. Prof. Christos Manopoulos, for attending my defense and providing their wealth of scientific experience.

Finally, I want to express my deepest gratitude to the people in my life that supported me and helped me accomplish, perhaps the biggest, goal of my life. My mother, Betty, my father, Antonis, my sister, Connie, and my partner, Ultan. Your continuous emotional support and everything you have done for me throughout the years is what allowed me to complete this PhD. Thank you, mom, dad, and Connie, for supporting me during my previous studies in biology and always encouraging me to aim high. This is yet another achievement to be proud of as a family. Thank you Ultan for being so supportive of my PhD, from initially accepting the position when we were in London, and later in Athens and abroad in my secondments, you were my rock throughout this PhD journey. Thank you all immensely, this accomplishment would not have been possible without you, I am extremely lucky to have you in my life.

Alexia Gali

Athens, May 2023

Summary

The Protein kinase D (PKD) family members are important proteins, found in mammals, that regulate the release of proteins from the cell, a process called secretion. In triple-negative breast cancer (TNBC), the most aggressive subtype of breast cancer, PKD appears to be involved in cancer cell growth. However, it remains unknown if PKD is responsible for the secretion of proteins that help TNBC cells survive and grow. We studied the roles of PKD2 and PKD3 in TNBC secretion by both blocking PKD activity, and by removing the proteins from the cells entirely in two TNBC cell lines, MDA-MB-231 and MDA-MB-468. Using proteomics techniques, we identified that PKD is responsible for the secretion of proteins that help cancer cells invade nearby tissues, hence aiding cancer metastasis. Interestingly, PKD2 was found to be responsible for most of this effect. This role of PKD was more evident in cells from metastatic TNBC i.e., cancer cells that have spread to other parts of the body, compared to primary tumors. Overall, this study helps us better understand the role PKD plays in TNBC secretion and how it might contribute to the spread of cancer cells. We also describe a new role for PKD2 in promoting the secretion of proteins that help cancer cells invade nearby tissues.

Extended Summary

Background and Aims:

The PKD family of serine-threonine protein kinases consists of three isoforms, PKD1, PKD2 and PKD3, which are best known for controlling secretion by participating in vesicle fission at the trans-Golgi network (TGN) and additionally participate in actin remodeling during cell migration. In triple negative breast cancer (TNBC), the main isoforms present are PKD2 and PKD3, following the epigenetic silencing of PKD1 during breast tumor progression. To date, several studies have linked PKD3 levels to increased proliferation, cell motility, invasion and cancer stem cell maintenance and PKD2 to drug resistance, cell adhesion and migration. Notably, the PKD2- and PKD3- regulated secretomes have exhibited pro-invasive and pro-motility properties in prostate and pancreatic cancer. Hence, it could be hypothesized that PKD contributes to TNBC secretion and may regulate the secretion of pro-oncogenic factors, therefore driving tumor progression.

In the present study, we aimed to investigate the PKD2 and PKD3-dependent secretome in TNBC and whether it promotes the secretion of tumor-promoting factors.

Methods:

To interrogate the PKD-dependent secretome, we initially used quantitative mass spectrometry (MS)-based proteomics (label-free GeLC-MS/MS) to analyze conditioned media (secretome) samples and respective cell lysates from control and PKD-inhibited TNBC cell lines MDA-MB-231 and MDA-MB-468. PKD inhibition was confirmed by immunoblotting and a custom developed PKD2 Ser 876 assay. Following statistical analysis of GeLC-MS/MS results, significantly changed secretome and cell lysate proteins were subjected to enrichment analysis. A panel of eight secreted proteins, with an established pro-invasive role in TNBC, were selected for validation by antibody-based assays.

Antibody-based multiplex assays (7-plex) were custom-developed, where appropriate, and were combined with enzyme-linked immunosorbent assay (ELISA) to validate the previously selected secretome proteins. Transcriptional analysis of three target genes of the validated proteins was used to identify if PKD signaling affects transcription and/or differential secretion. Following target protein validation, we used siRNA-mediated depletion of PKD2 and PKD3 to collect the respective isoform dependent secretome. We used the same 7-plex antibody-based assay and ELISA to interrogate the presence of the previously validated proteins in the collected secretomes and identify which isoform is responsible for their secretion. Knockdown efficiency was confirmed by immunoblotting.

To gain a systems level understanding of PKD contribution to TNBC secretion, we used a panel of TNBC cell lines, consisting of 6 cell lines originally established from the primary tumor and 4 metastatic cell lines from pleural effusions. We collected the PKD-dependent secretome and cell lysate and analysed the secretome samples with the same 7-plex antibody-based assay and ELISA and the cell lysates with a phosphoprotein 9-plex panel. This allowed us to identify if the previously validated proteins were also secreted in a PKD-dependent manner in additional TNBC cell lines and if PKD inhibition had an effect on the phosphorylation status of

9 kinases and kinase targets. PKD inhibition and stimulation were confirmed by immunoblotting and a custom developed PKD2 Ser 876 assay.

Results:

We have identified PKD signaling to be important for the composition of the TNBC cell secretome and provide a comprehensive understanding of the secreted and intracellular proteins regulated by the kinases. Intracellularly, we found PKD inhibition to reduce the secretion of several proteins related to ribosome biogenesis. In secretome samples, we discovered secreted proteins that were related to cell adhesion and proteins previously characterized as ECM regulators and invasion mediators in TNBC. We validated the PKD-regulated secretion of leukemia inhibitory factor (LIF), matrix metalloproteinase-1 (MMP-1), matrix metalloproteinase-13 (MMP-13), interleukin-11 (IL-11), colony-stimulating factor (M-CSF) and granulocyte-macrophage-colony-stimulating factor (GM-CSF), connecting PKD activity to a pro-tumorigenic secretome. Evidence from transcriptional analysis showed that PKD activity affects transcription and/or differential secretion to regulate secretion of invasion mediators.

Based on evidence obtained from the MDA-MB-231 cell line, we describe a predominantly PKD2-driven effect in the secretion of invasion mediators, with a smaller contribution from PKD3. Secretion of two additional proteins, stanniocalcin-1 (STC-1) and tenascin-C (TNC), although it was reduced upon pharmacological inhibition of PKD, as identified by LC-MS/MS and antibody-based assays, it was unchanged in PKD2/PKD3 depleted MDA-MB-231 and MDA-MB-468 cells.

Our results also show that PKD signaling regulates the secretion of a greater number of invasion mediators in established TNBC cell lines derived from metastatic sites than in TNBC cell lines derived from the primary tumor. This was evident based on both the greater number of mediators affected and magnitude of the effect (fold-change) in these cell lines. Finally, PKD inhibition was found to suppress c-Jun Ser 63 phosphorylation in a panel of six TNBC cell lines.

Conclusions:

Our findings suggest that PKD invasive functions could be exerted by the secreted proteins we have validated, which have been previously described to contribute to TNBC invasion. This is based on the identification of multiple invasion mediators in the PKD-regulated secretome which are known to contribute to different stages of TNBC invasion, from ECM remodelling to extravasation and finally to metastatic colonisation. Additionally, identification of pro-inflammatory in the PKD-dependent secretome suggests that PKD signalling contributes to immune cell recruitment in the TNBC tumor microenvironment as well. On a systems level, PKD plays a greater role in the secretion of TNBC invasion mediators in metastatic cell lines, suggesting that as cells become more capable of invasion and eventually metastasis, PKD enables tumor progression via the kinase regulated secretome. Initial screening identified that PKD signaling impacts on the phosphorylation status of c-JUN, suggesting it could regulate the transcriptional activities of the factor.

Περίληψη

Τα μέλη της οικογένειας των πρωτεϊνικών κινασών D (PKD) είναι σημαντικές πρωτεΐνες που βρίσκονται στα θηλαστικά και ρυθμίζουν την απελευθέρωση πρωτεϊνών από το κύτταρο, μια διαδικασία που ονομάζεται έκκριση. Στον τριπλά αρνητικό καρκίνο του μαστού (TNBC), έναν επιθετικό τύπο καρκίνου του μαστού, η PKD εμπλέκεται στην ανάπτυξη των καρκινικών κυττάρων. Ωστόσο, παραμένει άγνωστο εάν η PKD είναι υπεύθυνη για την έκκριση πρωτεϊνών που βοηθούν τα κύτταρα TNBC να επιβιώσουν και να αναπτυχθούν. Στην παρούσα διδακτορική διατριβή μελετήσαμε τους ρόλους των PKD2 και PKD3 στον εκκριτικό μηχανισμό του TNBC είτε με το μπλοκάρισμα της δραστηριότητας της PKD είτε με την αφαίρεση των πρωτεϊνών από τα κύτταρα σε δύο κυτταρικές γραμμές TNBC, MDA-MB-231 και MDA-MB-468. Χρησιμοποιώντας τεχνικές πρωτεϊνικής ανάλυσης, ανακαλύψαμε ότι η PKD ευθύνεται για την έκκριση πρωτεϊνών που βοηθούν τα καρκινικά κύτταρα να εισβάλλουν σε κοντινούς ιστούς και επομένως να αναπτύξουν μετάσταση σε άλλα όργανα. Συγκεκριμένα, η PKD2 βρέθηκε να είναι υπεύθυνη για το μεγαλύτερο μέρος αυτού του φαινομένου. Αυτός ο ρόλος της PKD ήταν πιο εμφανής στα κύτταρα μεταστατικού TNBC, δηλαδή στα καρκινικά κύτταρα που έχουν εξαπλωθεί σε άλλα μέρη του σώματος, σε σύγκριση με τους πρωτογενείς όγκους. Συνολικά, αυτή η μελέτη μας βοηθά να κατανοήσουμε καλύτερα το ρόλο που παίζει η PKD στον εκκριτικό μηχανισμό του TNBC και πώς μπορεί να συμβάλλει στη μετάσταση των καρκινικών κυττάρων. Επίσης, περιγράφουμε ένα νέο ρόλο για την PKD2 στην έκκριση πρωτεϊνών που βοηθούν τα καρκινικά κύτταρα να εισβάλλουν σε κοντινούς ιστούς.

Εκτενής Περίληψη

Εισαγωγή:

Η οικογένεια πρωτεϊνικών κινασών σερίνης-θρεονίνης PKD αποτελείται από τρεις ισομορφές, τις PKD1, PKD2 και PKD3, οι οποίες είναι γνωστές για τον έλεγχο της έκκρισης από το σύστημα trans-Golgi (TGN) και επιπλέον συμμετέχουν στην αναδιαμόρφωση της ακτίνης κατά την κυτταρική μετανάστευση. Στον τριπλά αρνητικό καρκίνο του μαστού (TNBC), οι κύριες ισόμορφες που υπάρχουν είναι οι PKD2 και PKD3, μετά την επιγενετική σίγαση της PKD1 που έχει παρατηρηθεί σε αυτό τον τύπο καρκίνου. Μέχρι σήμερα, αρκετές μελέτες έχουν συνδέσει τα επίπεδα της PKD3 με αυξημένο πολλαπλασιασμό, κινητικότητα κυττάρων, και μετάσταση και της PKD2 με την ανθεκτικότητα στα φάρμακα, την κυτταρική προσκόλληση και τη μετανάστευση. Ιδιαίτερα, οι ρυθμιζόμενες από τις PKD2 και PKD3 εκκρινόμενες πρωτεΐνες έχουν δείξει προ-μεταστατικές και προ-κινητικές ιδιότητες στον καρκίνο του προστάτη και του παγκρέατος.

Ως εκ τούτου, η PKD θα μπορούσε να συμβάλλει στον εκκριτικό μηχανισμό του TNBC και να ρυθμίζει την έκκριση προ-ογκογονικών παραγόντων, οδηγώντας επομένως στην εξέλιξη του όγκου. Στην παρούσα μελέτη, στοχεύσαμε να διερευνήσουμε το εξαρτώμενο από τις PKD2 και PKD3 πρωτεϊνικό έκκριμα στον TNBC και εάν οι κινάσες προάγουν την έκκριση παραγόντων που βοηθούν στη μετάσταση του όγκου.

Μέθοδοι:

Για να διερευνήσουμε το εξαρτώμενο από την PKD εκκρίτωμα, χρησιμοποιήσαμε αρχικά ποσοτική φασματομετρία μάζας (GeLC-MS/MS) για να αναλύσουμε δείγματα υπερκειμένου καλλιέργειας και αντίστοιχα κυτταρολύματα από τις κυτταρικές σειρές TNBC MDA-MB-231 και MDA-MB-468. Η αναστολή της PKD επιβεβαιώθηκε με ανοσοστυπωμα κατά Western. Μετά από στατιστική ανάλυση των αποτελεσμάτων GeLC-MS/MS, οι σημαντικά αλλαγμένες πρωτεΐνες υποβλήθηκαν σε ανάλυση εμπλουτισμού για Gene Ontology βιολογικές διεργασίες και κυτταρικό διαμέρισμα καθώς και για KEGG μονοπάτια. Ένα πάνελ οκτώ πρωτεϊνών, με καθιερωμένο προ-μεταστατικό ρόλο στη βιβλιογραφία του TNBC, επιλέχθηκε για επικύρωση.

Πολυπλεκτική ELISA σε συνδιασμό με απλή ELISA χρησιμοποιήθηκαν για την επικύρωση των επιλεγμένων πρωτεϊνών. Η μεταγραφική ανάλυση τριών γονιδίων-στόχων των επικυρωμένων πρωτεϊνών χρησιμοποιήθηκε για να προσδιοριστεί εάν η PKD επηρεάζει τη μεταγραφή ή/και τη διαφορική έκκριση. Μετά την επικύρωση των επιλεγμένων πρωτεΐνων, χρησιμοποιήσαμε τεχνολογια siRNA για την καταστολή της έκφρασής των PKD2 και PKD3 και συλλέξαμε το έκκριμα κάθε ισομορφής. Αναλύσαμε με πολυπλεκτική ELISA σε συνδυασμό με απλή ELISA την παρουσία των προηγουμένως επικυρωμένων πρωτεϊνών στα συλλεχθέντα εκκρίματα για να προσδιορίσουμε ποια ισομορφή της PKD είναι υπεύθυνη για την έκκρισή των πρωτεϊνών. Η αποτελεσματικότητα καταστολή της έκφρασής των PKD2 και PKD3 επιβεβαιώθηκε με ανοσοστύπωμα κατά Western.

Σε επίπεδο βιολογίας συστημάτων, θελήσαμε να κατανοήσουμε την συμβολή της PKD στον εκκριτικό μηχανισμό του TNBC μέσω της μελέτης ενός πάνελ δέκα κυτταρικών σειρών. Οι

σειρές αποτελούνταν από 6 κυτταρικές σειρές που αναπτύχθηκαν από πρωτοπαθή όγκο και 4 μεταστατικές κυτταρικές σειρές. Συλλέξαμε το εξαρτώμενο από την PKD εκκρίτωμα και κυτταρόλυμα και αναλύσαμε τα δείγματα εκκριμάτων με πολυπλεκτική ELISA σε συνδιασμό με απλή ELISA και τα κυτταρολύματα με ένα πάνελ φωσφοπρωτεϊνών. Αυτό μας επέτρεψε να αναγνωρίσουμε εάν η έκκριση των προηγουμένως επικυρωμένων εκκρινόμενων πρωτεϊνών γίνεται με τρόπο εξαρτώμενο από την PKD σε επιπλέον κυτταρικές σειρές TNBC και εάν η αναστολή της PKD έχει επίδραση στην φωσφορυλίωση 9 κινασών και στόχους κινασών. Η αναστολή και η διέγερση της PKD επιβεβαιώθηκαν με ανοσοστύπωση κατά Western και πολυπλεκτική ELISA με στόχο την PKD2 Ser 876.

Αποτελέσματα:

Η PKD βρέθηκε να έχει σημαντικό ρόλο στη σύνθεση του εκκριτώματος των κυττάρων TNBC. Ανακαλύψαμε εκκρινόμενες πρωτεΐνες που σχετίζονται με την κυτταρική προσκόλληση και πρωτεΐνες που έχουν προηγουμένως χαρακτηριστεί ως ρυθμιστές της εξωκυτταρικής μήτρας και βοηθούν στην μετάσταση του TNBC. Επιβεβαιώσαμε τη ρυθμιζόμενη από την PKD έκκριση των μεταστατικών παραγόντων ανασταλτικο παράγοντα λευχαιμίας (LIF), μεταλλοπρωτεϊνάση-1 (MMP-1), μεταλλοπρωτεϊνάση-13 (MMP-13), ιντερλευκίνη-11 (IL-11), παράγοντα διέγερσης αποικιών (M-CSF) και παράγοντα διέγερσης αποικιών κοκκιοκυττάρων-μακροφάγων (GM-CSF), το οποίο συνδέει τη δραστηριότητα της PKD με ένα προ-ογκογόνο εκκρίτωμα. Από τη μεταγραφική ανάλυση μερικών γονιδίων των συγκεκριμένων πρωτεϊνών διαπιστώσαμε ότι η δραστηριότητα της PKD επηρεάζει τη μεταγραφή και/ή τη διαφορική έκκριση για να ρυθμίσει την έκκριση μεταστατικών παραγόντων.

Περιγράφουμε επίσης, βάσει δεδομένων της κυτταρικής σειράς MDA-MB-231, ότι η PKD2 είναι κυρίως υπεύθυνη για την έκκριση μεταστατικών παραγόντων, με μια μικρότερη συμβολή από την PKD3. Η έκκριση δύο επιπρόσθετων πρωτεϊνών, της στανιοκαλσίνης-1 (STC-1) και της τενασκίνης-C (TNC), αν και μειώθηκε κατά τη φαρμακολογική αναστολή της PKD, όπως προσδιορίστηκε από LC-MS/MS και πολυπλεκτική ELISA, παρέμεινε αμετάβλητη στα κύτταρα MDA-MB-231 και MDA-MB-468 με μειωμένη έκφραση PKD2 ή PKD3.

Τα αποτελέσματά μας δείχνουν επίσης ότι η δραστηριότητα της PKD ρυθμίζει την έκκριση ενός μεγαλύτερου αριθμού μεταστατικών παραγόντων σε κυτταρικές σειρές TNBC που προέρχονται από μεταστατικό καρκίνο παρά σε κυτταρικές σειρές TNBC που προέρχονται από τον πρωτοπαθή όγκο. Τέλος, η αναστολή PKD βρέθηκε να καταστέλλει τη φωσφορυλίωση του c-Jun Ser 63 σε ένα πάνελ έξι κυτταρικών σειρών TNBC.

Συμπεράσματα:

Τα ευρήματά μας υποδηλώνουν ότι ο μεταστατικός ρόλος που έχει περιγραφεί για την PKD θα μπορούσε να οφείλεται στην έκκριση των μεταστατικών παραγόντων που ανακαλύψαμε. Αυτή η υπόθεση βασίζεται στην ταυτοποίηση πολλαπλών μεταστατικών παραγόντων στο ρυθμιζόμενο από την PKD έκκριμα, οι οποίοι είναι γνωστό ότι συμβάλλουν σε διαφορετικά στάδια μετάστασης του TNBC, από την αναδιαμόρφωση της εξωκυτταρικής μήτρας έως τον μεταστατικό αποικισμό. Επιπλέον, η ανακάλυψη προφλεγμονώδων παραγόντων στο

εξαρτώμενο από την PKD έκκριμα υποδηλώνει ότι η PKD συμβάλλει στη στρατολόγηση ανοσοκυττάρων στο μικροπεριβάλλον όγκου TNBC. Σε επίπεδο βιολογίας συστημάτων, η PKD παίζει μεγαλύτερο ρόλο στην έκκριση μεσολαβητών εισβολής TNBC σε μεταστατικές κυτταρικές σειρές, υποδηλώνοντας ότι καθώς τα κύτταρα γίνονται πιο ικανά για μετάσταση, η PKD επιτρέπει την εξέλιξη του όγκου μέσω του εκκριτώματος που ρυθμίζει. Επιπλέον, η PKD επηρεάζει την φωσφορυλίωση του c-JUN, υποδηλώνοντας ότι θα μπορούσε να ρυθμίσει τις μεταγραφικές δραστηριότητες του παράγοντα. Τα αποτελέσματα αυτής της μελέτης αυξάνουν την κατανόησή μας σχετικά με τη συμβολή των PKD2 και PKD3 στη σύνθεση του εκκρίματος του TNBC και υποδεικνύουν ότι οι κινάσες χρησιμοποιούν την εκκριτική οδό με έναν ειδικό για την ισομορφή τρόπο για να υποστηρίξουν τη συμπεριφορά μεταστατικών κυττάρων.

Contents

Abbreviations

1D-SDS-PAGE	One-dimensional gel electrophoresis
ABC	Ammonium Bicarbonate
ABCG2	ATP-binding cassette subfamily G member 2
ACN	Acetonitril
ADCs	Antibody–drug conjugates
ADF	Actin depolymerizing factor
ADP	Adenosine diphosphate
AKT	RAC-alpha serine/threonine-protein kinase
AKT1	AKT Serine/Threonine Kinase 1
ARFs	Adenosyl-ribosylation factor family of small G-proteins
ATP	Adenosine triphosphate
ATP6AP2	Adenosine triphosphatase H+ transporting accessory protein 2
BAPN	Beta-aminopropionitrile
BCA	Bicinchoninic acid assay
BGN	Biglycan
CAFs	Cancer associated fibroblasts
CCL11	Eotaxin
CCL5	C-C motif chemokine 5
CDK	Cyclin-dependent kinase
CERT	Ceramide transfer protein
c-JUN	transcription factor JUN
COPII	Coat protein complex ii
CRT	CRT0066101
CTF1	Cardiotrophin 1
DAG	Lipid diacylglycerol
DDX52	Probable ATP-dependent RNA helicase
DTT	Ditheotreitol
ECM	Extracellular matrix
ECM1	Extracellular matrix protein 1
EGFR	Epidermal growth factor receptor
ELISA	Enzyme linked immunosorbent assay
EMT	Epithelial-to-mesenchymal transition
EnR	Endoplasmic reticulum
ER	Estrogen receptor
ERES	ER exit sites
ERGIC	ER-to-Golgi intermediate compartment
ERK1	Extracellular signal-regulated kinase 1
FA	Formic acid
FTSJ3	pre-rRNA 2'-O-ribose RNA methyltransferase FTSJ3
g	Relative centrifugal force/ g force
GABP	GA-binding protein transcription factor
GAP	Gtpase-activating proteins
GDP	Guanosine diphosphate
GEFs	Guanine nucleotide exchange factors
GM2A	Ganglioside GM2 activator
GM-CSF	Granulocyte-macrophage colony-stimulating factor

GNL3	Guanine nucleotide-binding protein-like 3
GO	Gene Ontology
GOLPH3	Golgi phosphoprotein 3
GROα	Growth-regulated alpha protein
GSK3	Glycogen synthase kinase-3
GTP	Guanosine triphosphate
GTPase	Guanine nucleotide-binding protein
HDAC	Histone deacetylases
HER2	Human epidermal growth factor receptor 2
HGF	Hepatocyte growth factor
hr	Hour
IBP5	Insulin-like growth factor-binding protein 5
ICIs	Immune-checkpoint inhibitors
IL-11	Interleukin-11
IL31RA	Interleukin-31 receptor A
IL-6	Interleukin-6
IL-8	Interleukin-8
KEGG	Kyoto Encyclopedia of Genes and Genomes
L1CAM	Neural cell adhesion molecule L1
LAR	Luminal androgen receptor
LC	Liquid-chromatography
LGALS3BP	Galectin-3 binding protein
LGMN	Legumain
LIF	Leukemia inhibitory factor
LIMK1	LIM domain kinase 1
LMAN2	Lectin mannose-binding 2
LOX	Lysyl oxidase
M	Molar
m/z	Mass per charge
MARCKS	Myristoylated Alanine Rich C-Kinase Substrate
M-CSF	Macrophage colony-stimulating factor
MEK1	Mitogen-activated protein kinase kinase 1
mg	Microgram
min	Minutes
ml	Milliliter
MMP	Matrix metalloproteinases
MPHOSPH10	U3 small nucleolar ribonucleoprotein protein MPP10
mRNA	Messenger RNA
MS	Mass-spectrometry
mTORC1	Mammalian target of rapamycin complex 1
ng	Nanogram
nM	Nanomolar
NRCAM	Neuronal cell adhesion molecule
OD	Optical density
OS	Overall survival
OSBP	Oxysterol binding protein
P53	Cellular tumour antigen p53
PA	Phosphatidic acid

PAK4	P21-activated kinase 4
PARP	Poly(ADP-ribose) polymerase
PBS	Phosphate Buffered Saline
PD-1	Programmed cell death 1
PDCD11	protein RRP5 homolog
PD-L1	Programmed cell death receptor ligand 1
PI	Phosphatidylinositol
PI(4)P	Phosphatidylinositol (PI) 4-phosphate
PI3K	Phosphoinositide 3-kinases
PI3KCA	Phosphatidylinositol 3-kinase
PI4KIIIβ	Phosphatidylinositol-4 kinase iiiβ
PITPNC1	Phosphatidylinositol transfer protein cytoplasmic 1
PKC	Protein kinase C
PKCη	Protein kinase C η
PKD	Protein kinase D
PLC	Phospholipase C
PMSF	Phenylmethanesulfonyl fluoride
PPLP0	ribosomal protein lateral stalk subunit P0
PR	Progesterone receptor
RBM28	RNA-binding protein 28
Rho	Ras Homologous
RIN1	Ras and Rab interactor 1
RPF1	Ribosome production factor 1
rpm	Rounds per minute
RPS15	40S ribosomal protein S15
rRNA	Ribosomal RNA
S6K1	S6 kinase 1
SAPE	Streptavidin, R-Phycoerythrin conjugate
SCF	Kit ligand
sec	Seconds
Ser (or S)	Serine
SMAD3	SMAD family member 3
SNAI1	Snail
SNAI2	Slug
SOCS	Suppressor of cytokine signaling
SOX2	Sex-determining region Y-box2
Src	Src family kinases
SSH1	Slingshot protein phosphatase 1
STC-1	Stanniocalcin 1
TAMs	Tumor-associated macrophages
TGN	*Trans*-Golgi network
THBS1	Thrombospondin-1
TILs	Tumour-infiltrating lymphocytes
TME	Tumor microenvironment
TNBC	Triple negative breast cancer
TNC	Tenascin-C
TSLP	Thymic stromal lymphopoietin
uPA	Urokinase-type plasminogen activator

UPS	Unconventional protein secretion
UTP14A	U3 small nucleolar RNA-associated protein 14 homolog A
UTP18	U3 small nucleolar RNA-associated protein 18 homolog
VEGFR	Vascular endothelial growth factor
WDR46	WD repeat-containing protein 46
xMAP	Luminex multianalyte profiling
ZEB	Zinc finger E-box binding homeobox
µg	Milligram
µl	Microliters

List of Figures

List of Tables

Chapter 1
Introduction

1. Introduction

Cancer is the second leading cause of death globally, with an estimated 19.3 million new cases of cancer worldwide in 2020. The three most common cancer types identified were female breast cancer (2.26 million cases), lung (2.21) and prostate cancers (1.41). The most common causes of cancer death on the other hand had been witnessed in lung (1.79 million deaths), liver (830,000) and stomach cancers (769,000) [1]. The global death rate and the impact of these malignancies on the individuals and the health systems worldwide demonstrate the need for better prevention and treatment options; achieving this requires a better understanding of mechanisms of disease.

1.1. Breast cancer

Breast cancer is the most diagnosed cancer and the leading cause of cancer death in females. According to the World Health Organization (WHO) for the year 2020, an estimated 2.3 million new cases (11.7% of all cancer cases) and 685,000 deaths (6.9% of all cancer deaths) worldwide are attributed to breast cancer [2]. The incidence and mortality in men are distinctly lower, accounting for ~ 1 % of new cases of the disease [3].

Breast cancer incidence showed an increase during the period of 1980 to 2002, which can be attributed to various reproductive factors (i.e. menarcheal age, interval from menarche to first pregnancy, parity, number of children, oral contraceptives, etc.), such as the use of menopausal hormone replacement therapy and the adoption of preventive breast cancer screening [4]. The decline in the use of hormone replacement therapy in 2002-2003 resulted in a reduction in breast cancer incidence, which has since remained relatively stable in western countries. However, it is predicted that the number of breast cancer cases globally will continue to rise, reaching 2.4 million annually by 2030. This trend is believed to be driven by an aging population and an increasing number of breast cancer cases among women in developing countries [5]. The breast cancer death, primarily in western countries, has been decreasing since 1990, despite the increasing global incidence, thanks to early detection, increased awareness and education and improvement in treatment modalities [6].

Breast cancer is subclassified based on gene expression profiling, and the four major subtypes are Luminal A, Luminal B, HER2-enriched and Triple negative breast cancer (TNBC) [7]. The subtypes guide therapeutic selection and depict the expression profiles of estrogen receptor (ER), progesterone receptor (PR), human epidermal growth factor receptor 2 (HER2) and Ki-67 [8]. Figure 1 details the expression profile of each breast cancer subtype.

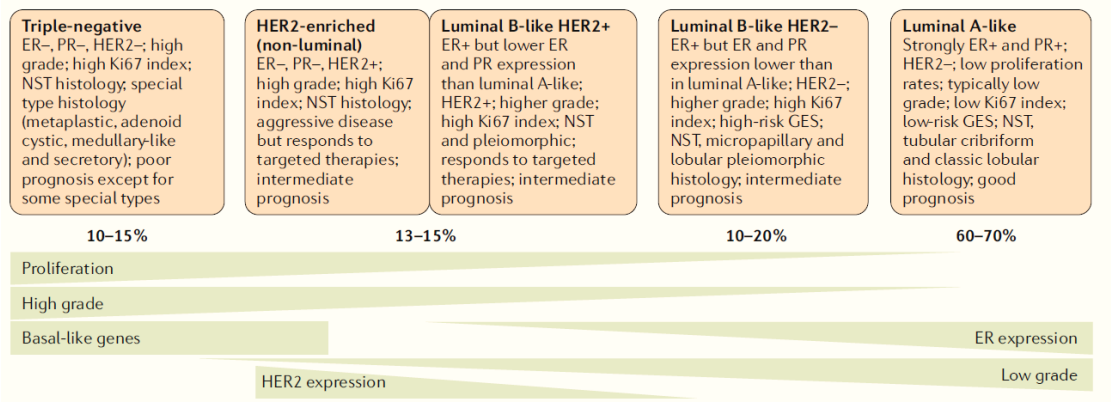

*Figure 1: **Breast cancer subtypes**. Breast cancer subtypes are based on histology and immunohistochemistry expression of key proteins: ER, PR, HER2 and the proliferation marker Ki67. Tumors expressing ER and/or PR are termed 'hormone receptor-positive'; tumors not expressing ER, PR and HER2 are called 'triple-negative'. Triple negative breast cancer is high-grade, exhibits high proliferation and expresses more basal-like genes. Adapted from Harbeck et. al. (2019) [9].*

1.2. Triple Negative Breast Cancer

TNBC accounts for ~ 15–20 % of breast cancers and is characterized by its poor prognosis due to heterogeneity, high proliferation rates and metastatic potential [10,11]. TNBC lacks expression of ER, PR and HER2, excluding thus the use of hormonal therapy and anti-HER2 agents as treatment options [12].

1.2.1. Risk factors and genomic background

The risk factors for TNBC include being female, being under the age of 40 years old [13] and being of non-Hispanic black or Hispanic race [14], suggesting the presence of genes or mutations that predispose these women to TNBC [15]. Other risk factors include multiparity, young age at first pregnancy and high waist/hip ratio [16].

The most important genomic alterations that have been identified in TNBC are mutations in the TP53 gene [17,18], such as heterozygous deletion of 17p, where TP53 is located [19], DNA damage response deficiency, specifically mismatch repair deficiency [20], mutations in *BRCA1/2* genes and gains [21–23] and amplifications of CD274 (the gene encoding Programmed cell death receptor ligand 1, PD-L1) [24]. Overall, TNBC is characterized by increased tumour mutational burden and clonal diversity [25]. Proteomic analysis of TNBC revealed that the most invasive TNBC types express high levels of proteins associated with metastasis such as extracellular matrix (ECM)-receptor interaction, cell adhesion, angiogenesis and epithelial-to-mesenchymal transition (EMT) and low levels of proteins involved in cell proliferation [26].

1.2.2. Classification

Initial efforts to characterize TNBC heterogeneity was performed by Lehmann and colleagues on the basis of gene-expression profiles, with six subtypes introduced: Basal 1 and 2 subgroups (basal-like 1 and 2), mesenchymal and mesenchymal stem-like subgroups, immunomodulatory and a luminal androgen receptor group [27]. As this approach was based on bulk mRNA analysis, it failed to decipher between the contribution of cancer cells and the tumor extrinsic features, such as the tumour-infiltrating lymphocytes (TILs) contributing to the immunomodulatory subtype and stromal cells to the mesenchymal stem-like. For this reason,

classification was updated to four TNBC subtypes: basal A and B, luminal androgen receptor (LAR), and mesenchymal [28], which have been validated at the cancer-cell level [29]. Basal A shows alterations in genes related to DNA repair (i.e., BRCA1, BRCA2) and a high TP53 mutation rate whereas Basal B is characterized by overexpression of growth factor signaling genes and myoepithelial differentiation genes. The Mesenchymal subtype is enriched for genes encoding regulators of cell motility, invasion, and mesenchymal genes, with a high expression level of stromal signatures. Finally, LAR overexpress regulators of the androgen receptor signaling pathway, genes coding for mammary luminal differentiation and increased mutations in the Phosphatidylinositol 3-kinase (PI3KCA) and AKT Serine/Threonine Kinase 1 (AKT1) genes [30].

1.2.3. Treatment landscape

Patients with early stage TNBC (stages I-III) are treated with surgery and the use of cytotoxic chemotherapy, which contains an anthracycline and a taxane, either prior (neoadjuvant) and/or after (adjuvant) the tumor resection [31]. Despite this treatment regiment, > 60% of the patients do not achieve a complete remission and ~ 46% of them will have distant metastasis [31–33], leading to this subtype of breast cancer having the worst overall survival (OS) rates amongst subtypes [11]. For patients with stage IV TNBC, the median OS is less than two years [34]. Thus, the necessity for new targeted therapies prompted the research of targetable TNBC drivers.

Multiple clinical trials have been testing novel treatment agents in the scope of key signaling pathways, DNA damage response and immunotherapy. FDA-approved agents include antibody–drug conjugates (ADCs), poly(ADP-ribose) polymerase (PARP) inhibitors and immune-checkpoint inhibitors (ICIs). In the field of ADCs, sacituzumab govitecan consists of a monoclonal antibody targeting the highly expressed transmembrane glycoprotein TROP2, that is coupled to the DNA topoisomerase I inhibitor SN-38. The agent is approved for patients with metastatic TNBC [35,36].

Olaparib and talazoparib, both PARP inhibitors, are approved for the treatment of patients with germline BRCA1/2-mutated HER2− metastatic breast cancer. The BRCA1/2 gene status is essential for the administration of these agents, as the loss of these genes in TNBC cells prompts PARP-mediated DNA repair for cell survival; the process can be harnessed to cause synthetic lethality following the administration of PARP inhibitors [37,38].

Atezolizumab and pembrolizumab are monoclonal antibodies targeting the programmed cell death 1 (PD-1) / PD-L1 axis and are approved in combination with chemotherapy as a first-line treatment for PD-L1+ advanced-stage TNBC. The PD-1/PD-L1 pathway is an immune checkpoint axis where PD-1 signaling negatively regulates T cell-mediated immune responses, providing an antigen-specific T cell immunologic evasion mechanism for the tumour. The FDA-approved compounds block the interaction of PD-L1, specifically on tumor cells and tumor-infiltrating immune cells, with PD-1, with atezolizumab being an anti-PD-L1 antibody [39,40] and pembrolizumab being an anti-PD-1 antibody [41,42].

Current clinical trials of targeted agents for TNBC are testing the use of vascular endothelial growth factor (VEGFR) inhibitors, Epidermal growth factor receptor (EGFR) inhibitors, Phosphoinositide 3-kinases (PI3K) inhibitors, AKT inhibitors, ADCs, Histone deacetylases

(HDAC) inhibitors and Cyclin-dependent kinase (CDK) inhibitors, amongst others, for the different stages of the disease [25,43].

1.2.4. TNBC Metastasis

TNBC has been associated with metastasis to the lung, liver, and brain [44]. Out of 433 women in the study of Jin et. al. (2018), 29% of these had 1 or more brain metastasis [44], which is a common site of metastasis for breast cancer [45]. TNBC metastasis is linked to poor patient outcomes since metastatic disease is currently incurable and causes the death of the majority of TNBC patients. The risk of death from breast cancer is higher for TNBC patients, and women with TNBC had an increased likelihood of distant recurrence within 5 years of diagnosis [11]. The finding of metastatic TNBC results in a fatal diagnosis, regardless of the chemotherapeutic intervention used to treat the disease [11].

During the metastatic process, tumor cells migrate from the primary site into the circulatory system and invade to ultimately colonize other organs. The metastatic cascade comprises of the steps a malignant cell takes to facilitate its dissemination from the primary tumor site to distant tissues for colonization. This process is extremely complex since it challenges the ability of cancer cells to survive and forces them to acquire a metastatic phenotype. Early metastasis has been attributed to cancer stem cells, which are a small subpopulation of undifferentiated cells within the tumor mass that show resistance to chemotherapy due to lack of proliferation [46].

Multiple events have been characterized during the metastatic cascade [47] (Figure 2). Initially, tumor cells locally invade and migrate into the stroma surrounding the primary tumor site. To enter the circulation and ultimately reach distant sites, metastatic cells need to intravasate into the vasculature or lymphatic system. Once into the circulation, metastatic cells are required to extravasate into parenchymal tissues at distant sites to the primary one. Finally, once able to form a micrometastasis at the new site, cells are selected for their ability to survive in the new site, start growing again and ultimately form a metastatic lesion. Tumors shed thousands of cells into the circulation each day, which shows how cells can easily overcome the initial barriers of the metastatic cascade involving dissociation and emigration from site of origin via the vascular system. The inefficient process of the metastatic cascade is ultimately the ability of cells to establish a new metastatic site within the metastatic niche [48], since studies has shown that only ~ 0.01 % of circulating tumor cells are capable of initiating some form of metastatic outgrowth [49].

The metastatic cascade is influenced by the ECM and the presence of the tumor microenvironment (Figure 2). The importance of these will be detailed in the following sections (1.2.5 and 1.2.6).

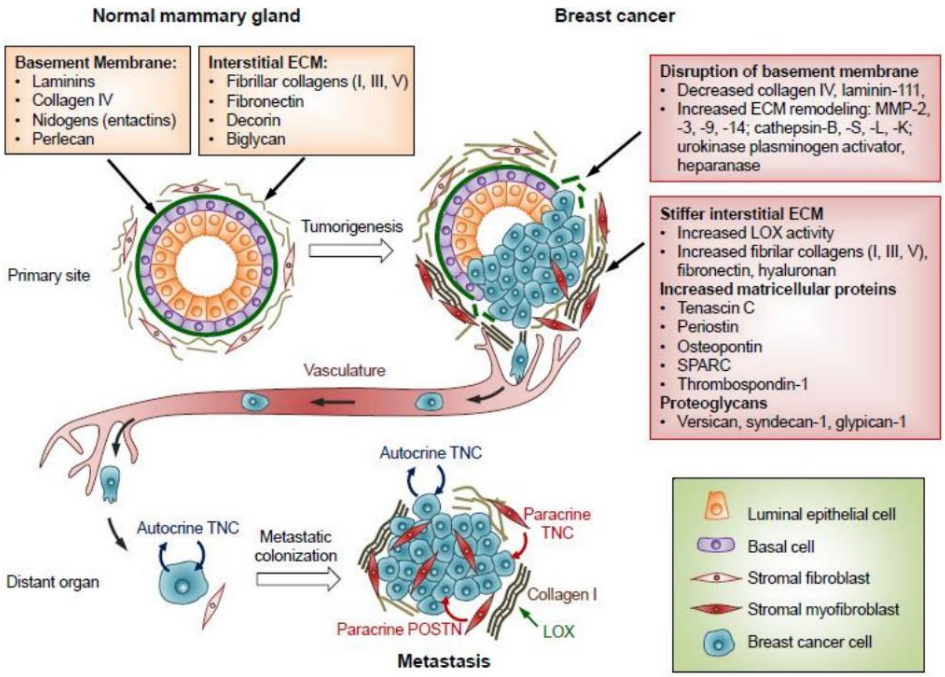

Figure 2: ***Extracellular matrix events leading to breast cancer metastasis****. Cancer cells originating from the primary breast tumor, with the potential to form metastasis, can enter the bloodstream and migrate to distant areas. Although most of these disseminated cancer cells are eliminated or become dormant due to the unfavorable conditions, a small number of these metastatic cells can withstand selective pressure and successfully create a metastasis in a distant site. A variety of extracellular matrix and tumor microenvironment factors aid the metastatic cascade at multiple steps. Adapted from Insua-Rodríguez and Oskarsson (2016)* [50]*.*

1.2.5. Extracellular matrix and related proteins in TNBC

The ECM is an intricate network comprised of 43 collagen subunits, 36 proteoglycans and ~ 200 complex glycoproteins, altogether amounting to roughly 300 macromolecules which constitute the core matrisome. The ECM surrounds cells in the tissues, providing physical support to ensure tissue integrity. The various ECM components interact with epithelial cells to regulate processes such as proliferation, adhesion, migration, polarity, differentiation, and apoptosis [51,52]. The ECM is a dynamic structure, continuously being remodeled through degradation, reassembly and chemical modifications [53].

In TNBC, alterations in the expression of ECM components results in abnormal deposition, remodeling and stiffening of the ECM, which in turn promotes TNBC motility, invasion and metastasis [54]. Tumour progression is facilitated by secretion of multiple growth factors, cytokines and chemokines as well as aberrant expression and organization of ECM components from cancer cells and cancer associated fibroblasts (CAFs) [55,56]. Indeed, in cancer patients, there is a clinical observation of increased expression of ECM components, such as tenascins and collagens [57].

Amongst the ECM modifying enzymes is the lysyl oxidase (LOX) family, which is composed of five paralogues, LOX and LOX-like 1–4 (LOXL1–4), all of which are secreted copper-dependent amine oxidases. Increased expression of LOX enzymes in breast cancer is associated with the induction of collagen crosslinking, which stiffens the ECM and subsequently promotes cell growth, survival, integrin signaling, focal adhesion formation and ultimately tumour progression (Figure 2) [58]. siRNA knockdown of LOX or inhibition by beta-aminopropionitrile

(BAPN), an irreversible inhibitor of LOX, in human MDA-MB-231 breast cancer cells reduced hypoxia-driven invasion in nude mice, demonstrating the clear involvement of LOX in hypoxia-driven metastasis. Additionally, injecting BAPN into mice along with MDA-MB-231 cells led to a reduced number of metastases [59], which is consistent with previous findings about the enzymes [60].

The ECM is known to be degraded by a family of zinc-dependent endopeptidases named Matrix metalloproteinases (MMPs). MMPs are divided into collagenases (e.g. MMP-1, MMP-13), stromelysins (e.g. MMP-10, MMP-12), gelatinases (e.g. MMP-2, MMP-9) or membrane-type enzymes (e.g. MMP-14, MMP-16). They exert their effects by cleaving a diverse group of substrates that include not only structural components of the extracellular matrix but also growth-factor-binding proteins, growth-factor precursors, receptor tyrosine kinases, cell-adhesion molecules, and other proteinases. This results in cancer progression via invasion and metastasis [61,62] (Figure 2). In TNBC, matrix metalloproteinases MMP-1, MMP-7, MMP-9, MMP-12, and MMP-13 were found to be highly expressed [63]. MMP-1 is known to be a mediator of breast cancer metastasis to the bone [64], the brain [65] and the lung [66], found to be more highly expressed in TNBC than in ER positive and HER2 positive breast cancer tissues [67]. Elevated levels of MMP-13 have been associated with decreased OS [68] and the protease is a marker of breast cancer metastasis in bone [69].

Various ECM proteins have been found to contribute to TNBC progression. Tenascin-C (TNC) is an ECM glycoprotein that is overexpressed in breast cancer [70]. It has been identified as a gene that mediates metastasis to the lung and is associated with poor metastasis free and OS when detected in the primary tumor or the metastatic lesions themselves [71] (Figure 2). TNC can also induce EMT-like changes, specifically loss of cell-cell junctions and acquisition of migratory behavior in breast cancer cells [72]. Another glycoprotein hormone, stanniocalcin 1 (STC-1) is upregulated in TNBC compared to other breast cancer subtypes [73–76]. STC-1 has been associated with TNBC invasion and metastasis, with evidence collected from both *in vitro* and *in vivo* experiments [74,75,77].

The members of the IL-6 family of cytokines, interleukin-11 (IL-11) and leukemia inhibitory factor (LIF) have been previously studied for their role in TNBC. IL-11 has been found to be overexpressed in breast cancer and associated with poor survival [78–80]. It was later identified that IL-11 is involved in the development of bone metastases through breast cancer-induced osteolysis [81–84]. LIF, a secreted glycoprotein, can signal via the LIF/ leukemia inhibitory factor receptor (LIFR) axis to promote tumor progression and metastasis in TNBC through activation of multiple signaling pathways such as Signal transducer and activator of transcription 3 (STAT3), AKT, and mammalian target of rapamycin (mTOR) [85,86]. Additionally, LIF is overexpressed in invasive breast carcinomas [87] and hence associated with a poorer relapse free survival in breast cancer patients [88].

1.2.6. Tumour microenvironment in TNBC

The heterogeneity of TNBC manifests in different clinical behavior for the different subtypes, for example sensitivity to cytotoxic agents and OS, as well as the tumor microenvironment (TME) composition [89]. TME is a complex mixture of noncancerous cell types and matrix components that has been found to contribute to disease progression and metastasis in solid tumors. The cell types encountered in the TME are CAFs, endotheliocytes, vascular smooth

muscle cells and immune cells such as T lymphocytes, macrophages and natural killer cells [90–92].

In TNBC, it was demonstrated that each of the four TNBC subtypes is associated with a specific TME profile [93]. All four subtypes were enriched in metabolic processes such as glycolysis and lipid metabolism, but differed in their expression levels of stromal signatures, with basal subtypes displaying low levels of stroma and LAR and mesenchymal subtypes showing high presence of stromal cells. In terms of immune signatures, TNBC tumors can depict immune cell infiltration, more specifically TILs, with CD8+ TIL spatial distribution determining four immune TME subtypes (immune desert, margin-restricted, stroma-restricted and fully inflamed) [94].

The TME employes the immune-related stromal cells tumor-associated macrophages (TAMs) to promote tumour growth, angiogenesis, and ECM remodeling. In breast cancer, TAMs have been found to promote tumor invasion and metastasis, and are associated with poor prognosis in cancer patients [95–97]. The bidirectional communication between tumor cells and TAMs is facilitated by the release of chemokines, inflammatory factors, and growth factors. The pro-inflammatory cytokines granulocyte-macrophage colony-stimulating factor (GM-CSF) and macrophage colony-stimulating factor (M-CSF) have been found to promote cancer aggressiveness by eliciting immune responses. M-CSF (also known as colony stimulating factor 1 - CSF1) is an established signaling molecule which facilitates the differentiation of monocytes into macrophages in the breast cancer TME [98]. It has been found that metastasized primary cancers had higher tumor epithelial and stromal expressions of CSF1 and colony stimulating factor 1 receptor (CSF1R) compared to non-metastatic cancers [99]. Additionally, M-CSF has been shown to act in a autocrine way via the CSF1/CSF1R signaling axis to promote invasion [100,101]. Similarly, GM-CSF is known to activate TAMs in breast cancer [102] and is associated with metastasis, tumor progression, and reduced survival in patients with breast cancer [103]. Experimental evidence has shown that breast cancer cells undergoing EMT can secrete GM-CSF to activate TAMs. Increased expression of GM-CSF is therefore associated with EMT and enhanced metastasis [102].

1.2.7. TNBC secretion as a therapeutic target

Given the aforementioned secreted factors of the ECM and TME and their role in TNBC progression via multiple processes, it is not surprising that this breast cancer subtype depends on its secretory machine for sustained proliferation [104,105] and invasive phenotype [106,107]. Dysregulated tumor cell secretion is a driver of cancer progression, deeming it a potential therapeutic target for the treatment of TNBC. A growing body of published work has associated the tumor secretome with the evasion of known hallmarks of cancer. For the promotion of metastasis, tumor secretion enables autocrine and paracrine signaling amongst different cell subtypes in the TME [108], cell-cell and cell-ECM interactions, ECM remodelling [109], activation of EMT, degradation of the basement membrane and formation of a pre-metastatic niche in distant organs [110].

Although it is intuitively clear that tumor growth and metastasis are linked to secretion, strategies for therapeutic exploitation of the secretory pathway are still in their infancy. This can be explained by the incomplete understanding of how the secretory pathway is

dysregulated by aberrant signalling in cancer cells [111]. This lack of knowledge hinders efforts to exploit the secretory pathway for therapeutic and diagnostic purposes.

1.3. Secretory pathway

The secretory pathway is responsible for protein synthesis and delivery of various macromolecules including exosomes, lipids, mRNAs, and proteins [104]. The collection of macromolecules secreted by a cell to the extracellular space are collectively referred to as the secretome [104]. The proteomic secretome is a tightly regulated network of cytokines, chemokines, growth factors and ECM components, that regulates cellular functions and cell-cell communication [112]. Two types of secretion have been identified: constitutive and regulated. Constitutive secretion is the default pathway in a cell, responsible primarily to replenish material at the plasma membrane and internal organelles. Regulated secretion aids the communication of the cell with its surroundings and depends on secretory vesicles, which store the secreted cargo until a signal triggers fusion with the plasma membrane. Sorting sequences within the structure of secreted cargo enables them to take the regulated secretion route [113].

1.3.1. Structure of the secretory pathway

The cellular compartments involved in the secretory pathway are the endoplasmic reticulum (EnR), ER exit sites (ERES), the ER-to-Golgi intermediate compartment (ERGIC), and the Golgi complex [114]. The EnR is the largest organelle of eukaryotic cells and consists of cisternae, a network of continuous membrane-enclosed tubules and sacs that extends from the nuclear envelop throughout the cytoplasm. Two distinct types of EnR have been identified: the rough EnR, where protein synthesis takes place due to the ribosomes present on its cytosolic surface and the smooth EnR, which is devoid of ribosomes, and steroid synthesis and drug metabolism occur. The EnR houses a plethora of enzymes that regulate assembly and correct protein folding as well as post-translational modifications of the newly synthesized proteins, such as N-glycosylation [115].

The proteins that require EnR translocation contain either a N-terminal sequence, consisting of 15-30 amino acids containing a hydrophobic core of at least 6 residues, or a transmembrane signal sequence, which instead contains a hydrophobic region of 16-25 amino acids [116]. When a newly synthesized protein contains one of the two sequences, they are transferred from the cytosol to the EnR, where the signal peptide is cleaved and the new protein is folded and leaves the EnR within vesicles, at the level of ERES [117].

Before being transported to the Golgi, secretory proteins enter in ribosome-free EnR-sub domains, namely ERES, to be packed into Coat Protein Complex II (COPII)-coated vesicles [118,119]. The process involves a wide range of signaling which ultimately leads to their transport to the ERGIC. It is still unknown whether COPII carriers vesicles fuse with the ERGIC or ERGIC is generated from the fused COPII carriers [120]. Once at the ERGIC, secretory cargos then move to the Golgi complex, the organelle where final protein processing and sorting occurs. Three functionally distinct Golgi regions have been identified, namely the *cis*-Golgi, which receives the secretory cargo and initial post-translational modifications of secretory proteins occur, and the *medial*-Golgi, and *trans*-Golgi, where final modifications take place. Finally, proteins are delivered to the *trans*-Golgi network (TGN), a tubulovesicular membrane compartment

that works as a sorting and distribution center, directing molecular traffic to endo-lysosomes, the plasma membrane, or the extracellular space. At the TGN proteins are packed into vesicles, sorted and delivered to their final destination [121].

In polarized cells, the possible directions of transport vesicles are either the apical surface, which faces the external environment, or the basolateral membrane, which faces adjacent cells and the extracellular matrix [122]. The sorting of apical proteins relies on post-translational modifications, such as glycans, while the sorting of basolateral proteins requires the serine/threonine protein kinase D (PKD) [123]. Loss of cellular apico-basal polarity, which relies on the Golgi complex, is an early stage of carcinogenesis and can result from incorrect delivery of proteins to the cell surface [124].

It has been found that certain proteins do not follow the classical pathway of secretion, therefore lacking a signal peptide or a transmembrane domain. These proteins may translocate across the plasma membrane, secreted through transporters, secreted via autophagosomes and endosomes or enter the EnR but bypass the Golgi apparatus on their way to the plasma membrane [125,126]. These process are known as unconventional protein secretion (UPS) and contributes to different cancer processes, such as growth, proliferation, invasion and metastatic colonization [127].

1.3.2. Vesicle trafficking and cancer development

Proper trafficking of proteins to the cell surface is of paramount importance to a cell, as loss of cell polarity is an early sign of carcinogenesis [124]. Vesicle trafficking pathways have been involved in processes such as cell migration, invasion, and metastasis. These pathways have been found to modulate the release of pro-tumorogenic proteins, such as proteases, ECM remodelling enzymes and immunosuppressive or protumorigenic cytokines [128].

The transport of constitutive cargo proteins from the Golgi complex to the plasma membrane is a process facilitated by tubular-saccular carriers moving along microtubules and actin filaments [128,129]. Molecular control of this process is facilitated by the small GTPases of the Rab and Arf families and, as recently discovered, by Rho (Ras Homologous) GTPases (Guanine nucleotide-binding proteins or G-proteins). RHO GTPases are guanosine triphosphate (GTP)-binding proteins, with a molecular weight in the range of 20kDa, belonging to the RAS superfamily, and are conserved in eukaryotic cells. As all the GTPases, RHO GTPases are able to switch between an active GTP-bound and an inactive guanosine diphosphate (GDP)-bound state under the regulation by guanine nucleotide exchange factors (GEFs), and GTPase-activating proteins (GAPs) [130]. In mammalian cells, the family of RHO GTPases comprise three main groups: RHO (with RHO A, B, C, D, E), RAC (with RAC1 and RAC2) and CDC42. They regulate numerous and divers cellular events, like cell growth [131], membrane trafficking [132] and cytoskeleton reorganization [133].

If there is a deficiency of GAPs or an excess of GEFs, this would lead to the accumulation of active GTP-bound small GTPases. Consequently, the interactions and activation of downstream effectors that bind to the GTP-bound small GTPases would be affected [128]. An important GEF, which has been found to promote the fission of carriers at the TGN by mediating PKD activation [134], is GEF-H1 (ARHGEF2). GEF-H1 is a microtubule-associated

RhoGEF that, when released from microtubules, stimulates the activation of RhoA and RhoB [135,136]. In breast cancer, GEF-H1 activity was regulated by ECM stiffness [137] and the protein was found to contribute to invasion of cells through 3D matrices [137].

1.3.3. Signaling at the Golgi during cancer progression

Under normal conditions, the secretory pathway plays a central role in cell growth, survival, and homeostasis by housing a variety of a variety of signaling molecules, typically G-proteins and kinases, which activate different signaling cascades as a response to external stimuli (i.e., hormones, nutrients, or growth factors). But during malignant transformation, the functions of glycosylation, secretion and transport of proteins [111] are hijacked, with up- and down-regulation of multiple factors [138], aberrant glycosylation of others [139] and transport regulators acting as oncogenes or tumor suppressors [140]. This enables the evasion of cancer hallmarks, such as deregulation of cell signaling, sustained proliferation, escape from immune surveillance, angiogenesis and metastasis [104]. Therefore, genetic and epigenetic alterations of secretory pathway molecules are positively selected during cancer progression.

As metastatic disease is the main cause of poor survival outcomes in cancer patients, efforts have been made to decipher the role of the Golgi complex and the signaling molecules it houses in the development of an invasive phenotype. Several kinases at the Golgi complex have been found to be deregulated during breast cancer progression (Figure 3). The Src family kinases (Src), which are present on the Golgi membranes, is frequently overexpressed in breast cancer, while there is a positive correlation between the activity of Src and the ability of TNBC cells to form metastases in the bone and lungs [141]. The TGN protein Phosphatidylinositol Transfer Protein Cytoplasmic 1 (PITPNC1), a kinase predominantly localizing at the TGN to promote the transfer of phosphatidylinositol (PI) and phosphatidic acid (PA) amongst membranes, is amplified in TNBC and is characterized as a pro-metastatic protein induced in breast cancer [142]. Golgi phosphoprotein 3 (GOLPH3), which is also localizing to the TGN thanks to the interaction with phosphatidylinositol 4-phosphate (PI4P), is overexpressed in breast cancer and involved in processes such as cell migration and invasion [143]. Finally, one of the most important signaling molecules of the TGN, which localizes also on TGN membranes and regulates protein secretion, is PKD. The kinase's established role in TNBC progression will be discussed in section 1.4.

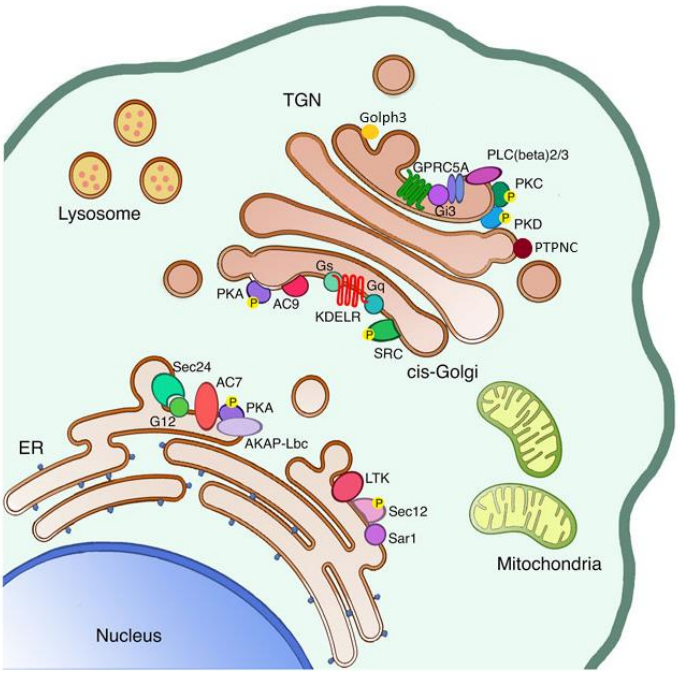

*Figure 3: **The secretory pathway hosts several signaling molecules**. TNBC cells hijack several TGN signaling molecules, and consequently the processes they regulate, to promote their aggressiveness. Several kinases (PITPNC1, GOLPH3, PKD etc.) that are employed in cancer progression are depicted. Adapted from Del Giudice et. al. (2022) [140].*

1.4. Protein kinase D

The serine-threonine protein kinase D consists of three isoforms, PKD1 [144], PKD2 [145] and PKD3 [146], which belong to the superfamily of calcium/calmodulin-dependent kinases [147]. The isoforms are Golgi protein kinases, where they control secretion by vesicle fission at the Golgi complex [148,149] and regulate actin remodeling [150,151]. The involvement of PKD in these processes has fueled its research in the context of cancer, where it was found to be involved in cell migration [151], invasion, metastasis [152] and proliferation [153]. Although PKD1 was the first isoform to be characterized and extensively studied, the importance of PKD2 and PKD3 are now recognized in different cancer subtypes with research on the isoforms continuously gaining ground.

1.4.1. Vesicle fission

PKD activation on TGN membranes is of paramount importance to ensure secretion of basolateral proteins. Basolateral protein exit from the TGN is regulated by PKD through the regulation of the lipid metabolism [149]. To enable the export of transport vesicles to the basolateral membrane, βγ subunits of heterotrimeric G-proteins are activated in a cascade that will ultimately activate PKD. Initially, phospholipase C (PLC) is activated to convert PI4P, an important lipid mediator in trafficking to the plasma membrane, to a second messenger, lipid diacylglycerol (DAG). DAG enables the activation of protein kinase C η (PKCη), a member of the protein kinase C (PKC) family, and at the same time recruits PKD to the TGN [123,154–156], into which it can bind with its cysteine-rich domains [157]. PKCη can phosphorylate two distinct serine residues of the “activation loop” of PKD, which differ amongst PKD isoforms. In two isoforms, a C-terminal autophosphorylated serine residue increases and stabilizes the active state, specifically in PKD1 (S916) and PKD2 (S876) [158,159]. PKD3 lacks the C-terminal

autophosphorylation site, but its activity can be detected by activation loop phosphorylation (pS744/748) [158]. It has been reported that upon PKD overexpression, the TGN is converted into small vesicles (also known as hypervesiculation) and upon PKD depletion, vesicle fission is blocked and long, tubular structures appear [148].

Different substrates of PKD have been identified, creating a signaling network that ensures the maintenance of constitutive secretory transport of cargo to the plasma membrane. One of PKD's substrates is phosphatidylinositol-4 kinase IIIβ (PI4KIIIβ) [160], whose role is the generation of PI4P, the precursor of DAG. PI4P can bind and recruit two lipid transfer proteins, ceramide transfer protein (CERT) and oxysterol binding protein (OSBP), to the TGN [161]. CERT controls the delivery of ceramide from the EnR to the TGN, where it is converted to sphingomyelin and PKD's most important messenger, DAG [162]. By phosphorylating CERT (S132) and OSBP (S240), PKD can negatively regulate their binding with PI4P, association with the TGN and ceramide transfer activity [163].

The transport of PKD cargo has been found to be regulated by crosstalk between microtubules and the Golgi complex. Active RhoA has been shown to localize at the Golgi and previous studies found that ligand binding to G-protein coupled receptors leads to the release of GEF-H1 from microtubules, which can activate RhoA at the TGN. RhoA can, in turn, activate PKD and result in the cargo delivery for localized exocytosis at focal adhesions [134].

Important regulators of protein transport from the TGN are also adenosyl-ribosylation factor family of small G-proteins (ARFs). Arfaptin-1 is recruited, through interaction with PI4P, to the TGN membrane and this recruitment is regulated by PKD1-mediated phosphorylation of arfaptin-1 at S132 [164]. This phosphorylation disrupts the ability of arfaptin-1 to inhibit the small GTPase Arf1 thereby allowing for vesicle fission to occur [165]. A functional protein complex discovered at the TGN comprised of the small GTPases ARF1 and ARL1, and Arfaptin2 which bound to cytosolic PKD2 to regulate the secretion of matrix metalloproteinase-2 and -7 (MMP-2 and MMP-7) [166].

1.4.2. Cell migration

The processes of cell adhesion and migration are dependent on the actin cytoskeleton. During cell migration, cells develop plasma-membrane protrusions, which can either be sheet-like (lamellipodia), or spike-like (filopodia) and are responsible for cell movement. In both types of protrusions, the main component is actin, in either the form of branched filaments in lamellipodia or bundles of filamentous (F)-actin in filopodia [167,168].

Both cell adhesion and migration through membrane protrusions have high requirements on efficient actin polymerization. Actin polymerization is a reversible process, in which Adenosine triphosphate (ATP)-loaded actin monomers associate with and dissociate from the barbed end of an actin filament. The ATP-loaded actin monomers undergo hydrolysis to be incorporated into the actin filaments, releasing phosphate, and allowing adenosine diphosphate (ADP) to remain bound to F-actin. The exchange of ADP for ATP occurs at the pointed end of the filament [169]. The disassembly of F-actin is regulated by proteins belonging to the Actin Depolymerizing Factor (ADF)/cofilin pathway, namely ADF, cofilin-1 and cofilin-2. Cofilin-1 (hereafter referred to as cofilin) facilitates subunit dissociation from the pointed end of actin

filaments, prompting actin filament severing, which is a fundamental process during cell migration, and multiple rounds of actin assembly are required as the cell moves forward [170,171].

LIM domain kinase 1 (LIMK1) and phosphatase slingshot 1L (SSH1L) proteins regulate the activity of cofilin during the disassembly of actin filaments [171]. Active (unphosphorylated) SSH1L, along with active p21-activated kinase 4 (PAK4), guarantees a functional cofilin activity cycle and cell migration. Cell migration depends on phosphorylation and dephosphorylation of cofilin in the lamellipodium, since when cofilin is phosphorylated at Ser3 it cannot bind actin and is therefore inactive. To promote directed cell migration, SSH1L localizes to the leading edge and mediates cofilin dephosphorylation [172].

Both SSH1L and PAK4 are direct targets of PKD [173,174]. Basal PKD3 activity activates LIMK via PAK4 leading to cofilin phosphorylation, which guarantees a functional cofilin activity and subsequent cell migration. PKD3 knockdown was found to decrease the activity of PAK4, while SSH1L stayed active; this led to an increase of non-phosphorylated (active) cofilin, imbalanced F-actin severing and decreased cell migration. On the other hand, when PKD2 and PKD3 are overactivated, they inactivate SSH1L by phosphorylation at S978 but do not affect the activity of PKA4; this results in the increase of phospho-cofilin levels, which prevents F-actin severing and directed cell migration [175].

Initial studies found that a kinase-dead version of PKD lead to an increase in directional cell migration [150]. This regulation of cell migration by PKD can be contributed in some part to the phosphorylation of cortactin [176], an actin binding protein enriched in lamellipodia of motile cells and invadopodia of invasive cancer cells [177], and Ras and Rab interactor 1 (RIN1), which modulates the activation of Abl kinases [178].

1.4.3. Protein Kinase D in TNBC

In breast cancer, the main isoforms present are PKD2 and PKD3, which function as oncoproteins. This is the result of PKD1 being epigenetically silenced during breast tumor progression, since it had been found to act as tumor suppressor by maintaining the epithelial phenotype and blocking invasion and metastasis [179,180]. This leads to an isoform switch towards PKD2 and PKD3 in TNBC. PKD1 has been found to prevent invasion and EMT via downregulation of MMPs at the mRNA level and the prevention of E-cadherin degradation via the transcription factor Snail [181,182], suggesting it acts as tumor suppressor. Interestingly, the loss of ER was found to be responsible for the upregulation of PKD3 in ER-negative tumors [179]. In the case of PKD2, the exact mechanism of PKD2 regulation is unknown, but it has been suggested that GA-binding protein transcription factor (GABP) is a potential regulator of PKD2 expression [183].

As a means of studying the PKD isoforms, scientists have been using the selective pan-PKD inhibitor CRT0066101. The inhibitor was discovered by Guha and co-workers and it has been studied extensively for its antiproliferative properties and its ability to reduce invasion in a variety of cancer subtypes [184–187]. It was initially found to inhibit proliferation of pancreatic cancer cell lines which expressed moderate to high levels of endogenous PKD1 and 2, an effect later replicated in xenograft mice of pancreatic cancer [184]. The effects of CRT0066101 were then studied in several other cancer models, including colorectal cancer, glioblastoma and

breast cancer, either singly or in combination with approved drugs. In breast cancer, CRT0066101 demonstrated its efficacy in reducing tumor growth of ER negative (HCC1954), multidrug-resistant (MCF-7-ADR) and TNBC (MDA-MB-231 & MDA-MB-468) cell lines [179,188].

PKD2 has been found to contribute to chemoresistance, based on correlation with high amounts of P-glycoprotein, a protein generating efflux pumps for various drugs [189]. Knockdown of PKD2 in MDA-MB-231 cells resulted in a significant decrease in resistance to paclitaxel, suggesting PKD2 as a regulator of paclitaxel-induced drug resistance and P-glycoprotein expression [190].

Elevated PKD3 expression has been found in TNBC, compared to normal human breast tissue, which was associated with significantly decreased distant metastasis-free survival [179]. It was later observed that PKD3 knockdown decreased proliferation, migration, and invasion *in vitro* and *in vivo*. The same study replicated these results by using the PKD inhibitor CRT0066101. The inhibitor was first found to decrease TNBC cell proliferation, migration, and invasion *in vitro* and then its efficacy was demonstrated in xenograft mouse models where it decreased primary tumor size, local invasiveness, and metastasis [179].

Increased PKD3 protein and transcript levels were later observed in TNBC cells and basal-like breast cancer tissues, further confirming its pro-oncogenic role in this breast cancer subtype. PKD3 was shown to increase proliferation through activating the mammalian target of rapamycin complex 1 (mTORC1) signaling cascade. PKD3 knockdown in TNBC cells led to reduced S6 kinase 1 (S6K1) phosphorylation, while overexpression of active PKD3 resulted in the hyperactivation of S6K1. This study provided further insight into the proliferative signaling PKD3 regulates [153]. PKD3 was later found to contribute, via the GEF-H1/PKD3 signaling axis, to the maintenance of TNBC stem cells [191]. Depletion of PKD3 in the TNBC cell line MDA-MB-231 reduced the cancer stem cell frequency *in vitro* and tumor initiation potential *in vivo*. Pharmacological PKD3 inhibition by CRT0066101 in combination with the chemotherapeutic paclitaxel synergistically decreased oncosphere and colony formation efficiency *in vitro* and xenograft recurrence *in vivo* [191].

PKD2 and PKD3 have been suggested to be positive regulators of EMT [192]. EMT is characterized by a switch from E-cadherin expression to N-cadherin, which mediates tumor cell invasion during the metastatic process [193]. Importantly, the transcription factors Snail (SNAI1), Slug (SNAI2), zinc finger E-box binding homeobox 1 and 2 (ZEB1, ZEB2) are important mediators of EMT through gene regulation [194]. Upon PKD inhibition by CRT0066101 in the MDA-MB-231 cell line, the cellular protein levels of EMT markers like Snail, N-cadherin, MMP-9, smooth muscle actin (SMA) and vimentin were all reduced [192]. It was later found that PKD3 depletion in MDA-MB-231 cells also decreased the EMT genes sex-determining region Y-box2 (SOX2), ATP-binding cassette subfamily G member 2 (ABCG2) and Slug expression [191].

Cell migration has been associated with both PKD2 and PKD3 in breast cancer. In doxorubicin-resistant MCF-7 cells, inhibiting the expression of PKD2 resulted in decrease of cell migration [195]. Both PKD2 and PKD3 can impact the cofilin phosphorylation status. Using the MDA-MB-468 cell line, which only expresses PKD2 and PKD3, it was observed that basal activity of PKD3 is responsible for regulating the activity of PAK4 and its downstream signaling, but it does not

significantly inhibit SSH1L. Therefore, complexes formed by PKD enzymes play a role in maintaining an equilibrium between phosphorylation and dephosphorylation processes necessary for a functional cofilin activity cycle [175].

1.4.4. *Protein Kinase D in cancer secretion*

Previous research has established that PKD is responsible for the constitutive secretion of proteins, and that PKD2 regulates the constitutive secretion of MMP-2 and MMP-7 [166]. In TNBC, re-introduction of active PKD-1, had a negative effect on the expression of MMPs (namely MMP-2, MMP-7, MMP-9, MMP-10, MMP-11, MMP-13, MMP-14 and MMP-15) [181]. Of note, all these isoforms have been known to promote MDA-MB-231 invasion [196]. These results were complimentary to impairment of MDA-MB-231 invasiveness upon re-introduction of active PKD-1 [181]. One possible interpretation of these findings is that PKD1 is epigenetically silenced in TNBC because it can regulate the expression of MMPs, which are necessary for the invasive characteristics of this breast cancer subtype. As mentioned in section 1.4.3, inhibition of PKD2 and PKD3 by CRT0066101 reduced the intracellular protein levels of MMP-9 in cellular lysates of the TNBC cell line MDA-MB-231, along with the protein levels of other EMT-related factors [192]. Nevertheless, MMP-9 extracellular levels were not quantified by the authors in the conditioned media to link this finding of intracellular protein levels to secretion.

A number of studies have focused on pancreatic cancer, where PKD2 and PKD3 have a tumor promoting role while PKD1 has demonstrated both pro- and anti-tumorogenic properties [197]. PKD1 was found to induce the expression of MMP-1, which was linked to cell migration and invasion [198]. PKD2 was shown to regulate secretion of MMP-7 and MMP-9, which was isoform specific, as the effect was not replicated upon PKD1 knockdown. Additionally, PKD2 enhanced invasion in three-dimensional extracellular matrix cultures by stimulating expression and secretion of the two MMP isoforms [199].

PKD2- and PKD3-regulated secretion has also been implicated in prostate cancer, where it was found to have a tumor promoting role. PKD3 was first implicated in the secretion of tumor-promoting factors MMP-9, interleukin-6 (IL-6), interleukin-8 (IL-8), and growth-regulated alpha protein (GROα) in prostate cancer. Secretion of these factors was not found to be a result of reduced transcript levels of the proteins, suggesting that PKD3 knockdown impaired the secretion but not transcription of these factors [200]. The application of conditioned medium collected from PKD3 knockdown cells significantly inhibited migration in normal PC3 prostate cancer cells. Additionally, the phenotype of PKD3 knockdown was reversed when conditioned medium from the parental PC3 cells was applied. This suggests that PKD3 promotes the secretion of factors that stimulate motility [200].

In another study on prostate cancer, PKD2 and PKD3 were also found to be regulators for expression of invasion- and metastasis-related genes in the urokinase-type plasminogen activator (uPA)-uPAR and MMP pathways [201], factors involved in ECM remodelling [202,203]. Additionally, prostate cancer cell migration and invasion were found to be positively regulated by NFκB (Nuclear factor kappa-light-chain-enhancer of activated B cells) signaling and histone deacetylase 1-mediated uPA [201]. The isoforms roles were further elucidated recently, when it was identified that PKD2 or PKD3 knockdown or inhibition of PKD activity resulted in decreased expression and secretion of pro-inflammatory chemokines SCF (Kit ligand), CCL5

(C-C motif chemokine 5) and CCL11 (Eotaxin) in two prostate cancer cell lines. Secretion of this set of proteins promoted mast cells recruitment and expression of angiogenic factors, which led to tumor angiogenesis [204].

In summary, PKD2 and PKD3 dependent secretomes can promote motility, invasion, and regulation of immune cells in the tumor microenvironment, deeming them as important contributors to the cancer secretome.

1.5. Proteomics technologies for cancer research

1.5.1. *Introduction to proteomics*

Proteomics is the large-scale study of all the proteins present in an organism, tissue, or cell. Proteomics technologies try to decipher the differences in protein expression levels between different conditions as well as networks of protein interactions and their respective interactions [205]. Overall, proteomics can give insight into the altered or activated signaling pathways in disease, enabling the identification of potential drug targets and biomarkers [206]. Current in-depth proteomics studies can both identify and quantify thousands of proteins in a single sample [207,208], thereby allowing for comprehensive analyses. As proteins usually exert their function depending on the cellular compartment they reside in, isolating and analyzing proteins from specific cellular compartments [209] can add further insight into the complexity of regulation and/or alternative functions.

A typical workflow of proteome-wide analysis includes sample preparation for isolation and separation of protein mixtures, biochemical fractionation in combination with protein digestion followed by mass-spectrometry-based protein identification and quantification [210]. One-dimensional gel electrophoresis (1D-SDS-PAGE) is used for robust protein fractionation in a single step. Subsequently, each lane from the gel is cut into several bands that are subjected to in-gel digestion with trypsin. The peptides generated from this digestion undergo a second fractionation using nano-liquid-chromatography, after which the separated peptides are introduced into the mass spectrometer. At the point of contact the peptides undergo an ionization process, whereby the peptides become charged. In the first mass-spectrometry step (MS1), the charged peptides eluting from the liquid-chromatography system are continuously scanned, whereby the peptides with highest intensities for a given scan window are selected for fragmentation by collision-induced dissociation. The spectrum of these fragments is detected in the second mass-spectrometry step (MS/MS or MS2) and allows for the identification of the peptide-sequence based on searching a database of known protein sequences using bioinformatics. Protein quantification for in-depth proteomics can largely be divided in two ways, labeled and unlabeled. In this thesis, protein quantification was based on an unlabeled approach. Unlabeled procedures have been extremely useful for biomarker discovery and validation studies [211], and be divided in two methods: 1) signal intensity measurement based on precursor ion spectra (MS1) and 2) spectral counting, which is based on counting the number of MS/MS spectra of peptides assigned to a certain protein. For this thesis, we employed spectral counting for differential protein expression analysis.

1.5.2. *Validation of proteomics findings by xMAP assays*

Results of proteomics discovery studies have traditionally been followed up by further validation, using antibody-based approaches for proteins with available antibodies. This is

because, when developed in a thorough manner, antibodies offer a high level of sensitivity and specificity. The enzyme linked immunosorbent assay (ELISA) is an example of an antibody-based technique, used to quantify proteins in biofluids reliably in a short amount of time. ELISA works by using an enzyme-conjugated antibody to detect the presence of a specific target molecule. In the assay, the target is immobilized/captured onto a solid support, such as a microplate. Next, a detection antibody is added in the mix that will bind the desired target. If the target molecule is present in the sample and has been bound by both the capture and detection antibodies, a colorimetric or chemiluminescent reaction will occur and present the levels of the target in the biofluid.

Current high throughput, proteomics discovery studies sometimes generate hundreds of interesting candidates, and selecting only a handful candidates for follow-up studies by antibody-based methods can be risky and costly. An alternative method to performing an ELISA assay for the validation of each candidate identified by mass spectrometry-based proteomics results is the Luminex Multianalyte Profiling (xMAP) technology (or multiplexed microsphere-based) assays [212]. Multiplex assays were introduced in the late 1990s by Luminex Corporation, a biotechnology company based in Austin, Texas [213]. The technology was developed to provide a high throughput multiplexed assay for the detection and quantification of multiple target molecules simultaneously in a single sample. Although the technology depends on the presence of suitable antibodies for the detection of targets, it is a timesaving, cost-effective technology [214] widely adopted in biomedical research and clinical diagnostics [215,216].

The technology employs color-coded microspheres which can be coated with different capture agents, such as antibodies, nucleic acids, or peptides. Each microsphere is color-coded with a unique combination of fluorescent dyes, allowing up to 500 different microsphere sets to be distinguished in a single assay. The microspheres are first incubated with the biofluid of interest (i.e., serum, plasma, conditioned media etc.) and bind to the desired target (for the validation of mass spectrometry-based proteomics validation, antibody coated microspheres are used). Using detection antibodies against each target, which are conjugated to a fluorescent dye, target quantification can be performed by detecting the amount of fluorescence associated with each microsphere. Therefore, the intensity of the fluorescent signal from each microsphere, hence each target, is converted into a quantitative measurement of the target molecule. The xMAP platform offers several advantages over traditional ELISA immunoassays, including high throughput, multiplexed detection of target molecules, and the ability to perform complex assays in a single reaction. A limitation in xMAP assays is cross-reactivity of antibodies, which hinders multiplexed reactions in cases where antibodies for different targets cross-react; during development of xMAP assays, it is ensured that no cross-reactivity is present amongst antibodies of the same assay.

An example of candidate validation by xMAP assays following mass spectrometry-based proteomics analysis are two studies by Birse at. al. (2015 and 2017) [217,218]. Lung cancer biomarkers were initially identified from cancer tissues, cell lines and conditioned medium samples using a label-free quantitative liquid LC/MS analysis [217]. A panel of nine candidate markers was identified as increased in serum collected from subjects with lung cancer, relative to controls. For all nine of the biomarkers, xMAP assays were developed and were tested in

diluted serum. These markers were then assessed in a training study, which resulted in five of those being selected to comprise a diagnostic tool for determining asymptomatic individuals with solitary pulmonary nodules [218]. These two studies demonstrate the effectiveness of validating LC-MS/MS findings by xMAP assays and the ability to create multi-marker panels that can be useful in clinical practice.

1.5.3. Proteomic profiling of the TNBC secretome

Proteomics technologies have enabled the study of breast cancer secretome. Several studies have analyzed the TNBC secretome, either in comparison with other breast cancer cell lines or individually characterize the proteins it contains.

The MDA-MB-231 secretome has been studied by Ziegler et. al. (2016), along with TNBC cell line secretomes of DT22 and DT28 cells [219]. Proteins in the MDA-MB-231 secretome included galectin-3 binding protein (LGALS3BP), a protein that modulates cell-cell and cell-matrix interactions, which is correlated with poor outcomes when found in breast cancer serum [220]. Thrombospondin-1 (THBS1), which was abundantly secreted from MDA-MB-231 cells, is known to be overexpressed in advanced stages of breast cancer. THBS1 is a major activator of the pro-metastatic cytokine transforming growth factor beta (TGF-β), and can be found in higher levels in the plasma of metastatic patients as compared to non-metastatic patients [221,222]. LOXL2, belonging as previously mentioned in the lysyl oxidase family [58], was secreted by MDA-MB-231 cells, promoting the cross-linking of collagen fibrils and hence ECM stiffening. Complimenting these findings, DT22 cells were found to secrete proteins such as extracellular matrix protein 1 (ECM1), biglycan (BGN), neural cell adhesion molecule L1 (L1CAM), and neuronal cell adhesion molecule (NRCAM), in addition to an unusually high level of TNC. Both ECM1 and TNC are associated with metastasis [223]. These findings gave insight into the ECM proteins secreted by TNBC cell lines to promote their aggressive phenotype.

Boersema et. al. (2013) [224] used the TNBC cell lines HCC1143, MFM223 and MDA-MB-453, amongst other breast cancer cell lines, to characterize their secretome and proteome. They detected the presence of growth factor receptors ErbB2 (HER2), ErbB3 (erb-b2 receptor tyrosine kinase 3), and FGFR1 (Fibroblast growth factor receptor 1) predominantly in TNBC cell lines. They also identified semaphorins, which are secreted proteins that can be shed from the membrane by ADAMs (A disintegrin and metalloproteinases) and MMPs. These proteins were first described as axon guidance factors in the nervous systems but have now been described to have tumor suppressors or tumor promoting roles in breast cancer [225]. The study detected semaphorins 3C, 4B, 4C, 4D, 5A, 7A, and their receptor Neuropilin 1 (NRP1) and plexins A1, A2, B1, B2, and D1. Finally, they identified TNC in the HCC1143 TNBC cell line, which is known to be produced by breast cancer cells and supports the survival and growth of initiating cells during the formation of metastases in the lungs [71].

A study by Shin et al. (2016) [226] analyzed the MDA-MB-231 secretome, along with secretome samples from breast cancer cell lines Hs578T, MCF-7, and SK-BR3. Enrichment analysis demonstrated that the major biological functions of these secretomes were related to cellular movement (30 %), cell death (23 %), cellular growth and proliferation (17 %), genetic disorder (14 %), cell–cell signaling and interaction (7 %), protein synthesis (6%), and gene expression (3 %). MDA-MB-231 secretome comprised of proteins legumain (LGMN), insulin-like growth factor-binding protein 5 (IBP5), adenosine triphosphatase H+ transporting accessory protein 2

(ATP6AP2), lectin mannose-binding 2 (LMAN2) and ganglioside GM2 activator (GM2A). The researchers confirmed the presence of ATP6AP2 and GM2A in breast cancer patients' plasma samples. When the authors knocked down GM2A, cell migration was decreased in all tested breast cancer cell lines, with the effect more pronounced in the TNBC cell lines MDA-MB-231 and SKBR3. In the literature, ATP6AP2 has been found to be upregulated in breast cancer tissues and promote breast cancer progression [227] .

The secretome of TNBC cells not only facilitates extracellular matrix interactions but also the interaction with the tumor microenvironment. Profiling of the MDA-MB-231-derived extracellular vesicles demonstrated that the vesicles contain M-CSF, which promoted a tumor immune microenvironment [228]. Secreted factors from TNBC cells also showed a greater ability to alter the blood–brain barrier and aid in breast cancer brain metastatic development. To gain brain metastatic specific features, MDA-MB-231 cells upregulated secreted factors involved in interleukin-6 signaling, namely Suppressor Of Cytokine Signaling 3 (SOCS3), IL-6, Interleukin-31 receptor A (IL31RA), and Cardiotrophin 1 (CTF1)) and interleukin-7 (Suppressor Of Cytokine Signaling (SOCS2), Thymic stromal lymphopoietin (TSLP), and Hepatocyte Growth Factor (HGF) [229].

Aims of the thesis

The molecular functions of PKD2 and PKD3 in TNBC have been the focus of several studies. Despite currently knowing the isoforms' contribution in various TNBC processes such as proliferation, migration and invasion, the secreted factors that PKD2 and PKD3 regulate in TNBC remain unknown.

Proteomic profiling of the cancer cell secretome is an efficient way to discover the secreted factors released from cancer cells. In this context, this study aimed to:

- Characterize the PKD-regulated secretome and cell lysate in TNBC by liquid chromatography–mass spectrometry, using two TNBC cell lines, MDA-MB-231 and MDA-MB-468, which are PKD2 and PKD3 positive and have been previously used as cellular models for the study of the isoforms.

- Validate a panel of secreted proteins with a pro-oncogenic role in TNBC, identified by liquid chromatography–mass spectrometry, using antibody-based xMAP assays and ELISA.

- Investigate the PKD2- and PKD3-dependent secreted proteins using siRNA technology to knockdown either PKD2, PKD3 or both isoforms and characterize their dependent secretome by xMAP assays and ELISA for the previously validated secreted factors.

- Systematically study the PKD-regulated secretome using a panel of TNBC cell lines to isolate the PKD-regulated secretome and characterize it by xMAP assays and ELISA for the previously validated secreted factors.

- Systematically study the PKD-regulated intracellular proteome using a panel of TNBC cell lines to detect phosphorylation of several kinases and kinase targets by xMAP assays following PKD-inhibition.

Chapter 2
Materials and Methods

2. Materials and Methods

2.1. Cell culture and reagents

MDA-MB-231 (CLS, RRID:CVCL_0062), MDA-MB-436 (RRID:CVCL_0623), MDA-MB-453 (RRID:CVCL_0418) cells were cultured in DMEM low glucose (Gibco, #41965-039). MDA-MB-468 (CLS, RRID:CVCL_0419), BT549 (RRID:CVCL_1092), HCC1806 (RRID:CVCL_1258), HCC38 (RRID:CVCL_1267), HCC70 (RRID:CVCL_1270), HCC1143 (RRID:CVCL_1245) and HCC1937 (RRID:CVCL_0290) cells were cultured in RPMI-1640 (Gibco, #21875-034). All media were supplemented with 10 % fetal bovine serum (Gibco, #10270106) and 1 % penicillin/streptomycin (Life Technologies, Cat# 15140-122). All cell lines were cultured at 37 ^{o}C in a humidified chamber with 5 % CO_2 and were authenticated in the last three years by SNP profiling.

The pan-PKD inhibitor CRT0066101 was purchased from Tocris Bioscience (Biotechne, #4975) and PMA was purchased from Merck Millipore (#P1585).

2.2. Cell viability measurements

Cell viability analysis was measured using the CellTiter-Glo luminescent cell viability assay (Promega, #G7570), according to manufacturer's instructions. The assay is a homogeneous method to determine the number of viable cells in culture based on quantitation of the ATP present, which signals the presence of metabolically active cells. The amount of ATP is directly proportional to the number of live cells present in culture. 96-well plates were prepared with mammalian cells in 100µl of culture medium. Control wells were prepared containing medium without cells to obtain a value for background luminescence. 100µl of CellTiter-Glo® Reagent, equal to the volume of cell culture medium present in each well, were added. The contents were mixed for 2 minutes on an orbital shaker to induce cell lysis. The plate was incubated at room temperature for 10 minutes to stabilize luminescent signal. Fluorescence was measured at Ex560nm/Em590nm, in Relative Fluorescent Units (RFU) and recorded on a VarioskanTM LUX multi-mode microplate reader (Thermo Fisher Scientific, MA, USA).

2.3. Western Blot

Whole cell extracts were obtained by solubilizing cells in lysis buffer (20 mM Tris pH 7.4, 150 mM NaCl, 1% Triton X-100, 1 mM EDTA, 1 mM ethylene glycol tetra acetic acid (EGTA), plus Complete protease inhibitors and PhosSTOP (Roche Diagnostics, #4906845001)). Whole cell lysates were clarified by centrifugation for 15 min at 16,000 g and 4°C. Equal amounts of protein were run on NuPage Novex 4–12% Bis-Tris gels (Life Technologies, #NP0336) and blotted onto nitrocellulose membranes using the iBlot device (Life Technologies, #IB301001). The PageRuler™ protein ladder was used in each gel (Thermo Fisher Scientific, #26616). Membranes were blocked for 30 min with 0.5% (v/v) blocking reagent (Roche Diagnostics, #11096176001) in PBS containing 0.05% (v/v) Tween-20 (Sigma-Aldrich, #P9416). Membranes were incubated with primary antibodies (see Table 1) overnight at 4°C, followed by 1 hr incubation with HRP-conjugated secondary antibodies (see Table 1) at room temperature. For quantitative Western Blotting chemiluminescence was detected at a depth of 16-bit in the linear detection range of an Amersham Imager 600 equipped with a 3.2 megapixel super-

honeycomb CCD camera fitted with a large aperture f/0.85 FUJINON lens. Densitometry was performed using Image Studio Lite 4.0 (Li-COR Biosciences, Bad Homburg, Germany).

Table 1: Antibodies used for Western Blot analysis.

Antibody target	Source	Catalogue number
Anti-GAPDH	Cell Signaling Technology	# 97166
Anti-Tubulin	Merck Millipore	#05-829
Anti-Phospho-PKD/PKCμ-(Ser916)-PKD	Cell Signaling Technology	#2051
Anti-Phospho-(Ser744/748)-PKD	Cell Signaling Technology	# 2054
Anti-PKD3	Cell Signaling Technology	# 5655
Anti-PKD2	Cell Signaling Technology	# 8188
anti-Rabbit IgG	Jackson ImmunoResearch Labs	# 111-035-144
anti-Mouse IgG	Jackson ImmunoResearch Labs	# 115-035-062

2.4. Sample preparation of secretomes and cell lysates for mass spectrometry

Conditioned medium and cell lysate from cell lines was collected and processed as previously described [230]. For mass spectrometry, 1 million MDA-MB-231 or MDA-MB-468 cells were seeded in 60 mm dishes in serum-complete medium without the presence of antibiotics and were allowed to reach ~ 90 % confluency over 24 hours. Cells were subsequently washed three times with PBS and treated with 2 ml of (a) serum free medium for 24 hours (b) 2.5 μM CRT0066101 (referred here as CRT(2.5uM)) in serum free medium for 2 hours and replacement with serum free medium for 22 hours (c) 1 μM CRT0066101 (referred here as CRT(1uM)) in serum free medium for 8 hours and replacement with serum free medium for 16 hours. Conditioned medium (secretome) was collected and centrifuged (15 min at 500 x g at 4°C followed by 20 min at 2000 x g at 4 ˚C) for the removal of cell debris. The supernatant was concentrated to ~ 30 μl by passing over an Amicon 3 kDa filter (Merck Millipore, #UFC500324). For the collection of cell lysates, cells were washed three times with ice-cold PBS and scraped following the addition of LDS-sample buffer/b-mercaptethanol. Lysed cells were centrifuged at 14000 x g for 15 min at 4 ˚C and kept at - 80 °C until further analysis.

2.5. Gel electrophoresis and in-gel digestion of proteins

Gel electrophoresis and in-gel digestion were performed as previously described [230]. Briefly, cell lysates (10 μl) and secretomes (30 μl) were separated on precast 4–12 % gradient gels using the NuPAGE SDS-PAGE system (Invitrogen). Following electrophoresis, gels were fixed in 50% ethanol/3% phosphoric acid solution and stained with Coomassie R250. Subsequently, the gels were washed once in 50 mM ABC and twice in 50 mM ABC/50 % ACN, followed by reduction in 10 mM DTT/50 mM ABC for 1 hour at 56 °C and alkylation in 50 mM iodoacetamide for 45 min at room temperature in the dark. After washing once in 50 mM ABC and twice in 50 mM ABC/50 % ACN, gel lanes were cut into 3 bands (for both cell line secretome and cell lysate samples) and each band was cut into ~1 mm^3 cubes. Gel cubes were first washed in 50 mM ABC/50 % ACN and then dried in vacuum centrifuge for 10 min at 50 °C. Following gel cube rehydration by trypsin solution (Promega, 6.25 ng/mL in 50 mM ABC), the gel cubes were covered with 50 mM ABC and incubated overnight at 25 °C. Peptides were

isolated from the gel cubes with 5% FA/50 % ACN (twice) and 1% formic acid (FA) (once). In a vacuum centrifuge at 60 °C the extracts were concentrated before LC–MS/MS after which volumes were adjusted to 50 µl with 0.05 % FA into LC autosampler vials after filtering through a spin filter of 0.45 µm [231].

2.6. LC-MS/MS proteomic analysis

Peptides were separated using an Ultimate 3000 nanoLC-MS/MS system (Thermo Fisher Scientific) equipped with a 40 cm × 75 µm ID fused silica column custom packed with 1.9 µm 120 Å ReproSil Pur C18 aqua (Dr Maisch GMBH, Ammerbuch-Entringen, Germany). After injection, peptides were trapped at 10 µl/min on a 10 mm × 100 µm ID trap column packed with 5 µm 120 Å ReproSil Pur C18 aqua in buffer A (buffer A: 0.1% formic acid in MQ; buffer B: 80% ACN + 0.1% formic acid in MQ) and separated at 300 nl/min in a 10–40% buffer B gradient in 90 min (130 min inject-to-inject) at 35 °C. Eluting peptides were ionized at a potential of + 2 kVa into a Q Exactive mass spectrometer (Thermo Fisher, Bremen, Germany). Intact peptide masses were measured at resolution 70.000 (at m/z 200) in the orbitrap using an AGC target value of 3 × 106 charges. The top 10 peptide signals (charge-states 2+ and higher) were submitted to MS/MS In the HCD (higher-energy collision) cell (1.6 m/z isolation width, 25% normalized collision energy) using an AGC target value of 1 × 106 charges an underfill ratio of 0.5% and a maxIT of 60 ms at resolution 17.500 (at m/z 200).

2.7. Protein identification and database searching

The FASTA protein sequence file of UniProtKB/Swiss-Prot human database (released in January 2021 with 42,383 entries) was used to match theoretical fragmented ions to the measured spectra using the MaxQuant search engine (version 1.6.10.43) [232]. Two missed cleavages were allowed. Peptide modification was set to cysteine carbamidomethylation, and methionine oxidation and N-terminal acetylation were added as variable modifications in the search parameters. The maximally allowed mass error for the precursor mass (MS) was 4.5 ppm and for and fragment mass (MS/MS) was 20 ppm, respectively. Both peptide and protein identifications were filtered at a false discover rate (FDR) 0.01 using the target-decoy strategy (default in MaxQuant). The mass spectrometry proteomics data have been deposited to the ProteomeXchange Consortium via the PRIDE [233] partner repository with the dataset identifier PXD041042.

2.8. Statistical analyses and data mining of LC-MS/MS data

Quantification of proteins was done using spectral counting, which is the sum of all MS/MS spectra for every detected protein [234]. Spectral counts for known proteins in a sample were normalized to the sum of spectral counts for that sample and subsequently multiplied by the mean of the sum for all samples. Normalization and statistical testing were performed using the R package countdata. Differential statistical analyses of samples was performed on the normalized spectral counts per sample using the inverted beta-binomial test [235] to compare protein expression between the paired control and treatment samples. Statistical significance was assessed with a *p*-value of ≤ 0.05 and log2FC < −0.1 or > 0.1. Statistical enrichment analysis for Gene Ontology (GO) Biological Processes and Cellular Compartment was performed using g:Profiler [236] (p-value$_{adj}$ ≤ 0.05, version e104_eg51_p15_2719230). KEGG (Kyoto Encyclopedia of Genes and Genomes) pathway enrichment analysis was performed using Enrichr (p-value$_{adj}$

≤ 0.05, KEGG_2021_Human) [237]. Prediction of classically secreted, intracellular, transmembrane and unconventionally secreted proteins was performed using OutCyte [238]. Protein-protein interaction networks were created by STRING [239] (interaction sources: experiments, databases and neighborhood/ confidence > 0.7).

2.9. Protein isolation

Total protein isolation protocols were followed for phospho-proteomic measurements. The lysis buffer (Protavio Ltd, Athens, Greece) was supplemented with a protease/phosphatase inhibitor mix (Protavio Ltd, Athens, Greece) at 100x v/v and with Phenylmethanesulfonyl fluoride (PMSF) (MilliporeSigma, #P7626) at 50x v/v. The samples were maintained at -80^{o}C. Before collection, thawed samples were first sonicated and then centrifuged at 2400 rpm for 30 min.

2.10. Protein quantification

Protein quantification was performed using the Pierce BCA Protein Assay Kit (Thermo Fisher Scientific, #23225). Working Reagent was prepared by mixing 50 parts of BCA Reagent A with 1 part of BCA Reagent B (50:1, Reagent A:B). Then, 25μL of each standard or sample was pipetted into a microplate well with a working range of 20–2000μg/mL. After that, 200μL of the Working Reagent was added to each well, and the plate was mixed thoroughly on a plate shaker for 30 seconds. Next, the plate was covered and incubated at 37°C for 30 minutes. Finally, the plate was cooled to RT and absorbance was measured at 562nm on a Tecan INFINITE F50 (Tecan, Switzerland).

2.11. ELISA

For quantification of TNC, analysis was performed using a commercially available human TNC (Abcam, #ab213831) enzyme-linked immunosorbent assay (ELISA) kit, according to the manufacturer's instructions. Samples were diluted 1:2 in sample diluent buffer. A 6,000 pg/mL Tenascin-C solution was prepared by adding 600 µL of a 10,000 pg/mL Tenascin-C stock solution into a tube with 400 µL sample diluent buffer. 300 µL of the sample diluent buffer was aliquoted into each standard tube. Next, 300 µL of the above 6,000 pg/mL Tenascin-C solution was added into the 1st tube and mixed. Then, 300 µL from the 1st tube was transferred to the 2nd tube and mixed. Subsequently, 300 µL from the 2nd tube was transferred to the 3rd tube and mixed, and so on. 100 µL of standard, blank or test sample were added on a TNC pre-coated 96-well plate. The plate was sealed and incubated at 37°C for 90 minutes. Following the incubation, the plate content was discarded, and the plate was blotted onto paper towels. After that, 100 µL of biotinylated anti-Human Tenascin-C antibody working solution was added into each well, and the plate was sealed and incubated at 37°C for 60 minutes. The plate was washed three times with 0.01M PBS following this incubation. Each well was then filled with 100 µL of prepared ABC working solution and the plate was sealed and incubated at 37°C for 30 minutes. Then, the plate was washed five times with 0.01M PBS. After the washing steps, the washing buffer was discarded, and the plate was blotted onto paper towels. Next, 90 µL of prepared TMB color developing agent was added into each well, and the plate was sealed with a new adhesive cover and incubated at 37°C in dark for 10 minutes. Finally, in each well 100 µL of prepared TMB Stop Solution were added and the optical density O.D. absorbance was read at 450 nm in a Tecan INFINITE F50 (Tecan, Switzerland) within 30 minutes after the TMB Stop Solution was added.

2.12. xMAP assays

Proteomics measurements were performed in triplicates using the Luminex Multianalyte Profiling (xMAP) technology. Briefly, Luminex xMAP is an instrument for multiplex detection of proteins in a single biological sample using bead-based sandwich immunoassays (ELISA-like). It is based on polystyrene or paramagnetic microspheres (beads) that are internally dyed with red and infrared fluorophores of differing intensities. Each dyed bead is given a unique number (bead region) allowing the differentiation of one bead from another. Multiple analyte-specific beads can then be combined in a single well of a 96-well microplate-format assay to detect and quantify multiple targets simultaneously, using the Luminex instrument (FlexMAP 3D) for analysis. The system can simultaneously detect many targets in a single sample depending on the system design. Using a dual laser system, the signature of each bead is identified, and the presence and intensity of reporter associated with the bead is detected. The intensities are reported by the median of all the beads with the same ID. This gives information about both the identity and concentration of targets in the sample. Protein antibodies are usually coupled to the beads.

As part of this PhD thesis, antibody-based Luminex assays for cytokine detection were developed using Protavio's (Athens, Greece) multiplex assay service. 7 of the Luminex assays (MMP-1, MMP-13, LIF, STC-1, IL-11, M-CSF, GM-CSF) were created for the detection of cytokines in biological fluids and 1 assay (PKD2 pSer876) for the detection of the autophosphorylation site of PKD2. Capture antibodies were coupled to the beads whereas detection antibodies were biotinylated (if not already biotinylated). Quality control confirmed biotinylation and coupling efficiency. In each assay, the optimal capture/detection antibody pair was selected based on signal-to-noise ratio measurement. All the different capture antibodies were coupled to Luminex magnetic beads, different bead regions, and were detected using analyte-specific biotinylated antibodies that bind to the appropriate epitope of the immobilized analyte.

Additionally, a custom-developed phosphoprotein 9-plex panel of Protavio was used for the detection of: Cellular tumour antigen p53 (P53, S15), SMAD family member 3 (SMAD3, S423/S425), Mitogen-activated protein kinase kinase 1 (MEK1, S217/S221), Myristoylated Alanine Rich C-Kinase Substrate (MARCKS, S170), RAC-alpha serine/threonine-protein kinase (AKT, S473), transcription factor JUN (c-JUN, S63), Glycogen synthase kinase-3 (GSK3, S9/S21), extracellular signal-regulated kinase 1 (ERK1, T202/Y204) and Epidermal growth factor receptor (EGFR, Y1068).

Briefly, 50µl of the coupled beads (bead mix where appropriate) were incubated with the samples on a flat bottom 96-well plate on a shaker at 900 rpm for 90 min at room temperature. Then, detection mix was added, and the samples incubated on a shaker at 900 rpm for 60 min at room temperature. The final step was the addition of freshly prepared SAPE solution (Streptavidin, R-Phycoerythrin conjugate, #SAPE-001, MOSS) for the detection of the signal. 15 min after the incubation with SAPE, samples were measured with the Luminex FlexMAP 3D instrument.

Proteomic measurements were accepted based on the following criteria:
- Bead Counts: A measurement is accepted if the corresponding bead count is above 100.
- R^2 values (for cytokine assays): A measurement is accepted if the corresponding standard curve for the analyte has an R^2 value > 0.85.
- Signal to noise ratio (for phosphoprotein assays): A measurement of a control samples (positive to negative cell lysate control) showed a ratio of > 2.

2.13. Transient siRNA Transfection

MDA-MB-231 cells were seeded at 200,000 wells per well. Lipofectamine® RNAiMAX Reagent (Thermo Fisher Scientific, #13778030) was diluted in Opti-MEM® Medium (Thermo Fisher Scientific, ##31985-047) using 250µl of Opti-MEM® Medium and 5µl of Lipofectamine® RNAiMAX Reagent per well), according to manufacturer's instructions. siRNAs were purchased from GE Healthcare Dharmacon Inc (spNon: #D-001810–10, spPKD3: #L-005029, spPKD2: #L-004197). siRNAs were diluted in Opti-MEM® Medium using 250µl of Opti-MEM® Medium and 0.75µl of siRNA. Diluted siRNA was added to diluted Lipofectamine® RNAiMAX Reagent in a 1:1 ratio and mixtures incubated for 5 minutes at room temperature. Cells were transfected with siRNAs for PKD2, PKD3 and both for PKD2 and PKD3. The siRNA-lipid complex was added to cells. Following 24 hours of transfection, cells were re-plated in a 96-well plate at a density of 20,000 cells per well. After an additional 24 hours, the media was replaced with newly added media. Cells were incubated for 24 hours in newly added serum containing medium and secretome samples were collected. Knockdown for PKD2, PKD3 and both for PKD2 and PKD3 was confirmed by Western Blot.

2.14. RNA Isolation

RNA extraction was performed using the NucleoSpin RNA kit for RNA purification (Macherey-Nagel, #740971). The cell culture medium was completely aspirated, and 350 µL of Buffer RA1 and 3.5 µL b-mercaptoethanol were added into each cell culture dish. The lysate was then cleared by filtration through NucleoSpin® filter. Next, 350 µL ethanol (70 %) was added to the homogenized lysate and mixed by pipetting. One NucleoSpin® RNA Column was taken for each preparation, placed in a Collection Tube and each lysate was loaded onto a column. Each column was then centrifuged for 30s at 11,000 x g and placed in a new Collection Tube. To each isolation, 10 µL of reconstituted rDNase was added to 90 µL Reaction Buffer for rDNase. The DNase reaction mixture was applied directly onto the center of the silica membrane of the column and incubated at room temperature for 15 min. Next, 200 µL Buffer RAW2 was added to the NucleoSpin® RNA Column, centrifuged for 30 sec at 11,000 x g. Buffer RAW2 was used to inactivate the rDNase. Then, 600 µL Buffer RA3 was added to the NucleoSpin® RNA Column and centrifuged for 30 sec at 11,000 x g. Finally, 250 µL Buffer RA3 was added to the NucleoSpin® RNA Column and centrifuged for 2 min at 11,000 x g to dry the membrane completely. The RNA was eluted in 40 µL RNase-free H2O after centrifugation at 11,000 x g for 1 min.

2.15. Quantitative polymerase chain reaction (qPCR)

Primer mix was created by adding 5 µl of each primer and 90 µl of sterile water. RNA samples were thawed on ice. RNA concentration for each sample was measured using the NanoDrop® ND-1000 UV-Vis Spectrophotometer (Thermo Fisher Scientific). 100ng of RNA, diluted in sterile water, were used for real-time PCR, using the Power SYBR® Green RNA-to-C T ™ 1-Step

kit (Thermo Fisher Scientific, #4389986). Power SYBR® Green RT-PCR Mix was mixed with RT Enzyme Mix and each primer mix. Reaction mix was added on PCR plate along with 1 µl of RNA. qPCR was performed using the CFX96 Touch Real-Time PCR Detection System (Bio-RAD, #1855196). qPCR conditions were as per Table 2. To analyze the fold change gene expression, the double delta Ct analysis was used (fold change = 2(-ΔΔCt)). RPLP0 (ribosomal protein lateral stalk subunit P0) served as control gene. Primers were obtained from Biomers.net and Microsynth and their sequence can be found in Table 3.

Table 2: qPCR conditions.

Stage	Step	Temperature	Time
Hold	Reverse Transcription	48 °C	30 min
Hold	Activation of AmpliTaq DNA Polymerase	95 °C	10 min
Cycling (40 cycles)	Denature	95 °C	15 sec
	Annealing	60 °C	1 min
Melt curve	Denature	95 °C	15 sec
	Anneal	60 °C	15 sec
	Denature	95 °C	15 sec

Table 3: Primer sequences for qPCR analysis.

Primer sequence of gene **F: Forward** **R: Reverse**	**Source**
TNC F: TCCCAGTGTTCGGTGGATCT; R: TTGATGCGATGTGTGAAGACA	Biomers.net
STC-1 F: GTGGCGGCTCAAAACTCAG; R: GTGGAGCACCTCCGAATGG	Biomers.net
LIF F: CCAACGTGACGGACTTCCC; R: TACACGACTATGCGGTACAGC	Biomers.net
RPLP0 F: CTCTGCATTCTCGCTTCCTGGAG R: CAGATGGATCAGCCAAGAAGG	Microsynth

Chapter 3
Results

3. Results

3.1. CRT0066101 inhibits PKD activity in MDA-MB-231 and MDA-MB-468 cells

As a cellular model, the TNBC cell lines MDA-MB-231 and MDA-MB-468 cells were selected. Both cell lines are known from literature to express PKD2 and PKD3, but not PKD1 [191,240]. To inhibit PKD activity by CRT0066101 treatment, two inhibition schemes were employed: CRT0066101 at 2.5uM (here referred to as CRT(2.5uM)) for a duration of 2 hours and CRT0066101 at 1uM (here referred to as CRT(1M)) for a duration of 8 hours. Both inhibition treatments were performed using serum free media, as these conditions would be used later for liquid chromatography-mass spectrometry analysis.

Since CRT0066101 is an ATP-competitive inhibitor, it can block the catalytic activity of PKD and prevent substrate phosphorylation. COOH-terminal phosphorylation of PKD2, an event that is catalyzed by autophosphorylation at S876, is known to be reduced upon CRT0066101 treatment. This is not the case for activation loop phosphorylation, which is known to increase upon CRT0066101 treatment [241]. For this reason, the effectiveness of CRT0066101 inhibition can be assessed by detection of PKD2 autophosphorylation at pS876, which also probes the effect for PKD3 inhibition. Both CRT(2.5uM) and CRT(1uM) were successful in reducing PKD phosphorylation, as detected by immunoblotting for PKD2 S876. CRT(2.5uM) resulted in greater blocking of PKD activity (approximately 85 %) in both cell lines, whereas CRT(1uM) reduced PKD activity by approximately 60 %. The total protein levels of PKD2 and PKD3 remain unaltered by the treatment. PKD was fully phosphorylated following PDBu (DAG analog phorbol 12,13-dibutyrate) treatment, which served as a positive control. A representative immunoblot is depicted in Figure 4.

Serum deprivation was shown to activate PKD, as determined by S876 phosphorylation. In MDA-MB-231, an exposure of 8 hours in serum-free conditioned media increased PKD activity by 50 %, compared to 2 hours. Similarly, in MDA-MB-468 cells, a 25 % increase in PKD activity was witnessed at 8 hours in serum-free conditions, compared to 2 hours (Figure 4).

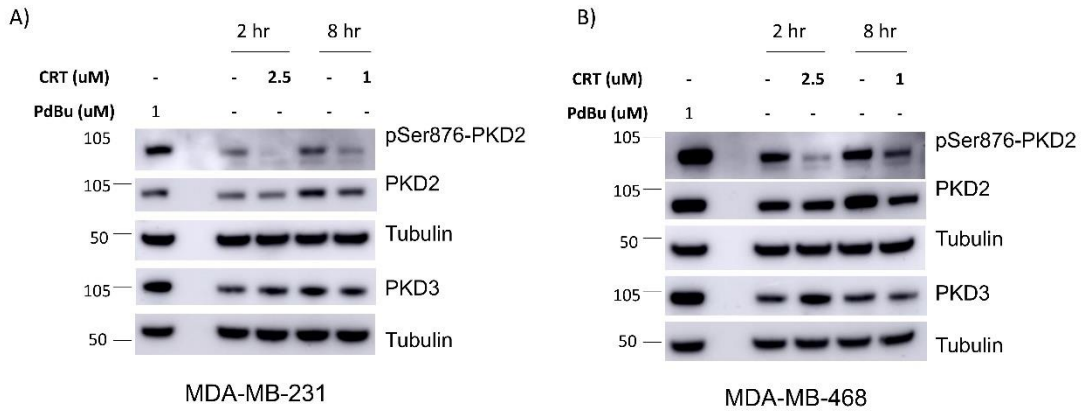

*Figure 4: **CRT0066101 inhibits PKD activity in MDA-MB-231 and MDA-MB-468 cells**. A, B) Western blots showing the autophosphorylation site (pS876) of PKD2 endogenous to A) MDA-MB-231 and B) MDA-MB-468 cells. Cell lines were treated with CRT(2.uM) for 2 hours and CRT(1uM) for 8 hours, under serum free conditions. PdBu treatment*

served as positive control. Immunoblotting was conducted, and membranes were probed with specific antibodies as indicated. Tubulin was used as loading control. Experiment was performed by Elena Gutiérrez-Galindo.

3.2. Development of a PKD2 S876 xMAP assay

An xMAP assay was custom developed for the detection of the autophosphorylation site (pS876) of PKD2. On a Luminex bead, a PKDSer876 specific antibody was coupled using Sulfo-NHS and EDC coupling conditions. A PKD2 antibody, detecting the total levels of the protein, was biotinylated using the NHS-PEG4-Biotin reaction. Quality control confirmed both coupling and biotinylation efficiency. The assay was then tested in control cell lysate samples for its ability to detect endogenous PKD2 S876 levels by quantifying the Median Fluoresence Intensity (MFI) values of the samples.

The assay was then used to assess CRT(2.5uM) and CRT(1M) in MDA-MB-231 and MDA-MB-468 cells and confirm it could replicate the results of immunoblotting and hence confirm PKD inhibition following CRT0066101 treatment. The assay demonstrated its effectiveness in detecting the reduced PKD2 S876 levels following both CRT0066101 treatment schemes under serum free conditions (Figure 5). Additionally, the inhibition schemes were tested under serum complete conditions in both cell lines. Both CRT(2.5uM) and CRT(1M) were successful in reducing PKD2 S876 levels under serum complete conditions in the MDA-MB-468 cell line. The endogenous PKD2 S876 levels in the MDA-MB-231 cell line were below the limit of detection of the assay under serum complete conditions, hence for the cell line the inhibition effectiveness was only confirmed under serum free conditions (Figure 5).

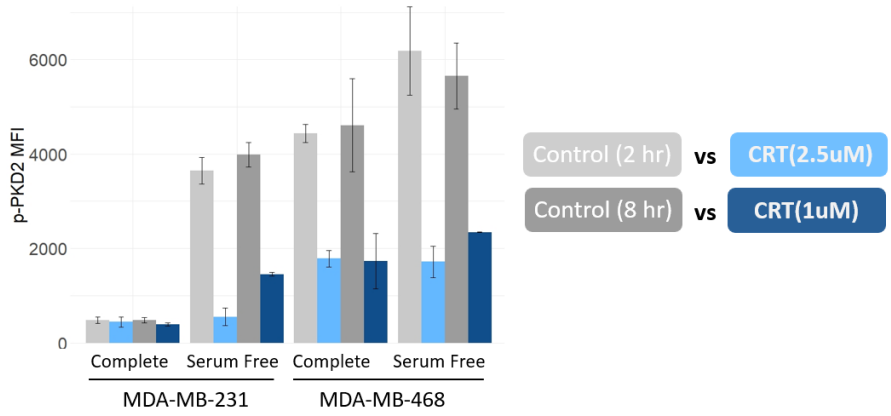

*Figure 5: **xMAP assay for the detection of pS876 PKD2 in MDA-MB-231 and MDA-MB-468 cells.** CRT(2.5uM) and CRT(1uM) were compared with respective controls, under serum free and serum containing conditions, using a custom-developed pS876 PKD2 xMAP assay. Data are reported as mean Median Fluorescence Intensity (MFI) values obtained from three biological replicates and error bars show standard deviation.*

3.3. Characterization of the PKD-regulated cell lysate and secretome by LC-MS/MS

Following the validation of inhibition effectiveness by CRT(2.5uM) and CRT(1M) under serum deprivation, both by immunoblotting and xMAP assay, the conditions were used to block PKD activity in the cell lines. Following treatment with the inhibitor, cells were left to recover for a total of 22 hours in the case of CRT(2.5uM) and 16 hours in the case of CRT(1uM) in serum free media. Sampling at 24 hours following treatment initiation allowed enough time for secretome changes to become evident in the conditioned medium [242] and for cell viability to be maintained under serum free conditions in control and CRT treated cells, as confirmed by

a CellTiter-Glo luminescent cell viability assay (Figure 6). Of note, cell viability was also unaltered in the cell lines following CRT(2.5uM) and CRT(1uM) under serum complete conditions (Figure 6).

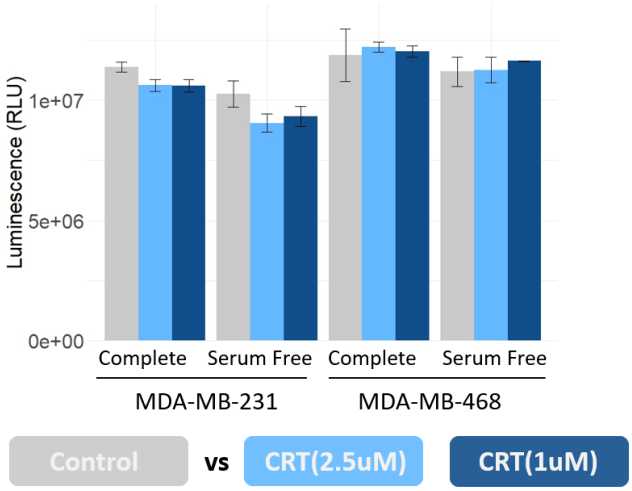

Figure 6: ***Confirmation of cell viability maintenance following CRT(2.5uM) and CRT(1uM).*** *Cell viability was assessed using the CellTiter-Glo reagent comparing CRT(2.5uM) and CRT(1uM) with control samples under serum free and serum containing conditions. Data are reported as mean luminescence values obtained from three technical replicates and error bars show standard deviation.*

Conditioned medium (here referred to as secretome) samples and their corresponding cell lysates were collected from control and CRT treated cells of the MDA-MB-231 and MDA-MB-468 cell lines. A label-free GeLC-MS/MS-based proteomics workflow [243] was employed to analyse 3 biological replicates for each sample in the treatment and control groups per cell line (Figure 7A).

Proteins were resolved using 1D SDS-PAGE and the gel lanes were sliced into three pieces, subsequently digested in-gel with trypsin. Peptides were extracted and then separated by a LC-MS/MS system. MS/MS spectra were then searched in MaxQuant [232]. The paired beta-binomial test was applied to find proteins with statistically significant differences in spectral count numbers between the control and CRT(2.5uM) and CRT(1uM) samples, in both secretome and cell lysate samples, using the R statistical software (Figure 7A).

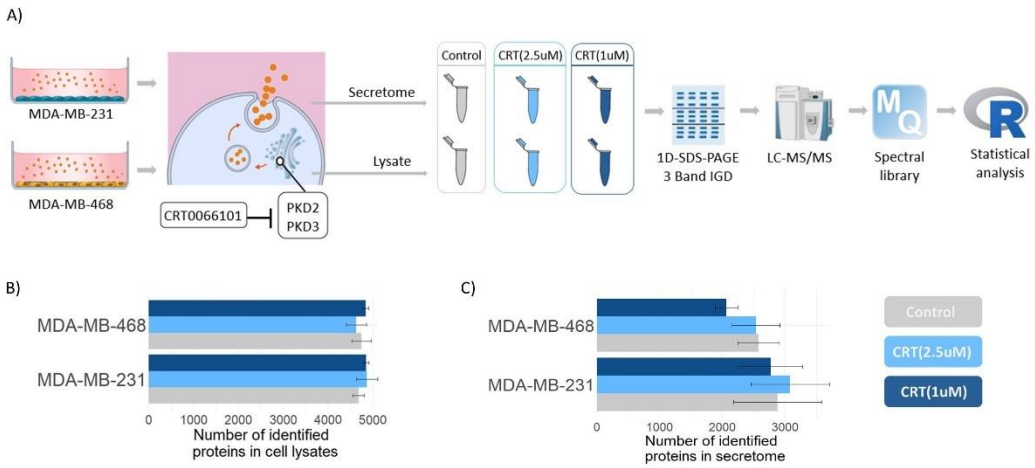

Figure 7: ***Proteomics workflow for the identification of the PKD-regulated secretome.*** *A) Overview of the proteomics workflow. Conditioned media (secretome) and cell lysate from PKD-inhibited MDA-MB-231 and MDA-MB-468 cells were collected for LC-MS/MS analysis. Samples were analyzed by 1D-SDS-PAGE, with each gel lane cut into 3 bands, in-gel digested (IGD) with trypsin and analyzed by LC-MS/MS. MS/MS spectra were then searched in MaxQuant spectral library and statistical analysis for the identification of statistically changed proteins was performed on the R statistical software. B, C) Number of proteins identified by LC-MS/MS in the B) cell lysate and C) secretome samples collected from each cell line and treatment condition, in three biological replicates. Numbers are reported as the mean of the three biological replicates and error bars show standard deviation.*

Prior to differential protein expression analysis, we assessed the number of proteins identified in each sample processed. An average of approximately 4,900 proteins were identified in the cell lysates samples, with no notable differences present between control and CRT treated samples per cell line (Figure 7B). For the secretome samples of the MDA-MB-231 cell line, an average of ~ 3,000 proteins were identified in the control and CRT treated samples, whereas an average of ~ 2,400 proteins were identified in the secretome samples of the MDA-MB-468 cell line (Figure 7C). Overall, the number of secreted proteins identified amongst the different groups per cell line was also not affected, in line with the preserved cell viability we had confirmed.

Unsupervised clustering analysis of secretome and lysate samples highlighted that samples clustered first according to sample type (secretome or cell lysate) and then by cell line (Figure 8). The changes in protein content between the control and CRT treated samples were not large enough to make the replicates from each condition cluster together, neither in secretome nor in cell lysate samples. This can be explained by our selection of short-time inhibition schemes, which had not completely blocked PKD activity. The heatmap of Figure 8 show the differences in protein content between secretome and lysate samples: a great number of proteins is predominantly found in cell lysates, and not in secretomes, and certain highly expressed proteins in secretome samples are absent in cell lysates. Additionally, cell line differences between the secretome or the cell lysate samples are evident in the heatmap.

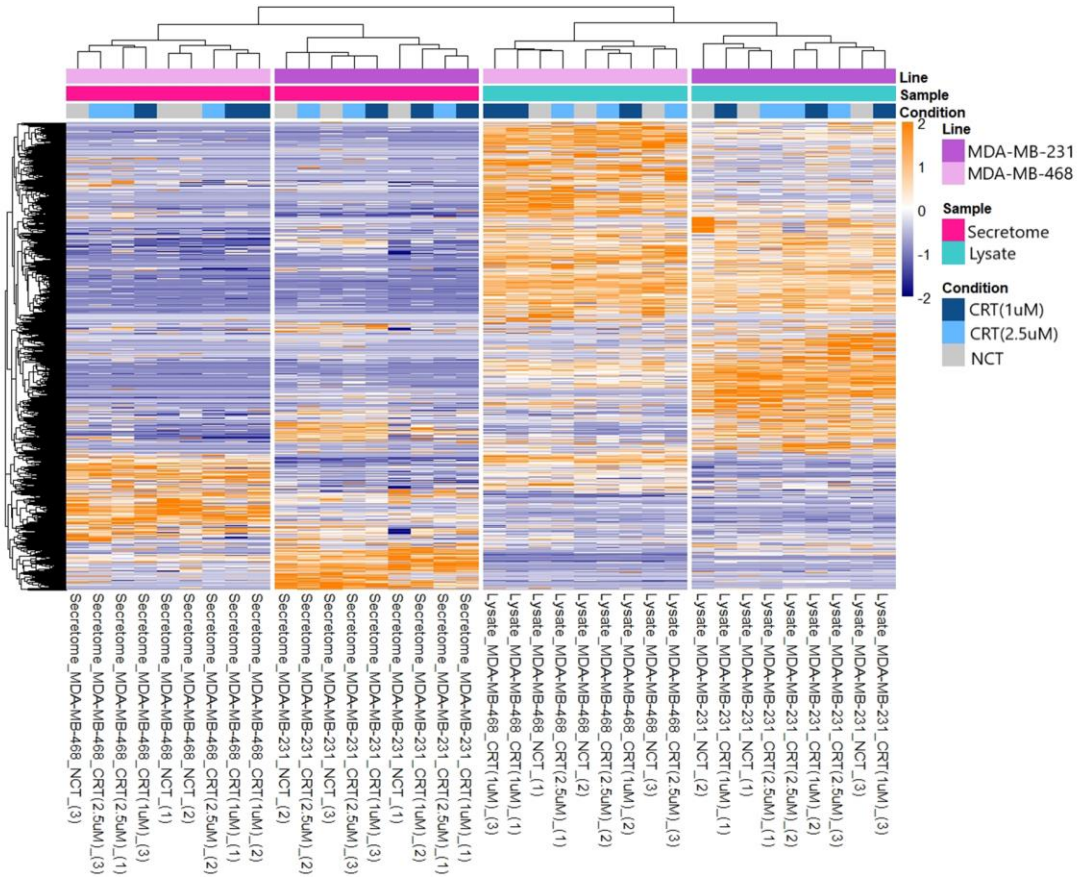

Figure 8: ***Unsupervised hierarchical clustering of the secretome and cell lysate samples analyzed by LC-MS/MS.*** *Samples are labelled according to their origin (secretome or lysate), their cell line (MDA-MB-231 or MDA-MB-468) and treatment condition (NCT/control, CRT(2.5uM) or CRT(1uM)). Relative protein abundances are shown from low (blue) to high (orange).*

To identify proteins that are regulated by PKD, either intracellularly or in the secretome, we quantitatively compared proteins found in CRT(2.5µM) and CRT(1µM) treated cells with control samples for each cell line and sample type using an inverted beta-binomial test [235], with significance established at p-value ≤ 0.05 and log2FC < −0.1 or > 0.1.

3.3.1. PKD inhibition results in reduction of intracellular levels of proteins related to ribosome biogenesis

In MDA-MB-231 cells, both CRT(2.5µM) and CRT(1µM) induced the significant change of approximately 100 proteins in cell lysate samples. The majority of these proteins were found to be upregulated, since CRT(2.5µM) induced the upregulation of 78 proteins and CRT(1µM) of 83 proteins (Figure 9A,B). 30 of these proteins were commonly upregulated between the inhibition schemes (Figure 9F) while 1 was commonly downregulated (Figure 9E).

In MDA-MB-468 cells, CRT(2.5µM) induced the significant change of 107 proteins whereas CRT(1µM) resulted in the change of 57 proteins (Figure 9C,D). In both cases, approximately half of the proteins were upregulated and the rest downregulated. 11 proteins were commonly upregulated proteins between the two inhibition schemes (Figure 9H) while 6 were commonly downregulated (Figure 9G).

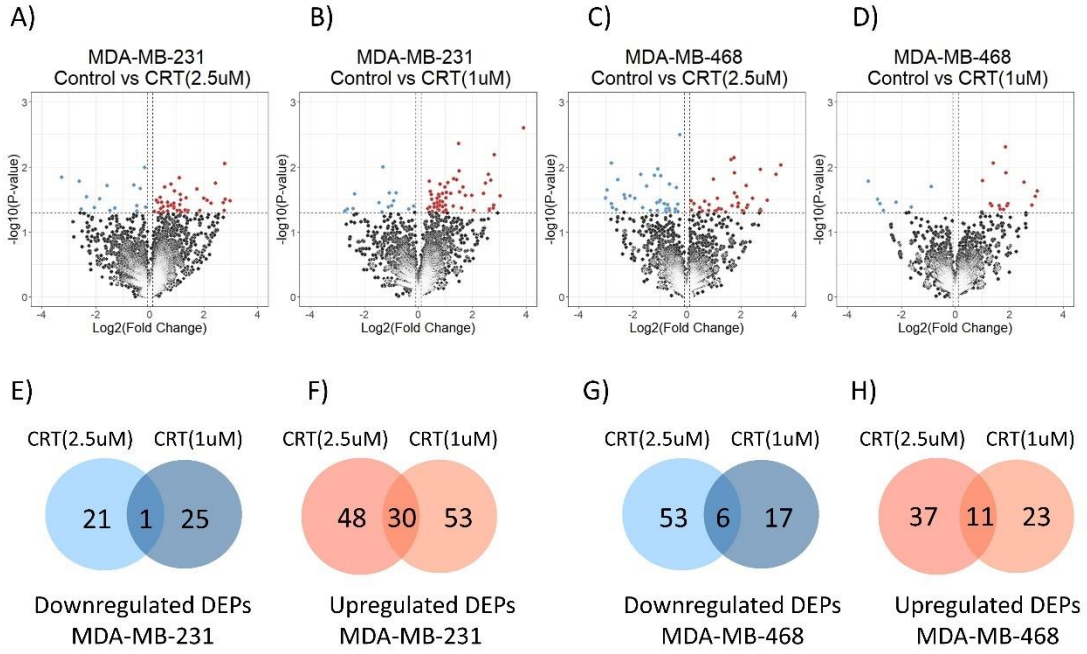

Figure 9: ***PKD inhibition results in significant abundance changes of intracellular proteins.*** *A - D) Identification of significantly changed cell lysate proteins upon CRT(2.5uM) and CRT(1uM), compared to control, per cell line. Volcano plots of log10 p values (statistical significance) against log2 protein abundance fold change between CRT(2.5μM) and CRT(1μM)-treated cells versus control for each cell line. In light and dark blue are downregulated secretome proteins upon CRT(2.5μM) and CRT(1μM), respectively, compared to control (log2FoldChange ≤ – 0.1 and p-value ≤ 0.05). Upregulated proteins following both CRT(2.5μM) and CRT(1μM) are found in red (log2FoldChange ≥ 0.1 and p-value ≤ 0.05). E - H) Overlap of significantly changed cell lysate proteins upon CRT(2.5uM) and CRT(1uM), compared to control, in the E -F) MDA-MB-231 cell line and G – H) MDA-MB-468 cell line.*

GO enrichment analysis [244] identified that in the MDA-MB-231 cell line, the significantly changed proteins were in nature cytosolic (adjusted *p* value=7.37×10^{-7}) (Figure 10A). In the MDA-MB-468 cell line, downregulated biological processes were related to ribosome biogenesis (adjusted *p* value=0.004), whereas upregulated proteins were associated with nuclear division, such as spindle (adjusted *p* value=0.005) and kinetochore formation (adjusted *p* value=0.0002).

GO enrichment analysis for biological processes in the MDA-MB-231 cell line did not present a great enough number of enriched terms in the identified significantly changed proteins, as depicted in Figure 10B. On the other hand, in the MDA-MB-468 cell line upregulated proteins were once again enriched for cell division processes (adjusted *p* value=0.0001) whereas downregulated proteins were enriched for protein regulation of JUN (adjusted *p* value=0.038) and MAP (adjusted *p* value=0.039) kinase activity.

Finally, KEGG pathways enrichment analysis further contributed to the understanding of the roles the significantly changed cell lysate proteins play. More specifically, in the MDA-MB-231 cell line the proteins downregulated belonged in ribosome biogenesis (adjusted p value = 0.019) and upregulated ones in different metabolic processes. In the MDA-MB-468 cell line downregulated proteins belonged in the formation of adherens, tight and gap junctions

(adjusted p values=0.001, 0.013 and 0.004, respectively) and upregulated ones were related to the ECM (adjusted p value=0.02) (Figure 10C).

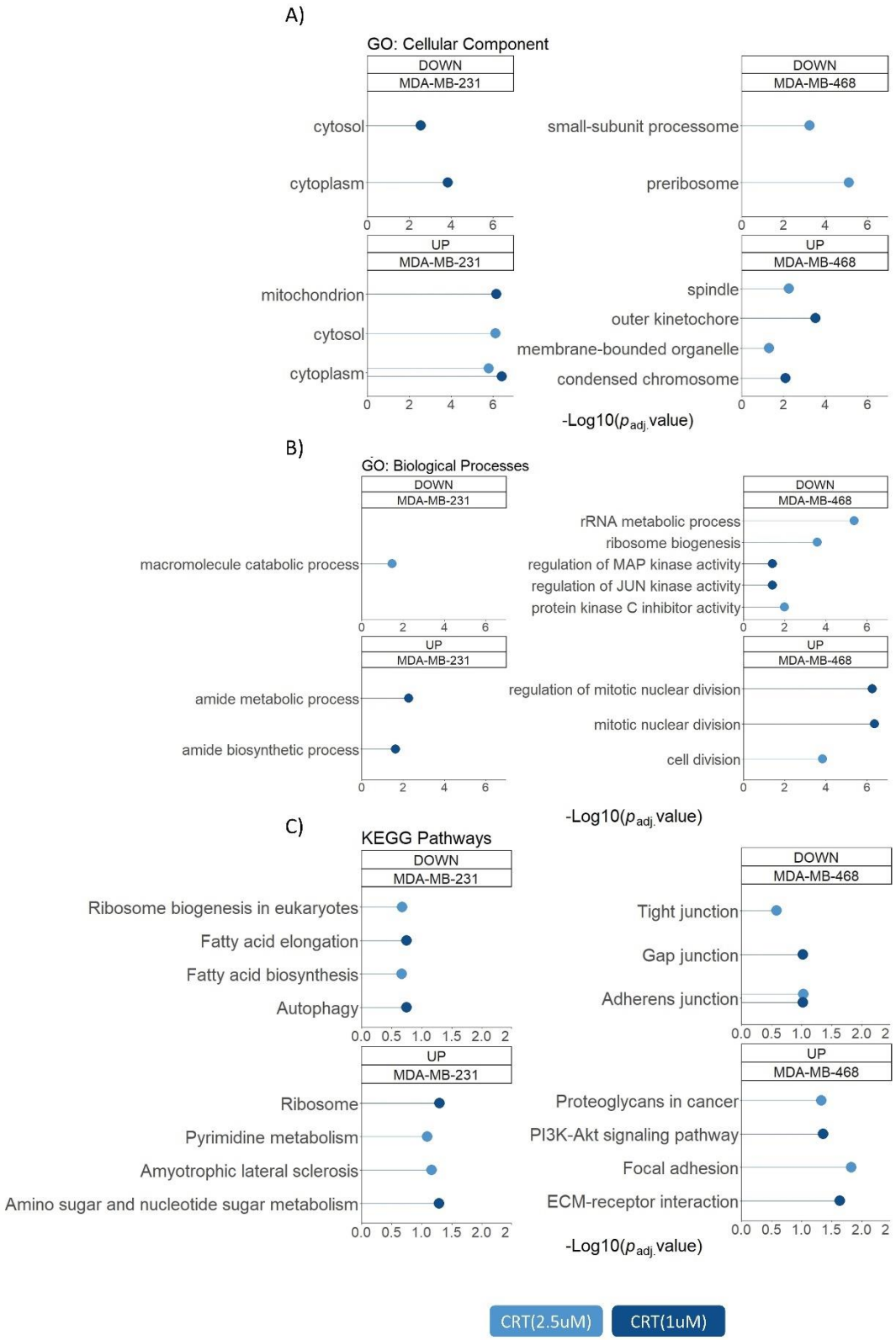

Figure 10: ***Enrichment analysis for the upregulated and downregulated proteins identified in cell lysates following PKD inhibition****. Top Gene Ontology (GO) biological processes terms and KEGG pathways identified to be upregulated (UP) or downregulated (DOWN) in the cell lysates of MDA-MB-231 and MDA-MB-468 following CRT(2.5μM) and CRT(1μM). X-axis indicates the enrichment scores [-log10 (adjusted p value)] for each term and y-axis the enriched term.*

A common enriched term that was identified in the downregulated proteins of both cell lines, following either GO biological processes or KEGG pathway enrichment, was ribosome biogenesis. Amongst the different ribosome-related proteins that were downregulated upon PKD inhibition by CRT(2.5μM) or/and CRT(1μM) in both the MDA-MB-231 and MDA-MB-468 cells were: small nucleolar RNA-associated proteins (UTP18, UTP14A) which are involved in nucleolar processing of pre-18S ribosomal RNA and ribosome assembly [245], ribosome production factor 1 (RPF1), which is required for pre- large ribosomal subunit (60S) biogenesis [246], methyltransferase FTSJ3 (pre-rRNA 2'-O-ribose RNA methyltransferase FTSJ3), involved in the modification of ribosomal RNA (rRNA) molecules within the ribosome [247] and RNA helicase DDX52 (Probable ATP-dependent RNA helicase DDX52), which is involved in the processing and maturation of rRNA molecules within the ribosome [248] (Figure 11A,B).

In MDA-MB-231 cells, we identified reduced levels of Guanine nucleotide-binding protein-like 3 (GNL3), a protein involved in the 60S ribosomal subunit biogenesis and shows enriched expression in multipotent stem cells across several invertebrate animals [249] (Figure 11A). In MDA-MB-468 cells we identified reduction in the levels of 40S ribosomal protein S15 (RPS15), a component of the small ribosomal subunit (40S) [250], U3 small nucleolar ribonucleoprotein protein MPP10 (MPHOSPH10), which is involved in ribosomal RNA processing and RNA-binding proteins [251], RNA-binding protein 28 (RBM28) which is involved in ribonucleoprotein complexes [252], protein RRP5 homolog (PDCD11) which is essential for the generation of mature 18S rRNA [253] and WD repeat-containing protein 46 (WDR46), which is required for rRNA processing and intra-nuclear transport of 60S ribosomal subunits [254] (Figure 11B).

Protein abundance of the aforementioned proteins before and after CRT treatment in the cell lysates of each cell line can be found in Figure 11. A protein-protein interaction network of these downregulated proteins using the STRING database created a highly connected network, depicting FTSJ3 to be interacting with the most proteins in the network (UTP18, UTP14A, MPHOSPH10, PDCD11, WDR46 and GNL3) (Figure 11C).

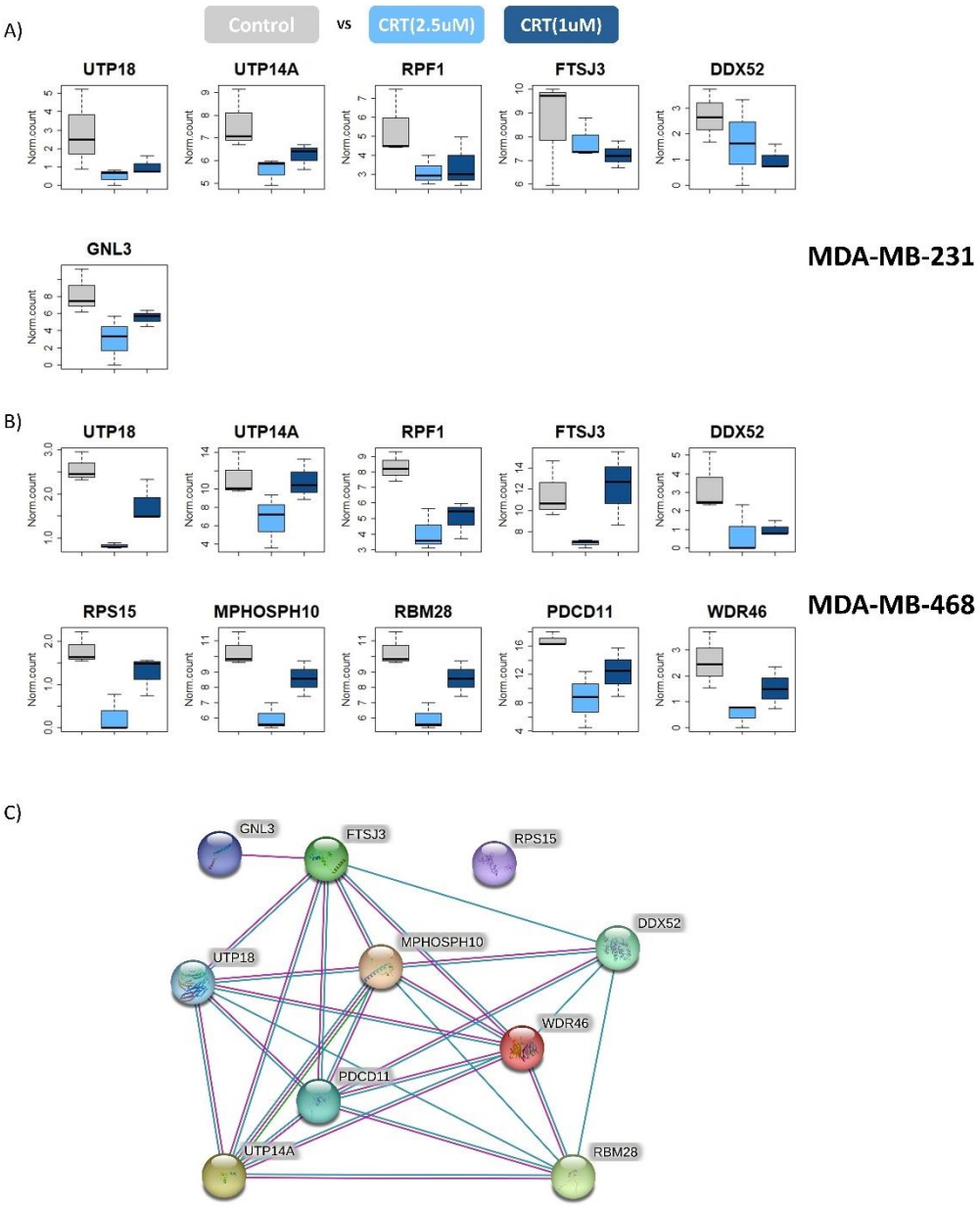

Figure 11: ***PKD inhibition reduces intracellular levels of proteins related to ribosome biogenesis.*** *A – B) Boxplots illustrating protein abundance of several ribosome related proteins found to be downregulated in the A) MDA-MB-231 and B) MDA-MB-468 cell lines following CRT(2.5µM) and CRT(1µM). Y-axis indicates the normalized count quantified during LC-MS/MS and x-axis the condition (control vs treatment). C) Protein – protein interactions analysis of downregulated intracellular proteins related to ribosome biogenesis using String network.*

3.3.2. PKD contributes to the composition of the TNBC secretome

In MDA-MB-231 cells, CRT(2.5µM) and CRT(1µM) induced the significant change of 61 and 66 proteins, respectively, whereas in MDA-MB-468 the same inhibition schemes changed significantly 143 and 244 proteins, respectively (Figure 12A,B,C,D).

As expected, most of the significantly changed proteins were downregulated in response to CRT(2.5µM) and CRT(1µM), in both cell lines, with 44 and 39 proteins, respectively, found in MDA-MB-231 cells and 110 and 182 showing reduced secretion in MDA-MB-468 cells (Figure 12A,B,C,D). These findings were in line with our hypothesis that PKD regulates the secretion of proteins in TNBC cell lines.

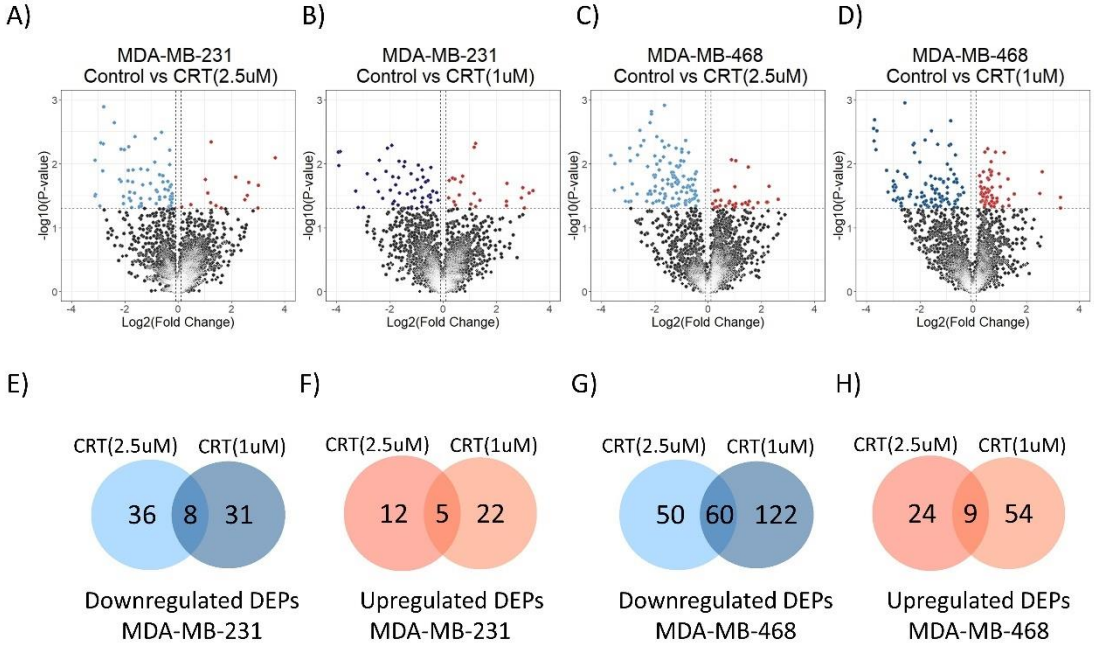

*Figure 12: **PKD contributes to the composition of the TNBC secretome**. A-D) Identification of significantly changed secretome proteins upon CRT(2.5uM) and CRT(1uM), compared to control, per cell line. Volcano plots of log10 p values (statistical significance) against log2 protein abundance fold change between CRT(2.5µM) and CRT(1µM)-treated cells versus control for each cell line. In light and dark blue are downregulated secretome proteins upon CRT(2.5µM) and CRT(1µM), respectively, compared to control (log2FoldChange ≤ − 0.1 and p-value ≤ 0.05). Upregulated proteins following both CRT(2.5µM) and CRT(1µM) are found in red (log2FoldChange ≥ 0.1 and p-value ≤ 0.05). E-H) Overlap of significantly changed secretome proteins upon CRT(2.5uM) and CRT(1uM), compared to control, in the E -F) MDA-MB-231 cell line and G – H) MDA-MB-468 cell line.*

In the MDA-MB-231 cell line, CRT(2.5µM) induced the upregulation of 17 proteins and CRT(1µM) of 27 proteins. 5 of these proteins were commonly upregulated between the inhibition schemes (Figure 12F). Similarly, 33 proteins were upregulated following CRT(2.5µM) and 63 following CRT(1µM) in the MDA-MB-468 cell line, with 9 proteins commonly upregulated between the inhibition schemes (Figure 12H).

The MDA-MB-231 upregulated secretome proteins were related to translation, as evidenced by the enriched GO biological processes (adjusted *p* value=0.0045) and KEGG pathway (adjusted *p* value=1.05×10^{-4}), whereas in the MDA-MB-468 cell line upregulated proteins were related to nicotinamide adenine dinucleotide (NADH) metabolic processes (adjusted *p* value=0.002) and glycolysis (adjusted *p* value=0.02) (Figure 13).

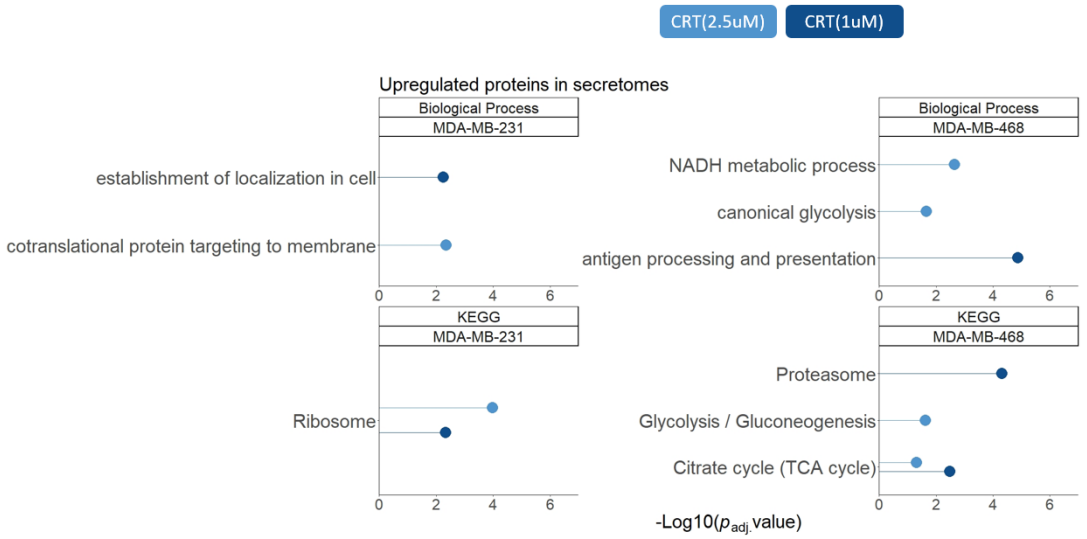

Figure 13: ***Enrichment analysis for the upregulated proteins identified in secretomes following PKD inhibition.*** *Top Gene Ontology (GO) biological processes terms and KEGG pathways identified to be upregulated in the secretome samples of MDA-MB-231 and MDA-MB-468 following CRT(2.5μM) and CRT(1μM). X-axis indicates the enrichment scores [-log10 (adjusted p value)] for each term and y-axis the enriched term.*

We aimed to identify whether the results of the two inhibition schemes were comparable, with respect to the downregulated proteins identified per cell line. 8 proteins were significantly downregulated upon both MDA-MB-231 CRT(2.5μM) and CRT(1μM), whereas 60 were found to overlap between MDA-MB-468 CRT(2.5μM) and CRT(1μM) (Figure 14). The levels of overlap in both cell lines were significant at $p < 0.001$ (one-sided Fisher's exact test). Notably, protein overlap was more evident within the same cell line following CRT treatment rather than between the two cell lines (Figure 14).

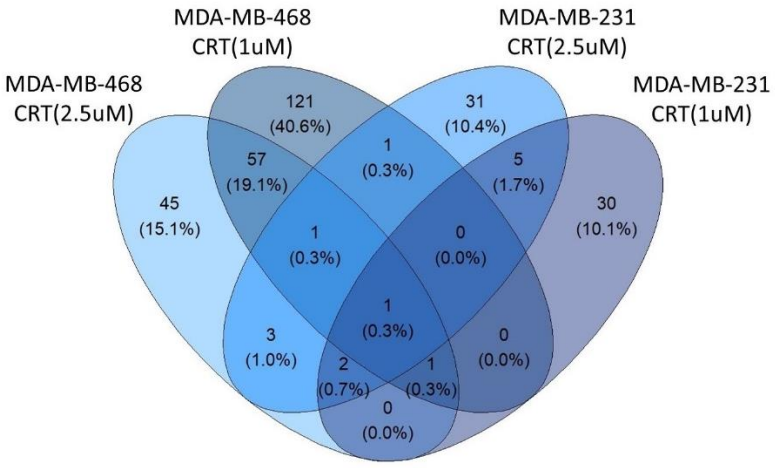

Figure 14: ***Secretome downregulated proteins show overlap within same cell line****. Venn diagram showing the overlap of downregulated proteins among the four treatment conditions (MDA-MB-231 and MDA-MB-468 cell lines treated with CRT(2.5μM) and CRT(1μM)).*

OutCyte analysis [238] was used to interrogate the class of downregulated secretome proteins identified from both cell lines. Out of the total 299 downregulated proteins, 170 (56.8 %) contained a signal peptide, 26 (8.7 %) a transmembrane domain and 79 (26.4 %) proteins were classified as intracellular. Finally, a total of 24 (8 %) proteins were predicted to be unconventionally secreted by the algorithm (Figure 15A). Our analysis confirmed that PKD-dependent protein cargo is, in its majority, classically secreted, which is in agreement with the kinase's role in regulating constitutive secretion from the trans Golgi network [255,149]. Interestingly, the proteins that were predicted as intracellular from OutCyte were enriched in the GO cellular compartment "extracellular exosome" (adjusted *p* value=2.65 × 10^{-7}) and "extracellular vesicle" (adjusted *p* value=3.21 × 10^{-7}), suggesting PKD could be involved in secretion of proteins via exosomes.

We initially aimed to investigate the processes that were altered upon PKD inhibition, irrespective of cell line-specific differences. Following GO enrichment, we confirmed that the proteins downregulated in the secretomes of both cell lines were, in nature, extracellular proteins (adjusted *p* value =1.67 × 10^{-43}), and proteins of the extracellular matrix (adjusted *p* value =8.76 × 10^{-24}) (Figure 15B) with roles in "cell adhesion" (adjusted *p* value=2.82 × 10^{-24}) and the "extracellular matrix organization" (adjusted *p* value=1.23 × 10^{-17}) (Figure 15C). Similarly, the two most enriched KEGG pathways to which the downregulated proteins belonged were "Axon guidance" (adjusted *p* value=9.18 × 10^{-11}) and the "Extracellular matrix-receptor interaction" (adjusted *p* value=2.19 × 10^{-8}) (Figure 15D).

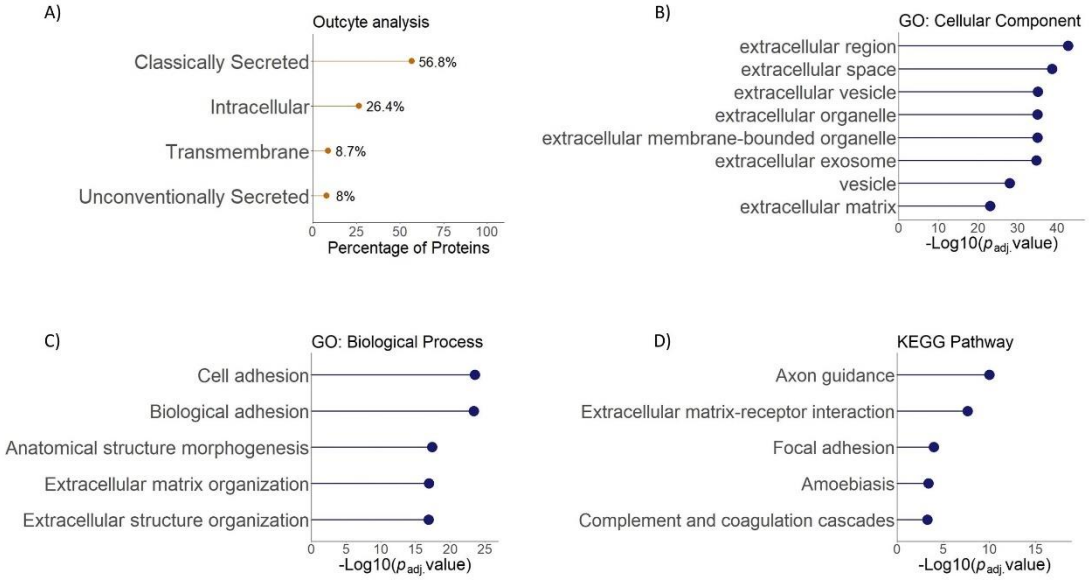

Figure 15: ***Enrichment analysis for all the downregulated proteins identified in secretomes following PKD inhibition.*** *A) Percentage of secreted, intracellular, transmembrane, and unconventionally secreted proteins predicted by the Outcyte algorithm in the downregulated proteins of CRT(2.5μM) and CRT(1μM) in both MDA-MB-231 and MDA-MB-468 cells. B - D) Top GO cellular compartments C) top GO biological processes and D) top KEGG pathways for the downregulated proteins identified in MDA-MB-231 and MDA-MB-468 cells following CRT(2.5μM) and CRT(1μM). X-axis indicates the enrichment scores [-log10 (adjusted p value), p-value cut-off of 0.05] for each term and y-axis the enriched term.*

In the MDA-MB-231 cell line, secretome proteins were "extracellular matrix" proteins (CRT(2.5uM) adjusted *p* value=1.01 × 10^{-14}, CRT(1uM) adjusted *p* value=0.003) (Figure 16A), which facilitated the "extracellular matrix organization" (CRT(2.5uM) adjusted *p* value=7.92 × 10^{-10}, CRT(1uM) adjusted *p* value=0.004) (Figure 16C) and "Extracellular matrix receptor interaction (CRT(2.5uM) adjusted *p* value=6.57 × 10^{-5}) (Figure 16E).

On the other hand, the most enriched cellular compartment to which the downregulated MDA-MB-468 cell line proteins belonged was the "cell periphery" (CRT(2.5uM) adjusted *p* value=4.89 × 10^{-20}, CRT(1uM) adjusted *p* value = 2.09 × 10^{-15}) (Figure 16B), with role in "cell adhesion" (CRT(2.5uM) adjusted *p* value = 1.06 × 10^{-19}, CRT(1uM) adjusted *p* value=2.2 × 10^{-13}) (Figure 16C) and "Axon guidance (CRT(2.5uM) adjusted *p* value=1.45 × 10^{-10}, CRT(1uM) adjusted *p* value=2.45 × 10^{-7}) (Figure 16F). More specifically, the "cell periphery" GO term describes the region around and including the plasma membrane of a cell and "axon guidance" defines the migration of an axon growth cone to a specific target site, facilitated by various cell adhesion molecules.

PKD predominantly localizes at the TGN to facilitate vesicle fission [255] but has also been found to be recruited at the leading edge of migration, specifically at the plasma membrane, where actin remodelling occurs [150]. Enrichment analysis provided an indication of both the localization of these proteins and their possible role, which was in line with the existing literature.

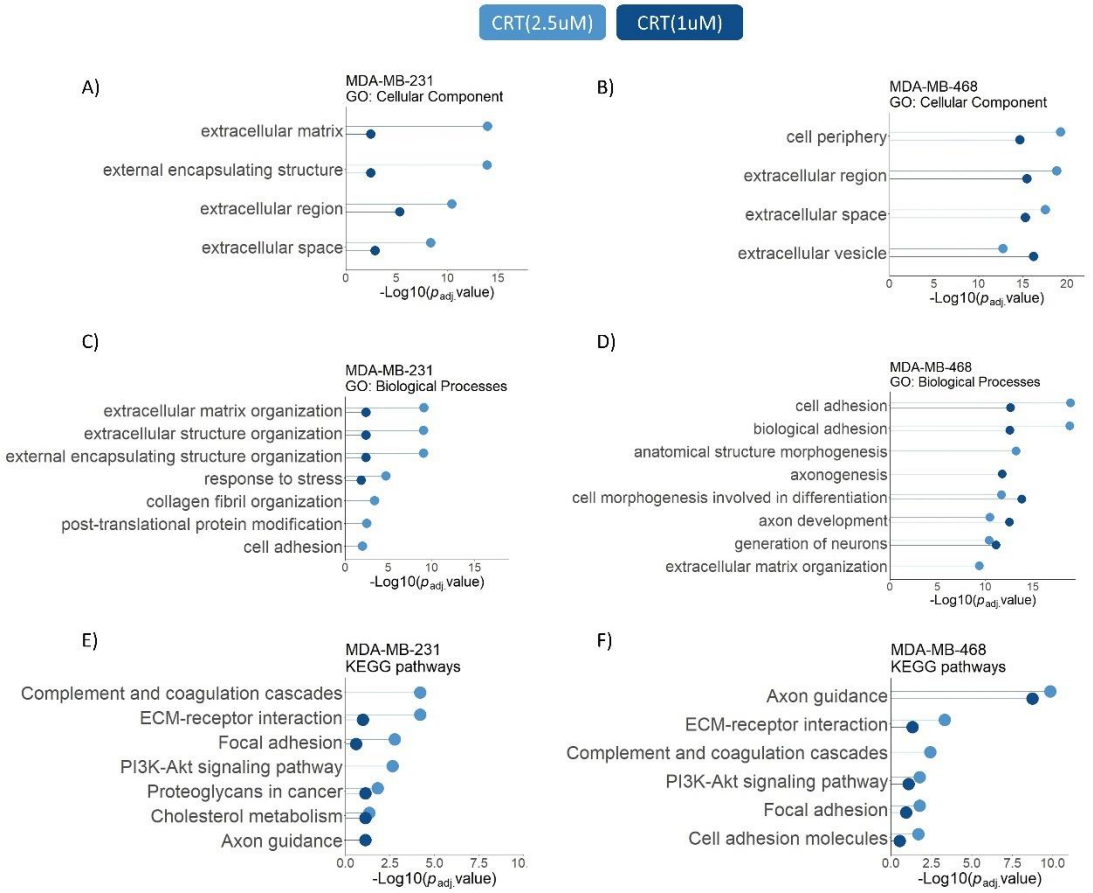

Figure 16: ***Enrichment analysis for the downregulated proteins identified in secretomes of each cell line following PKD inhibition.*** *A, B) Top Gene Ontology (GO) cellular compartment terms identified from the downregulated*

proteins of CRT(2.5µM) and CRT(1µM) in A) MDA-MB-231 and B) MDA-MB-468 cells. C, D) Top GO biological processes enriched in the downregulated proteins identified in C) MDA-MB-231 and D) MDA-MB-468 cells following CRT(2.5µM) and CRT(1µM). E, F) Top KEGG pathways enriched in the downregulated proteins identified in E) MDA-MB-231 and F) MDA-MB-468 cells following CRT(2.5µM) and CRT(1µM). X-axis indicates the enrichment scores [-log10 (adjusted p value), p-value cut-off of 0.05] for each term and y-axis the enriched term.

From the MDA-MB-468 cell line, downregulated proteins involved in cell adhesion comprised of several axon guidance molecules such as semaphorins (SEMA3A, SEMA3C, SEMA3E, SEMA3F, SEMA4B, SEMA4D), their primary receptors neuropilins (NRP1) and plexins (PLXNA1, PLXNB2), as well as ephrins (EFNA5, EFNB3) and their Eph receptors (EPHA4, EPHB2, EPHB4, EPHB6). Additionally, protein tyrosine phosphatases (PTPRF, PTPRS), protocadherin 7 (PCDH7), Protein tyrosine kinase 7 (PTK7) and MDA-9/syntenin (SDCBP), among others, all have established roles in regulating cell adhesion. An extended list of the downregulated cell adhesion related proteins following PKD inhibition in the MDA-MB-468 cell line can be found in Figure 17.

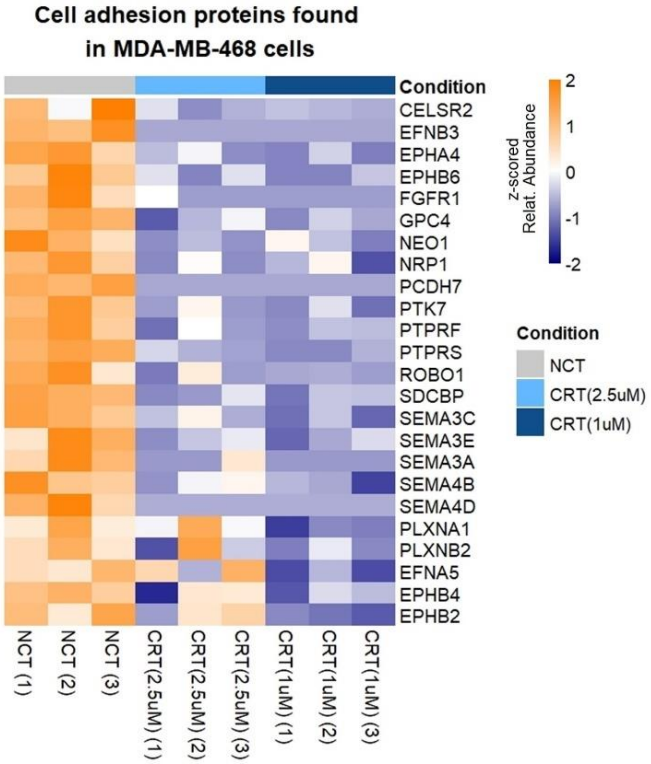

Figure 17: ***PKD inhibition reduces the secretion of cell adhesion related proteins.*** *Heatmap of Z-scores for relative protein abundances of downregulated cell adhesion proteins found in MDA-MB-468 secretome samples by LC-MS/MS. Each column represents a biological replicate (n=3). Relative protein abundances are shown from low (blue) to high (orange).*

Different classes of ECM proteins were identified in the downregulated proteins found from both cell lines, such as glycoproteins, proteoglycans, ECM regulators and secreted factors, as per Naba et al [256,257]. Literature review highlighted that amongst these downregulated ECM proteins were multiple invasion mediators that have been previously described in TNBC.

In the MDA-MB-231 set of downregulated proteins, we identified matrix metalloproteinase-1 (MMP-1), macrophage colony-stimulating factor (M-CSF), stanniocalcin-1 (STC-1), lysyl

oxidase homolog 2 (LOXL2), c-Met (also called tyrosine-protein kinase Met or hepatocyte growth factor receptor), procollagen-lysine,2-oxoglutarate 5-dioxygenase 2 (PLOD2), procollagen-lysine,2-oxoglutarate 5-dioxygenase 1 (PLOD1), Pentraxin-related protein (PTX3), lumican (LUM) and programmed cell death 10 (PDCD10).

The MDA-MB-468 set of significantly reduced secretome proteins included the ECM markers STC-1, Glypican 1 (GPC-1), tenascin-C (TNC), leukemia inhibitory factor (LIF), lysyl oxidase (LOX), Laminin subunit beta 1 (LAMB1), Integrin subunit alpha 6 (ITGA6), Transforming growth factor beta induced (TGFBI) and Interleukin 6 cytokine family signal transducer (IL6ST).

MMP-1 is one of the top over-expressed genes in breast invasive carcinoma TNBC [258], contributing to brain [65], bone [64] and lung [66,259] metastasis formation via basement membrane/ECM degradation and extravasation [260]. M-CSF (CSF1), an established signaling molecule which facilitates the differentiation of monocytes into macrophages in the breast cancer TME [98], has been shown to act in a autocrine way via the CSF1/CSF1R signaling axis to promote invasion [100,101]. An important ECM glycoprotein, TNC is overexpressed in breast cancer [261] and aids the metastatic process, as its deposition helps in the formation of a metastatic niche in distant organs [71,262]. LIF, a member of the interleukin-6 family of cytokines, can signal via the LIF/LIFR axis to promote tumor progression and metastasis in TNBC through activation of multiple signaling pathways [85–88]. STC-1 is a glycoprotein found to promote invasion and metastasis of TNBC [263,264,77,74]. Finally, collagen posttranslational modification proteins lysyl oxidase (LOX), lysyl oxidase homolog 2 (LOXL2) and procollagen-lysine,2-oxoglutarate 5-dioxygenase 2 (PLOD2) were identified in the set of downregulated proteins and are responsible for collagen crosslinking, resulting in ECM stiffness. Figure 18 illustrates several ECM proteins found to be downregulated following PKD inhibition in the MDA-MB-231 and MDA-MB-468 cell line.

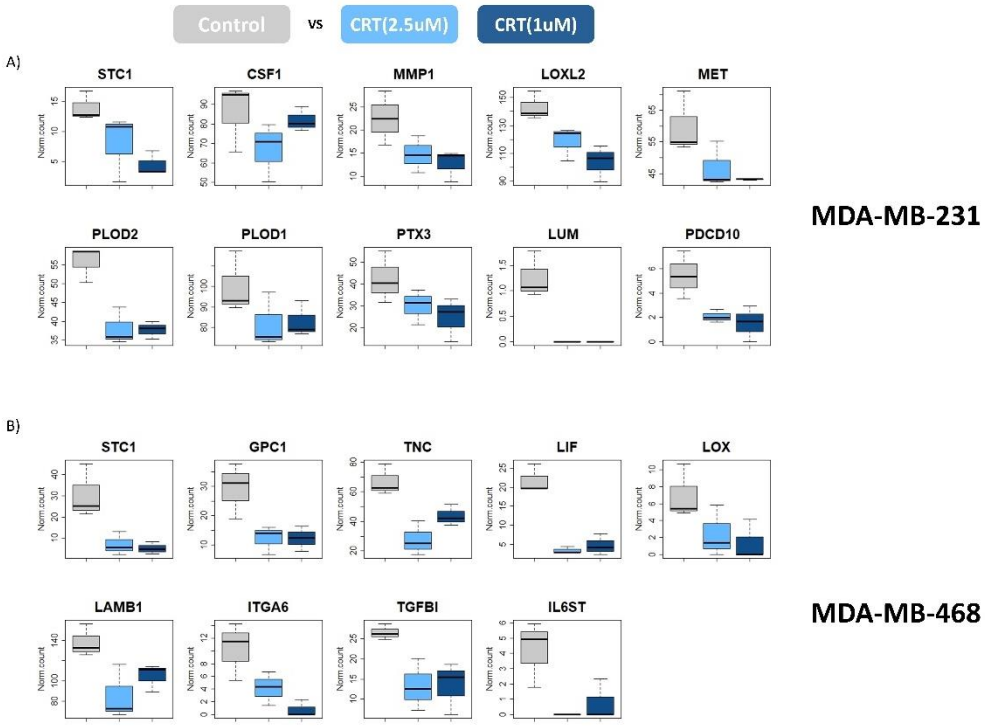

Figure 18: ***PKD inhibition reduces the secretion of ECM proteins and TNBC invasion mediators****. A – B) Boxplots illustrating protein abundance of several ECM proteins found to be downregulated in the A) MDA-MB-231 and B) MDA-MB-468 cell lines following CRT(2.5µM) and CRT(1µM). Y-axis indicates the normalized count quantified during LC-MS/MS and x-axis the condition (control vs treatment).*

3.4. PKD activity induces the secretion of TNBC invasion mediators

The identification of invasion mediator proteins in our dataset suggested a potential mechanism upon which PKD exerts its pro-invasive role in TNBC. We therefore focused our subsequent work on elucidating the role of the different PKD isoforms on the regulation of the secretion of these mediators. We first validated our proteomic results for STC-1, TNC, LIF, M-CSF and MMP-1 using antibody-based methods (multiplex assays and ELISA). The subcellular location of these proteins was annotated as "secreted" in UniProt, and they were only quantified in the secretome samples and not in the cell lysates during mass spectrometry analysis, due to low abundance. We included in the validation set three additional proteins, granulocyte-macrophage-colony-stimulating factor (GM-CSF), interleukin 11 (IL-11) and matrix metalloproteinase-13 (MMP-13), which although not identified in the secretome samples during LC-MS/MS possibly due to low abundance, they have an established role in TNBC progression [64,265,68,266,79,83,102].

Validation was initially performed on the MDA-MB-231 cell line which exhibited the most ECM protein enriched dataset and under the same conditions used for proteomic profiling. Samples from cells recovering under serum-free and serum-containing (10% fetal bovine serum - FBS) conditions were tested to account for the potential effect of serum deprivation on PKD activity, and therefore regulation of protein secretion. Equal protein content of cell lysates pre and post treatment was confirmed by BCA analysis before secretome sample analysis by multiplex assays and ELISA.

Reduced secretion of STC-1, TNC, LIF, GM-CSF, M-CSF, IL-11, MMP-1 and MMP-13 in the MDA-MB-231 cell line was partially confirmed under serum-free conditions (Figure 19A) after PKD inhibition in both CRT(2.5µM) and CRT(1µM). More specifically, STC-1, TNC, LIF, IL-11, MMP-1 and MMP-13 were downregulated upon CRT(2.5µM) or CRT(1µM) or both inhibition schemes. GM-CSF and M-CSF were not found to be downregulated by neither CRT(2.5µM) nor CRT(1µM), possibly due to high variability of the concentration results obtained.

In the MDA-MB-468 cell line, STC-1, TNC, LIF and M-CSF were downregulated following both CRT(2.5µM) and CRT(1µM) under serum-free conditions. GM-CSF, IL-11, MMP-1 and MMP-13 were either not quantified in the secretome samples or not quantified in all replicates of the cell line under these conditions (Figure 19B).

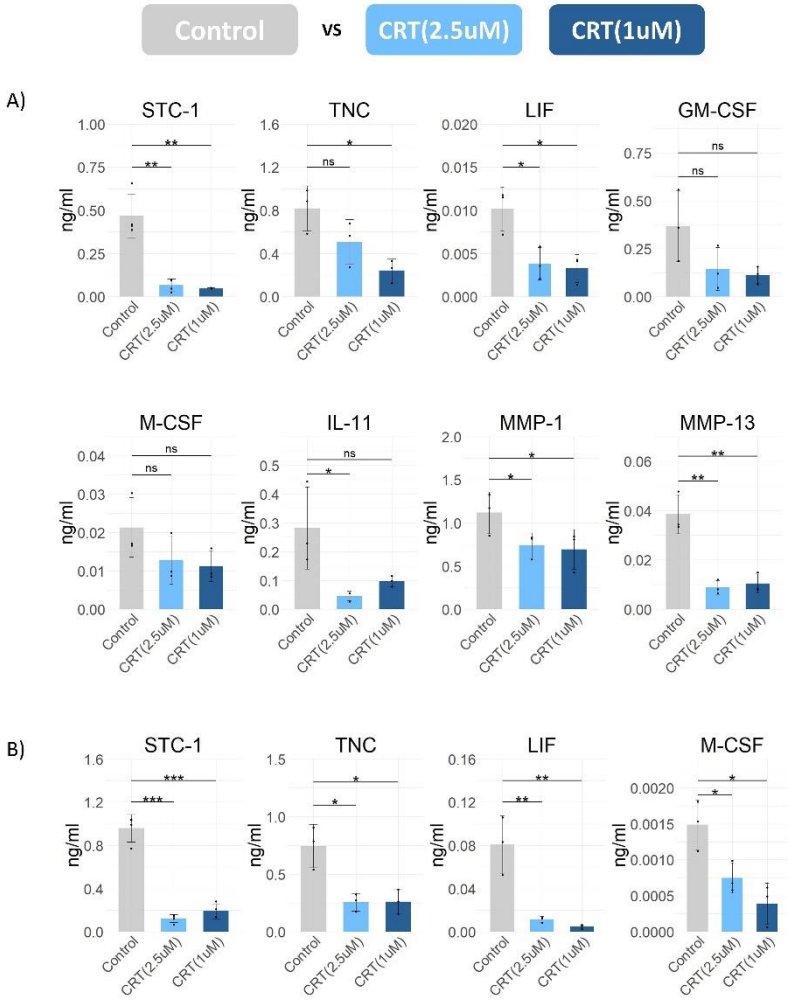

Figure 19: ***PKD activity induces the secretion of TNBC invasion mediators under serum-free conditions.*** *A, B) Quantification of eight selected secretome proteins in the A) MDA-MB-231 cells and B) MDA-MB-468 cells under serum free conditions. Protein secretion was quantified in secretome samples using multiplex assays for STC-1, LIF, GM-CSF, M-CSF, IL-11, MMP-1, MMP-13 and ELISA for TNC. Data are reported as mean of three or four biological replicates and error bars show standard deviation. P values were assessed by unpaired, two-tailed Student's t-test. ∗p < 0.05; ∗∗p < 0.01; ∗∗∗p < 0.001.*

Additionally, we validated the reduced secretion of STC-1, TNC, LIF, GM-CSF, M-CSF, IL-11, MMP-1 and MMP-13 in the MDA-MB-231 cell line and the reduced secretion of STC-1, TNC, LIF and GM-CSF in the MDA-MB-468 cell line under serum containing conditions (Figure 20A,B). Our results indicate that although TNC and LIF were not quantified during LC-MS/MS in the secretome samples of MDA-MB-231 cell, we were able to quantify the proteins using multiplex assays and ELISA and discovered their PKD-dependent secretion in the cell line. Additionally, GM-CSF was present in detectable levels in the MDA-MB-468 secretome samples collected under serum containing conditions and we were able to validate the protein as secreted in a PKD-dependent manner. M-CSF was present in detectable levels in the MDA-MB-468 secretome samples but due to high variability we were not able to validate the protein as secreted by PKD regulation. Additionally, and as per serum free conditions, IL-11, MMP-1 and MMP-13 were either not quantified in the MDA-MB-468 secretome samples or not quantified in all sample replicates.

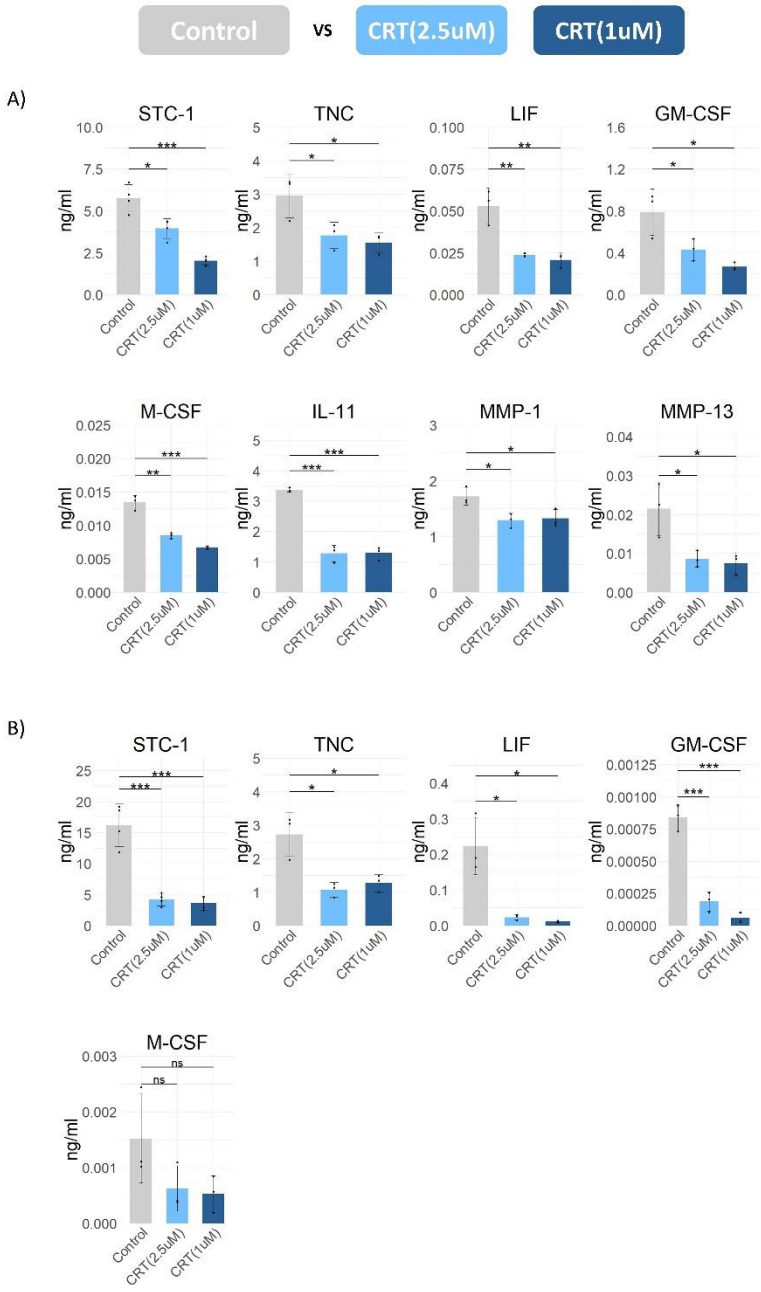

Figure 20: ***PKD activity induces the secretion of TNBC invasion mediators under serum containing conditions*** *A, B) Quantification of eight selected secretome proteins in the A) MDA-MB-231 cells and B) MDA-MB-468 cells under serum containing conditions. Protein secretion was quantified in secretome samples using multiplex assays for STC-1, LIF, GM-CSF, M-CSF, IL-11, MMP-1, MMP-13 and ELISA for TNC. Data are reported as mean of three or four biological replicates and error bars show standard deviation. P values were assessed by unpaired, two-tailed Student's t-test. ∗p < 0.05; ∗∗p < 0.01; ∗∗∗p < 0.001.*

3.5. PKD activity affects transcription and/or differential secretion to regulate secretion of invasion mediators

To understand if reduced secretion of the validated proteins upon PKD inhibition was a result of altered transcription or differential secretion, we selected three proteins (STC-1, TNC and LIF) that were secreted in a PKD-dependent manner in both MDA-MB-231 and MDA-MB-468 cells. We assessed the transcript levels of these three genes by qPCR using CRT(2.5µM) and CRT(1µM) in both cell lines and recovery under serum containing conditions.

In the MDA-MB-231 cell line, PKD inhibition reduced the expression of *TNC* by 1.7-fold after CRT(2.5µM) and by 1.3-fold in CRT(1µM), with a similar effect observed for *STC-1*, where mRNA expression reduced by 2.22-fold after CRT(2.5µM) and by 2.07-fold after CRT(1µM). No differences in the transcript levels of *LIF* were observed following the two CRT treatments (Figure 21A). In the MDA-MB-468 cell line, PKD inhibition did not affect the transcript levels of any of the three genes (Figure 21B).

To assess if the mRNA levels corresponded with intracellular protein levels following PKD inhibition in the MDA-MB-231 cells line, we used antibody-based multiplex assays and ELISA to quantify the intracellular protein levels of STC-1, TNC and LIF. The intracellular protein levels of STC-1 and TNC were downregulated upon both CRT(2.5µM) and CRT(1µM), whereas the levels of LIF were unchanged in the cell lysate following PKD inhibition using the two CRT schemes (Figure 21C). It is evident that for these three proteins, the mRNA levels matched the intracellular protein levels following PKD inhibition in the MDA-MB-231 cell line. In the case of STC-1 and TNC, reduced secretion of the proteins appears to be a result of decreased gene transcription, leading to less protein being synthesized and secreted upon PKD inhibition. In contrast, the fact that LIF is secreted less when PKD activity is blocked suggests differential protein secretion, as mRNA and intracellular protein levels remained unchanged. These observations provide the first evidence for a dual role of PKD in regulating transcription and secretion in TNBC.

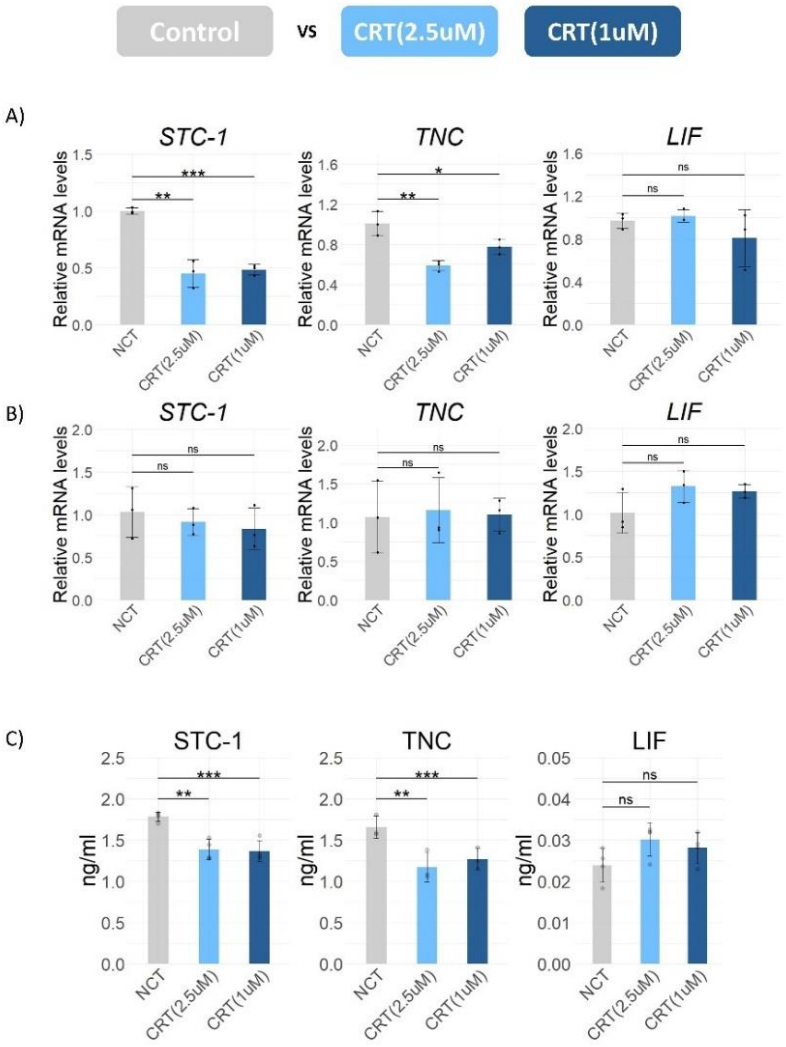

*Figure 21: **PKD activity affects transcription and/or differential secretion in TNBC**. A-B) Expression of STC-1, TNC and LIF genes after CRT(2.5uM) and CRT(1uM) in A) MDA-MB-231 cells and B) MDA-MB-468 cells. Expression levels are relative to RPLP0. Data are reported as mean of three biological replicates and error bars show standard deviation. C) Quantification of STC-1, TNC and LIF secretome proteins in the cell lysates of MDA-MB-231 cells. Levels of proteins were quantified in cell lysate samples using multiplex assays for STC-1 and LIF and ELISA for TNC. Data are reported as mean of three or four biological replicates and error bars show standard deviation. P values were assessed by unpaired, two-tailed Student's t-test. ∗p < 0.05; ∗∗p < 0.01; ∗∗∗p < 0.001*

3.6. PKD2, and to a lesser extent PKD3, regulates secretion of TNBC invasion mediators in MDA-MB-231 cells

To investigate isoform-specific regulation of secretion and confirm that the effect observed is not due to reported off-target effects of the inhibitor [267], MDA-MB-231 and MDA-MB-468 cells were transiently transfected with non-targeting control siRNA (siCTRL), PKD2 siRNA (siPKD2), PKD3 siRNA (siPKD3), and both PKD2 and PKD3 siRNA (siPKD2/3), and their secretome was analysed for the previously validated set of proteins (in the case of MDA-MB-231: STC-1, TNC, LIF, GM-CSF, M-CSF, IL-11, MMP-1 and MMP-13 and in MDA-MB-468 cells: STC-1, TNC, LIF and GM-CSF).

Knockdown efficiency of PKD2 and PKD3 was confirmed by immunoblotting (Figure 22A). Equal protein content of cell lysates amongst knockdown conditions was confirmed by BCA

analysis before the respective secretome samples were analyzed by multiplex assays and ELISA.

In the MDA-MB-231 cell line, with the exception of STC-1 and TNC, PKD2 knockdown and dual PKD2/PKD3 knockdown reduced the secretion of the tested proteins compared to the non-targeting siRNA control (Figure 22B). PKD3 knockdown reduced the secretion of IL-11 by 1.4-fold and of MMP-13 by 2-fold but had no effect on the other proteins. No additive effect was observed upon double PKD2 and PKD3 knockdown on the secretion of IL-11 and MMP-13.

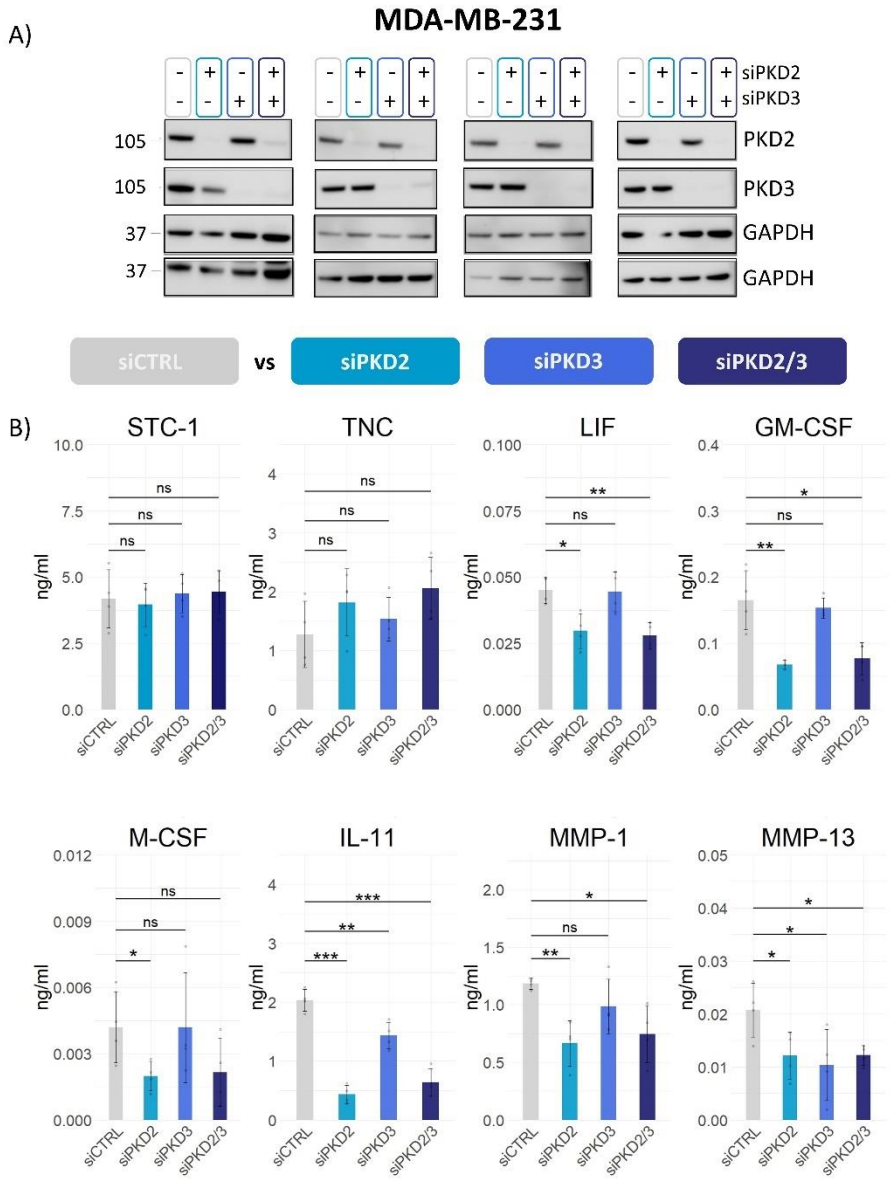

Figure 22: ***PKD2, and to a lesser extent PKD3, knockdown reduces the secretion of TNBC invasion mediators in MDA-MB-231 cells****. A) Quantification of PKD2 and PKD3 protein expression levels in MDA-MB-231 cells following siRNA-mediated PKD2, PKD3 or PKD2 and PKD3 knockdown (siPKD2, siPKD3, siPKD2/3), compared to cells transfected with a non-targeting control siRNA (siCTRL). Representative immunoblots of four independent experiments are shown. B) Bar plots showing protein quantification in ng/ml. Protein levels were quantified in secretome samples using multiplex assays for STC-1, LIF, GM-CSF, M-CSF, IL-11, MMP-1, MMP-13 and ELISA for TNC. Data are reported as mean of four biological replicates and error bars show standard deviation. P values were assessed by unpaired, two-tailed Student's t-test. ∗p < 0.05; ∗∗p < 0.01; ∗∗∗p < 0.001; ns: not significant.*

In the MDA-MB-468 cell line, knockdown efficiency of PKD2 and PKD3 was also confirmed by immunoblotting (Figure 23A) and equal protein content of cell lysates was confirmed by BCA analysis. PKD3 knockdown reduced the secretion of LIF by 1.2-fold. The levels of STC-1 and TNC were unaltered by PKD2 or PKD3 knockdown and GM-CSF could not be quantified in any of the collected secretome samples (Figure 23B).

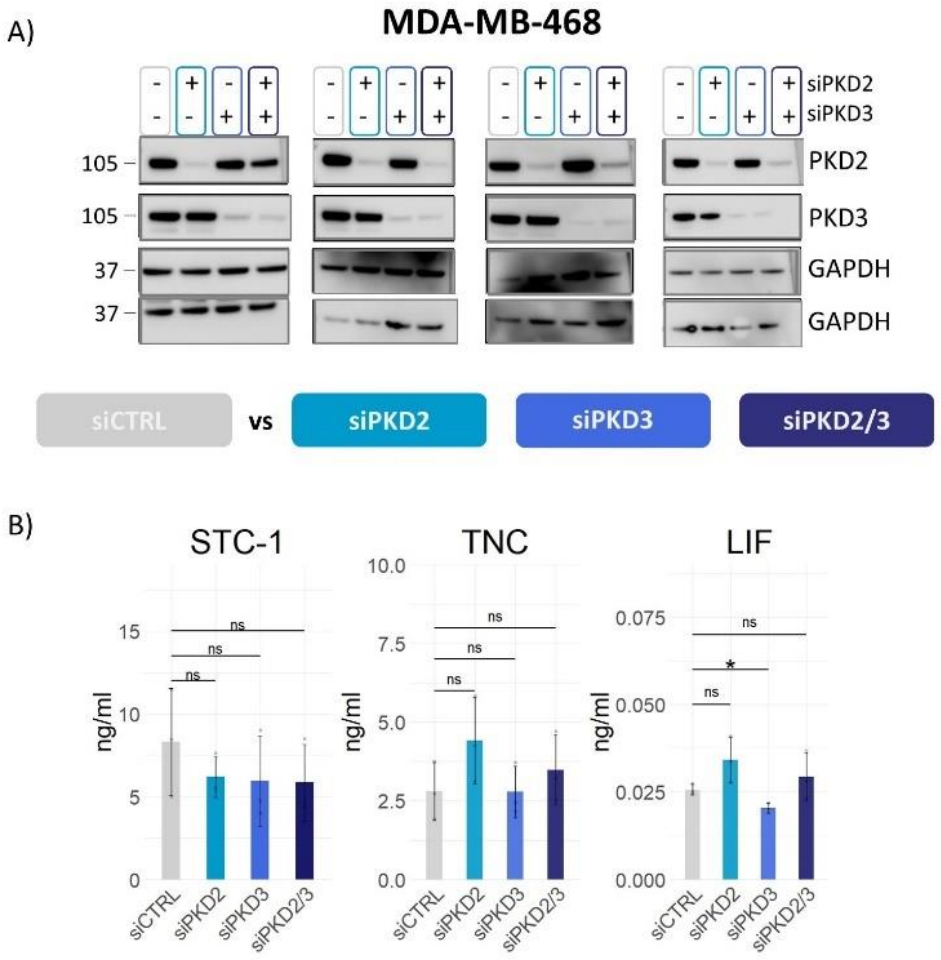

Figure 23: ***PKD2 and PKD3 knockdown have minimal effect on the secretion of TNBC invasion mediators in MDA-MB-468 cells.*** *A) Quantification of PKD2 and PKD3 protein expression levels in MDA-MB-468 cells following siRNA-mediated PKD2, PKD3 or PKD2 and PKD3 knockdown (siPKD2, siPKD3, siPKD2/3), compared to cells transfected with a non-targeting control siRNA (siCTRL). Representative immunoblots of four independent experiments are shown. B) Bar plots showing protein quantification in ng/ml. Protein levels were quantified in secretome samples using multiplex assays for STC-1 and LIF and ELISA for TNC. Data are reported as mean of four biological replicates and error bars show standard deviation. P values were assessed by unpaired, two-tailed Student's t-test. ∗p < 0.05; ∗∗p < 0.01; ∗∗∗p < 0.001; ns: not significant.*

These results suggest that PKD2 is the predominant isoform driving the secretion of invasion mediators in TNBC, with only a minor contribution from PKD3. Additionally, the reduced secretion of STC-1 and TNC upon pharmacological inhibition could not be replicated by the knockdown study neither in the MDA-MB-231 nor the MDA-MB-468 cell line, suggesting it may have been an off-target effect of the inhibitor.

3.7. PKD regulates the secretion of invasion mediators predominantly in TNBC metastatic cell lines

To gain a systems level understanding of PKD contribution to TNBC secretion, we assessed the effect of PKD inhibition on the previously validated invasion mediators in an expanded panel of TNBC cell lines consisting of 6 cell lines originally established from the primary tumor and 4 metastatic cell lines from pleural effusions [268–272] (Table 4). PKD2 and PKD3 were expressed in all cell lines with varying intracellular levels as observed by immunoblotting (Figure 24A). These results are in line with public expression data acquired from DepMap (Public 22Q4) (Table 4).

*Table 4: **Panel of TNBC cell lines.** TNBC cell line characteristics, including TNBC subtype and original site of cell line establishment (Primary/Metastasis). Transcript per million (TPM) values of PKD2 and PKD3 expression obtained from DepMap (Public 22Q4).*

Cell Line	Subtype	Primary/Metastasis	PRKD2 TPM	PRKD3 TPM
HCC1143	BasalA	Primary	5.39	3.65
HCC1806	BasalA	Primary	5.60	4.35
HCC1937	BasalA	Primary	5.52	3.20
HCC70	BasalA	Primary	5.28	4.46
MDA-MB-468	BasalA	Metastasis	5.38	5.08
BT549	BasalB	Primary	3.90	4.47
HCC38	BasalB	Primary	5.06	6.09
MDA-MB-231	BasalB	Metastasis	3.88	4.33
MDA-MB-436	BasalB	Metastasis	3.99	4.69
MDA-MB-453	Luminal	Metastasis	4.90	0.41

The inhibition scheme CRT(2.5uM) was evaluated in the panel of TNBC cell lines to establish its effectiveness on blocking PKD activity. Stimulation with PMA (1 uM for 15 minutes), a potent inducer of PKD activity [273], and inhibition by CRT(2.5uM) followed by stimulation with PMA, served as controls. We detected PKD2 activity by its autophosphorylation (pS876) using both immunoblotting and a custom-developed xMAP assay. Treatment with CRT(2.5uM) was able to block PKD activity in all cell lines albeit to a different extent as verified by the decrease in the phosphorylation of pS876 in PMA-stimulated cells. (Figure 24A, B).

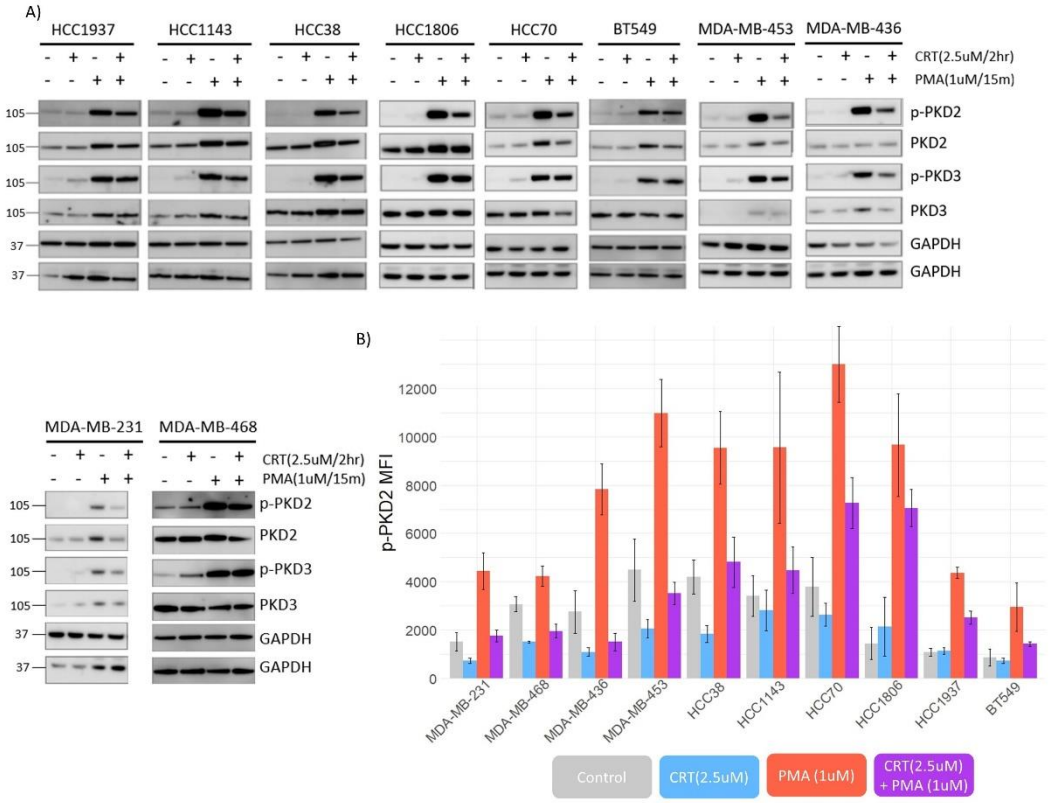

Figure 24: ***PKD inhibition and stimulation confirmation in a panel of ten TNBC cell lines.*** *A) Western blot comparing CRT(2.5uM), PMA(1uM) and CRT(2.5uM) followed PMA(1uM) in TNBC cell line panel. Immunoblotting was conducted, and membranes were probed with specific antibodies as indicated. GAPDH was used as loading control. B) xMAP assay for the detection of pS876 PKD2 in TNBC cell line panel using the same conditions as in Western Blot. Data are reported as mean Median Fluoresence Intensity (MFI) values obtained from three to four biological replicates and error bars show standard deviation.*

Results from the analysis of invasion mediators LIF, M-CSF, GM-CSF, IL-11, MMP-1 and MMP-13 in the secretome samples from the CRT(2.5µM)-treated cell lines are presented in Figure 25A. Equal protein content of cell lysates before and after treatment was confirmed by BCA analysis prior to secretome samples being analyzed by multiplex assays and ELISA. PKD signaling was found to drive the secretion of invasion mediators predominantly in cell lines originally established from pleural effusions and therefore metastasized. This was evident based on both the greater number of mediators affected and magnitude of the effect (fold-change) in these cell lines. Specifically, LIF and GM-CSF secretion was PKD-dependent in the metastatic cell lines MDA-MB-231, MDA-MB-468 and MDA-MB-436, compared to one primary tumor cell line whilst secretion of IL-11 and MMP-13 was found to be regulated by PKD only in metastatic TNBC cells. Protein measurements in the secretome of TNBC cell lines that showed statistically significant reduction following CRT(2.5µM) can be found in Figure 25B.

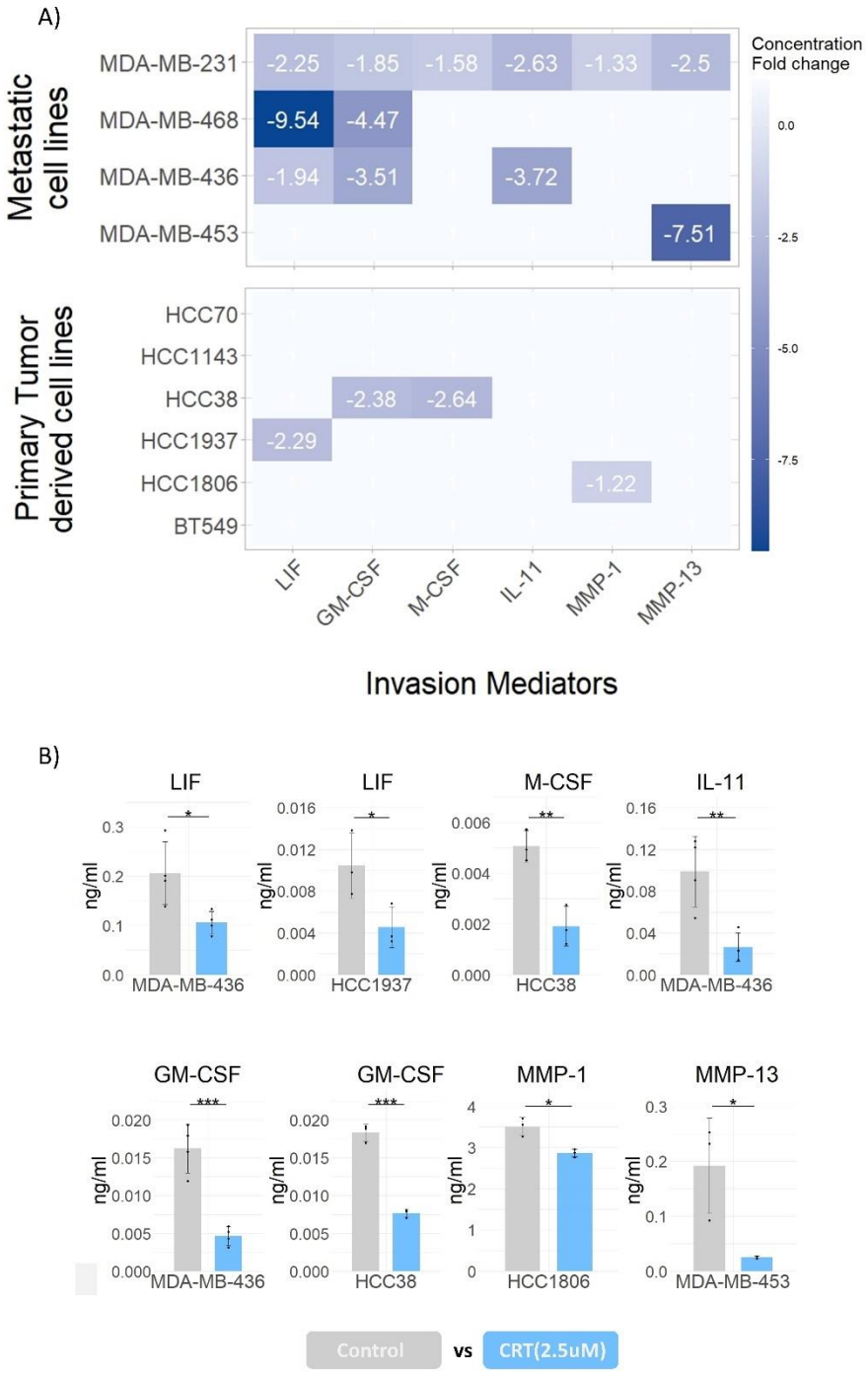

Figure 25: ***PKD regulates the secretion of invasion mediators predominantly in TNBC metastatic cell lines****. A) Heatmap of protein concentration fold change values (CRT(2.5µM) / control ≤ − 1.2) for the eight invasion mediators measured per cell line following PKD inhibition by CRT(2.5µM). Cell lines are ordered by the site from which they were originally established (metastasis or primary tumor). B) Protein levels (ng/ml) that showed significant reduction following CRT(2.5µM) in the TNBC cell line panel. LIF, GM-CSF, M-CSF, IL-11, MMP-1 and MMP-13 were quantified in secretome samples using multiplex assays. Data acquired from three or four independent biological replicates. Significance established at p ≤ 0.05 by unpaired, two-tailed Student's t-test. ∗p < 0.05; ∗∗p < 0.01; ∗∗∗p < 0.001.*

PKD had no effect on the secretion of some of these proteins on one or more cell lines despite their quantifiable levels in the secretome of these cells (Figure 26). This is in line with the observation that PKD does not reduce secretion globally, as initially detected by LC-MS/MS, but appears to have specific effects on a subset of invasion mediators in metastatic cell lines. All protein measurements in the secretome of TNBC cell lines can be found in Figure 26.

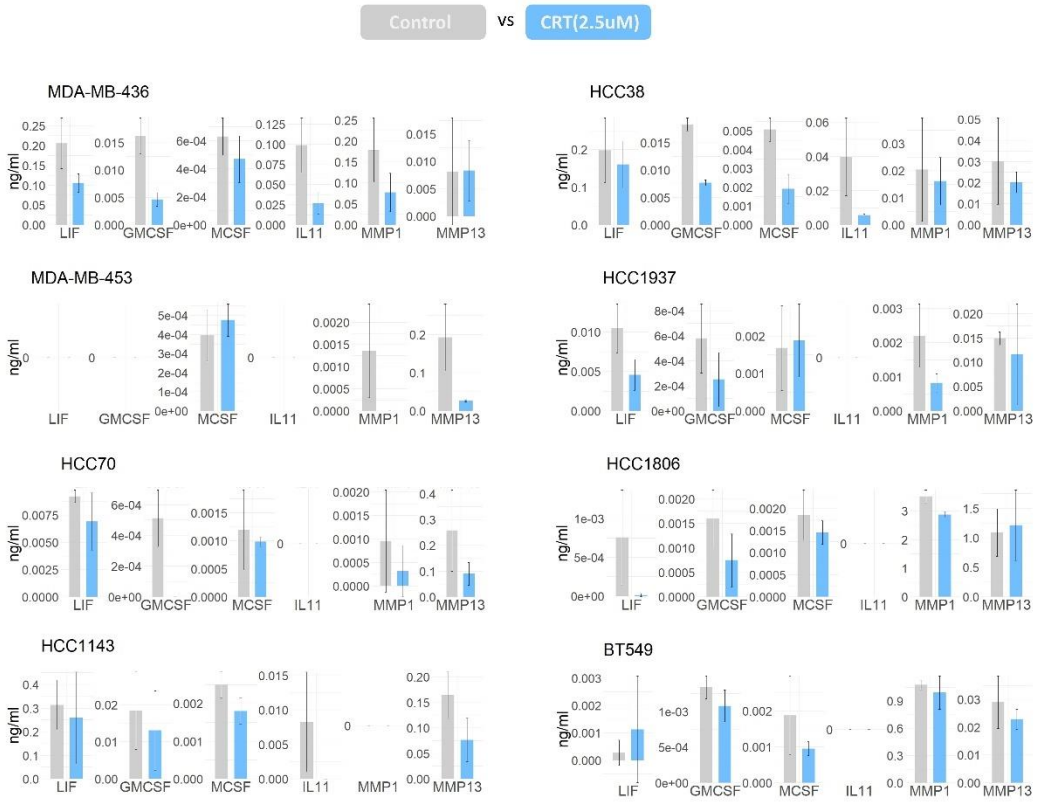

Figure 26: ***Protein measurements of invasion mediators in TNBC secretomes following PKD inhibition****. Protein measurements in the secretome of TNBC cell lines following CRT(2.5uM), compared to DMSO control. Levels of proteins were quantified in secretome samples using multiplex assays for LIF, GM-CSF, M-CSF, IL-11, MMP-1 and MMP-13. Data are reported as mean of three or four biological replicates and error bars show standard deviation. Protein measurements in the secretome of TNBC cell lines that showed statistically significant reduction following CRT(2.5µM) can be found in Figure 23.*

3.8. PKD inhibition suppress c-Jun phosphorylation at Ser63

To gain a systems level understanding of the signalling events occurring upon PKD inhibition, we initially selected 4 TNBC cell lines (MDA-MB-231, MDA-MB-468, MDA-MB-453 and HCC1937) and quantified the phosphorylation of 9 kinases and kinase targets following inhibition at 2.5uM CRT 0066101 for 2 hr CRT(2.5uM), stimulation at 1uM PMA for 15 min PMA(1uM) and inhibition followed by stimulation at 2.5uM CRT 0066101 for 2 hr followed by 1uM PMA for 15 min.

We aimed to identify commonly affected targets following PKD inhibition and stimulation conditions. In MDA-MB-468 cells, MEK1 pS217/S221 was reduced following CRT(2.5uM) as well as at CRT(2.5uM) followed by PMA(1uM) and remained unaltered following PMA(1uM). This effect was not replicated in any other cell lines. AKT1 pS473 was reduced upon PMA(1uM) in all 4 TNBC cell lines. More specifically, in all cell lines except MDA-MB-453, AKT1 pS473 was reduced after both PMA(1uM) and CRT(2.5uM) followed by PMA(1uM). More interested in targets affected following PKD inhibition, we identified c-JUN pS63 to be downregulated following CRT(2.5uM) as well as at CRT(2.5uM) followed by PMA(1uM) in cell lines MDA-MB-468, MDA-MB-453 and HCC1937 (Figure 27).

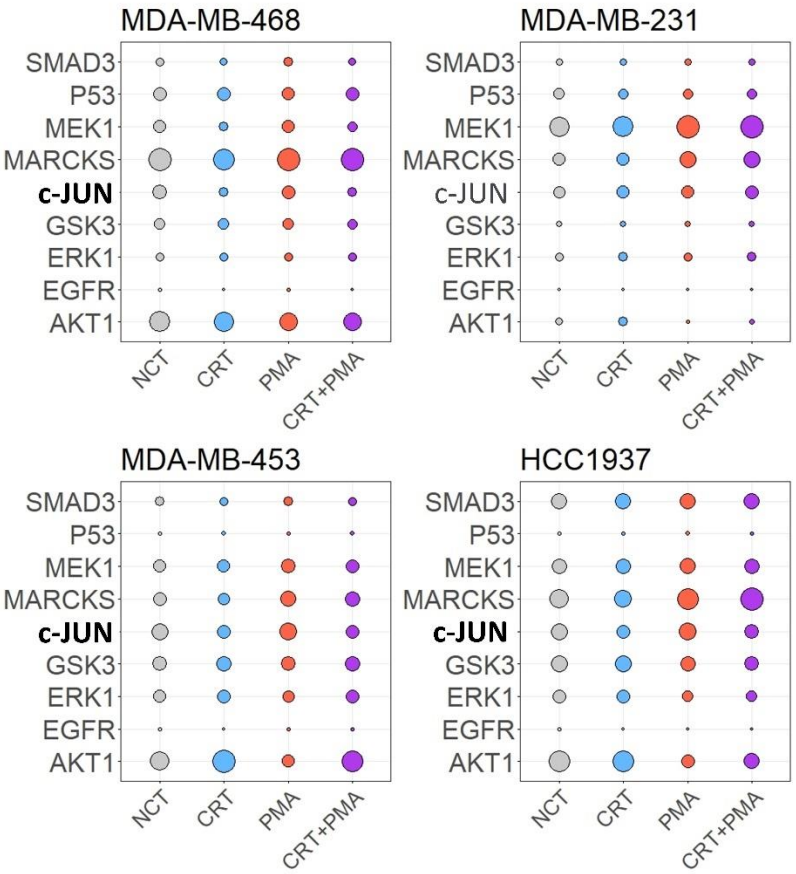

Figure 27: ***Effect of PKD inhibition in a panel of 9 phosphoproteins.*** *Heatmaps of Z-scores for relative MFI values of 9 kinases and kinase targets quantified following CRT(2.5uM), PMA(1uM) and CRT(2.5uM) followed PMA(1uM) in cell lines MDA-MB-468, MDA-MB-231, MDA-MB-453 and HCC1937. Each column represents the mean of three biological replicates (n=3).*

We investigated if the reduction in c-JUN pS63 levels following CRT(2.5uM) could be replicated in additional TNBC cell lines of our 10-cell line panel. Following CRT(2.5uM) and CRT(2.5uM) followed by PMA(1uM), c-JUN pS63 was reduced in a total of six cell lines (MDA-MB-453, MDA-MB-468, HCC1937, HCC1143, HCC70 and HCC38) out of the ten in our TNBC panel. PMA did not increase c-JUN pS63 in these six cell lines, but did so in the HCC1806 cell line. Additionally, c-JUN pS63 was increased upon CRT(2.5uM) and CRT(2.5uM) followed by PMA(1uM) in the MDA-MB-436 cell line (Figure 28).

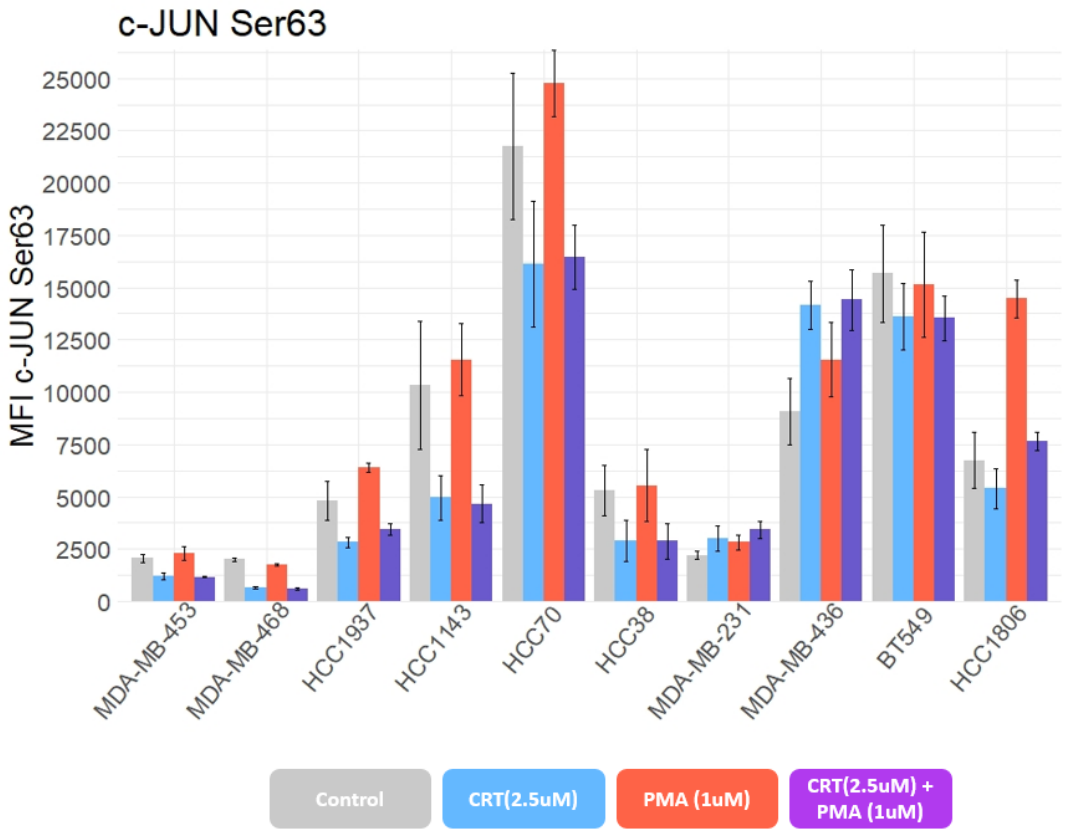

Figure 28: ***PKD inhibition suppress c-Jun phosphorylation at Ser63 in six TNBC cell lines****. xMAP assay for the detection of pS63 c-JUN in TNBC cell line panel following CRT(2.5uM), PMA(1uM) and CRT(2.5uM) followed PMA(1uM). Data are reported as mean Median Fluoresence Intensity (MFI) values obtained from three to four biological replicates and error bars show standard deviation.*

We aimed to validate the multiplex assay results by immunoblotting in the cell lines that showed reduced pS63 c-JUN following CRT(2.5uM) and CRT(2.5uM) followed by PMA(1uM). Immunoblotting confirmed for one biological replicate of cell lines HCC1937, HCC1143, HCC70, HCC38, MDA-MB-453 and MDA-MB-468 that pS63 c-JUN is reduced upon PKD inhibition by CRT(2.5uM). c-Jun is known to autoregulate its own gene expression [274,275] and, consistent with this, the total protein levels of c-JUN in these replicates were also reduced following the same inhibition conditions (Figure 29). Confirmation of PKD inhibition and stimulation was performed in the same blots by detection of PKD2 total levels and pS876 PKD2.

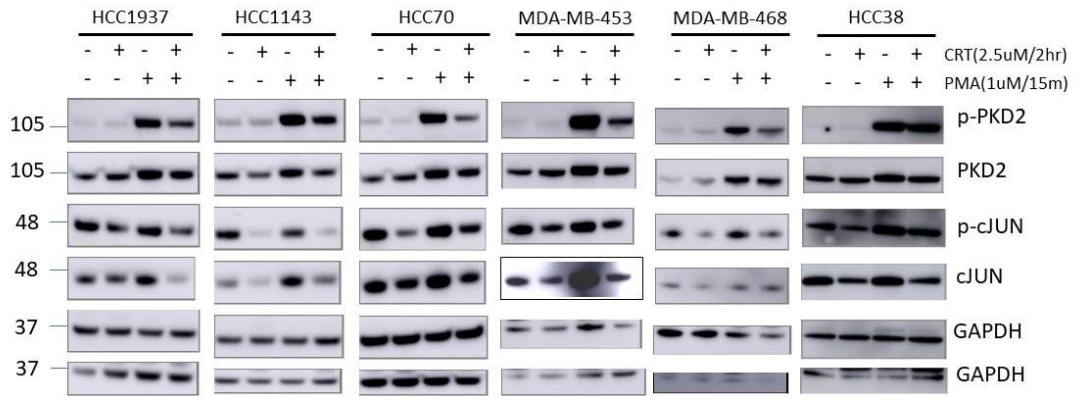

Figure 29: ***Confirmation of reduced c-Jun phosphorylation at Ser63 following PKD inhibition by immunoblotting.*** *Immunoblotting of HCC1937, HCC1143, HCC70, HCC38, MDA-MB-453 and MDA-MB-468 cells treated with CRT(2.5uM), PMA(1uM) or CRT(2.5uM) followed by PMA(1uM).*

Chapter 4
Discussion

4. Discussion

Protein kinase D is a fundamental kinase of the trans-Golgi network regulating vesicle fission and trafficking. Recent studies have highlighted that PKD2 and PKD3 are involved in signaling pathways linked to tumor progression in different cancer subtypes, including TNBC [153,179,180,190,199–201,240], however, the role of PKDs in regulating TNBC progression has not yet been associated with the secretion of pro-oncogenic factors. In this thesis, we have identified PKD signaling to be important for the composition of the TNBC cell secretome and provide a comprehensive understanding of the secreted proteins regulated by the kinases. Proteomic analysis, including LC-MS/MS and antibody-based multiplex assays, revealed that LIF, GM-CSF, M-CSF, IL-11, MMP-1 and MMP-13 are invasion-promoting factors whose secretion is regulated in a PKD-dependent manner in TNBC.

PKD family members regulate the fission of cargo vesicles at the Golgi complex, therefore regulating classical protein secretion [149,255]; this was reflected in the secretome samples analysed by LC-MS/MS as the majority of the identified downregulated proteins contained a signal peptide and several proteins were annotated as transmembrane. The second biggest percentage of proteins were annotated by the prediction algorithm as intracellular, and GO enrichment showed that most of these proteins were related to exosomes. Exosomes can contain different types of intracellular proteins arising from the plasma membrane, the endocytic pathway, and the cytosol [276]. One of the ways exosomes are secreted is via the TGN [277], it can therefore be hypothesized that PKD could be involved in the secretion of a subset of intracellular proteins via exosomes to enable intercellular communication. Exosomes are also generated within and released from endosomal compartments, with PKD being an important kinase for the integrity of the endolysosomal system [153]. PKD inhibition could therefore have impacted endolysosomal trafficking and subsequent exosome release.

In an early TNBC study, inhibition by CRT0066101 reduced migration, invasion and metastasis [179], an effect later linked with reduced protein levels of MMP-9 and other EMT-related factors in cellular lysates of MDA-MB-231 cells [192]. Our discovery, therefore, that the PKD-regulated secretome contains proteins involved in the organisation of the ECM and cell adhesion was in line with the previously described PKD functions.

We hypothesized that PKD invasive functions could be exerted by secreted proteins with a previously described role in TNBC invasion, hence selecting for validation a panel of eight such proteins. The factors identified by mass spectrometry, combined with evidence from previous literature, suggest that PKD is a contributing factor in ECM remodelling occurring during TNBC invasion. The collagenases we found to be secreted in a PKD-regulated manner, MMP-1 and MMP-13, are released by tumor cells to degrade both the basement membrane and the ECM to allow cancer cell invasion and metastasis to distant organs [64–66,68,258,259,265,278]. PKD2 is known to regulate the secretion of MMP-2, MMP-7 and MMP-9 via a multiprotein complex with ARF1 and ARL1, and Arfaptin2 [166,199], and in pancreatic cancer this PKD2-mediated secretion of matrix metalloproteinases aided invasion of cells *in vitro* and *in vivo* [199]. Similarly, in prostate cancer cell lines, PKD3 contributed to the composition of the secretome by regulating the secretion of MMP-9 [200] and the expression of urokinase-type plasminogen activator (uPA) [201], both factors involved in ECM remodelling [202,203]; conditioned medium from PKD3 knockdown

pancreatic cancer cell lines reduced the migration of control cells, indicating the presence of secreted factors in the PKD3-regulated secretome that stimulate cell motility [200].

The tumor microenvironment supports not only ECM remodelling but also the presence of inflammation in the surrounding tissue [279,280]. Tumor-secreted factors have been found to recruit various immune cell types to promote a tumorigenic microenvironment. We have identified the immunomodulatory cytokines M-CSF and GM-CSF, which have been found to act in an autocrine and/or paracrine way to promote TNBC invasion [100–102], as two factors whose secretion is regulated by PKD in different TNBC cell lines. Secretion of GM-CSF has been strongly associated with PKD signalling, with evidence that it is regulated in the MDA-MB-231, MDA-MB-468, MDA-MB-436 and HCC38 cell lines. Recent work in prostate cancer identified that PKD2 or PKD3 knockdown results in decreased expression and secretion of pro-inflammatory chemokines SCF, CCL5 and CCL11 in two prostate cancer cell lines, with the proteins contributing to chemotactic migration of mast cells *in vitro* [204]. In another study in prostate cancer, PKD3 knockdown was responsible for reduced secretion of pro-inflammatory cytokines IL-6, IL-8, and GROα [200]. These findings may suggest that PKD signalling contributes to immune cell recruitment of in the TNBC tumor microenvironment.

Not limited to matrix metalloproteinases and pro-inflammatory cytokines, we identified that pharmacological inhibition as well as depletion of PKD2 regulates the secretion of invasion mediators and IL-6 family members, LIF and IL-11. In the MDA-MB-231 cell line, exogenous LIF treatment was found to promote invasion and metastasis [88]. Additionally, knockdown of LIF decreased the expression levels of mesenchymal markers Vimentin and N-cadherin, suggesting that LIF can promote EMT [87]. Secretion of LIF could, therefore, exert PKD2's pro-invasive [179,281] and pro-EMT functions [192] in an autocrine and/or paracrine manner. An activator of osteoclast differentiation [282], IL-11 has been an important factor for breast cancer metastasis to the bone [79–83]. CRT0066101 treatment in an MDA-MB-231 mouse model reduced the number and size of lymph node and lung metastases. The study, however, did not assess bone metastasis in the mouse model [179]. In prostate cancer, on the other hand, decreased invasion and expression of genes related to bone metastasis was observed upon PKD2/3 knockdown or CRT0066101 inhibition. In the study's mouse model, reduced bone metastasis of prostate cancer cells was observed upon CRT0066101 treatment [283]. The identification of IL-11, as well as of MMP-1 and MMP-13, which are also mediators of breast cancer metastasis to the bone [64,284], supports the hypothesis that PKD2 and PKD3 contribute, via their dependent secretome, to the colonization of the bone for TNBC metastasis.

Secretion of STC-1 and TNC was reduced upon pharmacological inhibition of PKD with CRT0066101, however, it was unchanged in PKD2/PKD3 depleted MDA-MB-231 cells. Therefore, we cannot exclude an off-target effect of the kinase inhibitor with respect to the secretion of these two proteins. Nevertheless, the effect of short-term PKD inhibition by CRT0066101 may not be consistent with the phenotype of a three-day PKD knockdown in terms of secretion regulation of these two factors [285]. Further experiments with CRT0066101 on PKD knockdown cells may provide more insight into whether the secretion of STC-1 and TNC is an off-target effect or whether the cytokines are secreted by compensatory mechanisms after PKD knockdown.

Our data indicates a previously unknown function of PKD2 in TNBC secretion that can be linked to invasion, based on secretome data obtained from MDA-MB-231 cells. PKD2 has so far been associated with drug resistance in breast cancer [190] and has been found to be located at focal adhesions in MDA-MB-231 cells, contributing to cell adhesion and migration [281]. We validated the PKD2-regulated secretion of LIF, GM-CSF, M-CSF, IL-11, MMP-13 and MMP-1 and the reduced secretion of IL-11 and MMP-13 upon PKD3 knockdown. These results indicate isoform-specific rather than redundant functions of PKD2 and PKD3 in the secretion of pro-invasive proteins. Although it has been suggested that PKD2 and PKD3 may have similar pro-invasive functions in TNBC [179], a body of literature has been highlighting PKD3 as the main isoform driving motility and invasion [153,179,191,286]. Our findings suggest that PKD2 also contributes to TNBC invasion via the kinase-dependent secretome, which is distinct from that of PKD3. Assays using cell-conditioned media will provide further insight into whether the PKD2/PKD3-dependent secretome contributes to invasive cell behavior and immune cell recruitment. Nevertheless, to limit the secretion of pro-invasive and pro-inflammatory proteins, CRT0066101 is needed to block the secretion of both isoform-specific cargos.

The identification of multiple invasion mediators in the PKD-regulated secretome suggests that the kinases may be contributing to different stages of TNBC invasion, from ECM remodelling to extravasation and finally to metastatic colonisation. Importantly, we demonstrated on a systems level that PKD signalling has a greater role in the secretion of invasion mediators in TNBC cell lines established from metastatic sites, providing evidence from a panel of ten cell lines with different sites of origin. Our findings suggest that as cells become more capable of invasion and eventually metastasis, PKD plays a greater role in the secretion of TNBC invasion mediators, presumably to allow tumor progression. Therefore, inhibiting PKD activity by CRT0066101 could limit the secretion of pro-invasive proteins in TNBC cells, with the effect more evident in metastatic cell lines.

Not limited to ECM proteins, our proteomics dataset contained several cell adhesion-annotated proteins that were downregulated following PKD inhibition. More specifically, we have discovered semaphorins, their primary receptors neuropilins and plexins to be downregulated in MDA-MB-468 cells following PKD inhibition. Activation of plexins by semaphorins modulates cell adhesion and induces changes in the organization of the cytoskeleton of the target cells [225]. Some semaphorins and their receptors have been considered tumor suppressors whereas others are known to activate tumor formation. Interestingly, SEMA3C was the only protein downregulated in both cell lines with both CRT treatments. Currently, the protein's role remains contradictory in the literature, with reports finding SEMA3C to have a tumor suppressor role in breast cancer [287] and others associating it with tumor growth and invasion [288]. We also identified ephrins and their Eph receptors as downregulated upon PKD inhibition in MDA-MB-468 cells. EPH receptors and their cognate ephrin ligands constitute the largest family of receptor tyrosine kinases, with aberrant expression of these molecules found to contribute to the invasive characteristics of breast carcinoma cells or also act as tumor suppressors, depending on the cellular context [289–292]. Additional cell adhesion proteins comprised of protein tyrosine phosphatases and protocadherins, amongst others. Due to the large presence of proteins related to cell adhesion, the term was highly enriched amongst the MDA-MB-468 cell line downregulated proteins and was also present in the downregulated proteins of the MDA-MB-231 cell line. It

can be hypothesized that the secretion of this set of molecules serves as a migration cue, regulated by PKD, commanding the cells to migrate. Future research may uncover what functions these secreted axon guidance and cell adhesion molecules trigger in a PKD-dependent manner and whether they contribute to the regulation of cell motility by the kinase.

To analyze the effect of PKD2 and PKD3 on intracellular proteins, we employed PKD inhibition to analyze the cell lysates corresponding to the collected secretome samples by LC-MS/MS and assess the phosphorylation levels of 9 kinases and kinase targets by xMAP assays. Enrichment analysis revealed that the downregulated upon PKD inhibition intracellular proteins were related to ribosome biogenesis in both MDA-MB-231 and MDA-MB-468 cells. In eukaryotes, ribosome biogenesis is the main factor that determines the cell's translational capacity, and as a result, it plays a critical role in regulating cell growth [293]. Amongst the different ribosome-related proteins were UTP18, UTP14A, WDR46, FTSJ3, DDX52, GNL3, RPS15, MPHOSPH10, RBM28 and PDCD11, which network analysis revealed that are highly interconnected. The reduction of multiple proteins related to ribosomes, from RNA-associated proteins to proteins required for the formation of 60S and 40S ribosomal subunits, following PKD inhibition depicts a possible connection between the kinase and ribosome biogenesis, hence translation capacity. mTOR signaling is a master regulator of protein synthesis and cell growth, and the pathway is known to play a pivotal role in regulating ribosome biogenesis by facilitating the translation of mRNAs that encode cytoplasmic ribosomal proteins, as well as promoting the transcription of rRNAs [294]. In TNBC, PKD3 is known to trigger the activation of S6 kinase 1 (S6K1), a main downstream target of mTORC1 [153]. Therefore, PKD3 might be regulating mTORC1-S6K1 signaling to enhance proliferation via ribosome biogenesis.

Phosphoprotein profiling of PKD inhibited cells revealed the reduced phosphorylation of c-JUN at S63 in cell lines MDA-MB-453, MDA-MB-468, HCC1937, HCC1143, HCC70 and HCC38. Screening of PKD inhibited cells was initially performed using an xMAP c-JUN pS63 assay and the target was later validated by immunoblotting. Interestingly, the GO term “regulation of JUN kinase activity” had been found to be enriched amongst the downregulated by CRT(1μM) cell lysate proteins of MDA-MB-468 cells (due to the presence of proteins EPHA4, DAB2IP and PDCD4). The *JUN* proto-oncogene encodes a key transcription factor, c-Jun, that is activated by JNK-induced phosphorylation of serines 63 and 73, and forms homo- or heterodimers with members of the FOS, ATF, and MAF protein families to constitute the transcription factor activator protein-1 (AP-1) [295]. In breast cancer, JNK signaling is exploited by cells to promote tumor growth and metastasis. More specifically, c-JUN was found at particularly high levels at the invasive front of breast cancer tumors compared to benign breast cells in a study involving samples from breast cancer patients [296], with increased c-Jun levels regulating the activity of downstream target genes involved in processes governing cell growth, invasion, and tumor stem cell expansion [297]. In a prostate cancer study, Wnt Family Member 5A (Wnt5a) was found to activate JNK via PKD, with the inhibition of PKD found to suppress Wnt5a-dependent cell migration and invasion [198]. It can be hypothesized that PKD modulates JNK signaling, and as an effect c-JUN phosphorylation, to promote the invasive function of cells through transcription of c-JUN target genes. Assays using siRNA-mediated depletion of PKD2 and PKD3

will provide further insight into whether this effect can be replicated by knockdown, or if it is an off-target effect of the inhibitor CRT0066101.

To conclude, the results of this PhD project increase our understanding of the contribution of PKD2 and PKD3 to the composition of the TNBC secretome and indicate that the kinases employ the secretory pathway in an isoform-specific manner to support invasive cell behavior.

5. References

1. Ferlay, J. *et al.* Cancer statistics for the year 2020: An overview. *International Journal of Cancer* **149**, 778–789 (2021).

2. Arnold, M. *et al.* Current and future burden of breast cancer: Global statistics for 2020 and 2040. *Breast* **66**, 15–23 (2022).

3. Liu, N., Johnson, K. J. & Ma, C. X. Male Breast Cancer: An Updated Surveillance, Epidemiology, and End Results Data Analysis. *Clinical Breast Cancer* **18**, e997–e1002 (2018).

4. Glass, A. G., Lacey, J. V., Carreon, J. D. & Hoover, R. N. Breast cancer incidence, 1980-2006: combined roles of menopausal hormone therapy, screening mammography, and estrogen receptor status. *J Natl Cancer Inst* **99**, 1152–1161 (2007).

5. Jemal, A., Center, M. M., DeSantis, C. & Ward, E. M. Global patterns of cancer incidence and mortality rates and trends. *Cancer Epidemiol Biomarkers Prev* **19**, 1893–1907 (2010).

6. Allemani, C. *et al.* Global surveillance of cancer survival 1995-2009: analysis of individual data for 25,676,887 patients from 279 population-based registries in 67 countries (CONCORD-2). *Lancet* **385**, 977–1010 (2015).

7. Goldhirsch, A. *et al.* Strategies for subtypes--dealing with the diversity of breast cancer: highlights of the St. Gallen International Expert Consensus on the Primary Therapy of Early Breast Cancer 2011. *Ann. Oncol.* **22**, 1736–1747 (2011).

8. Yanagawa, M. *et al.* Luminal A and luminal B (HER2 negative) subtypes of breast cancer consist of a mixture of tumors with different genotype. *BMC Res Notes* **5**, 376 (2012).

9. Harbeck, N. *et al.* Breast cancer. *Nat Rev Dis Primers* **5**, 1–31 (2019).

10. Newman, L. A., Reis-Filho, J. S., Morrow, M., Carey, L. A. & King, T. A. The 2014 Society of Surgical Oncology Susan G. Komen for the Cure Symposium: Triple-Negative Breast Cancer. *Ann Surg Oncol* **22**, 874–882 (2015).

11. Dent, R. *et al.* Triple-Negative Breast Cancer: Clinical Features and Patterns of Recurrence. *Clin Cancer Res* **13**, 4429–4434 (2007).

12. Untch, M., Konecny, G. E., Paepke, S. & Minckwitz, G. von. Current and future role of neoadjuvant therapy for breast cancer. *The Breast* **23**, 526–537 (2014).

13. Kim, E.-K., Noh, W. C., Han, W. & Noh, D.-Y. Prognostic significance of young age (<35 years) by subtype based on ER, PR, and HER2 status in breast cancer: a nationwide registry-based study. *World J Surg* **35**, 1244–1253 (2011).

14. Stark, A. *et al.* African Ancestry and Higher Prevalence of Triple-Negative Breast Cancer. *Cancer* **116**, 4926–4932 (2010).

15. Kumar, P. & Aggarwal, R. An overview of triple-negative breast cancer. *Arch Gynecol Obstet* **293**, 247–269 (2016).

16. Millikan, R. C. *et al.* Epidemiology of basal-like breast cancer. *Breast Cancer Res Treat* **109**, 123–139 (2008).

17. Wellenstein, M. D. *et al.* Loss of p53 triggers WNT-dependent systemic inflammation to drive breast cancer metastasis. *Nature* **572**, 538–542 (2019).

18. Ghosh, M. *et al.* Mutant p53 suppresses innate immune signaling to promote tumorigenesis. *Cancer Cell* **39**, 494-508.e5 (2021).

19. Li, Y. *et al.* Targeted immunotherapy for HER2-low breast cancer with 17p loss. *Sci Transl Med* **13**, eabc6894 (2021).

20. Parkes, E. E. *et al.* Activation of STING-Dependent Innate Immune Signaling By S-Phase-Specific DNA Damage in Breast Cancer. *J Natl Cancer Inst* **109**, (2017).

21. Lakhani, S. R. *et al.* The pathology of familial breast cancer: predictive value of immunohistochemical markers estrogen receptor, progesterone receptor, HER-2, and p53 in patients with mutations in BRCA1 and BRCA2. *J Clin Oncol* **20**, 2310–2318 (2002).

22. Atchley, D. P. *et al.* Clinical and pathologic characteristics of patients with BRCA-positive and BRCA-negative breast cancer. *J Clin Oncol* **26**, 4282–4288 (2008).

23. Samstein, R. M. *et al.* Mutations in BRCA1 and BRCA2 differentially affect the tumor microenvironment and response to checkpoint blockade immunotherapy. *Nat Cancer* **1**, 1188–1203 (2021).

24. Prestipino, A. & Zeiser, R. Clinical implications of tumor-intrinsic mechanisms regulating PD-L1. *Science Translational Medicine* **11**, eaav4810 (2019).

25. Bianchini, G., De Angelis, C., Licata, L. & Gianni, L. Treatment landscape of triple-negative breast cancer - expanded options, evolving needs. *Nat Rev Clin Oncol* **19**, 91–113 (2022).

26. Lawrence, R. T. *et al.* The proteomic landscape of triple-negative breast cancer. *Cell Rep* **11**, 630–644 (2015).

27. Lehmann, B. D. *et al.* Identification of human triple-negative breast cancer subtypes and preclinical models for selection of targeted therapies. *J Clin Invest* **121**, 2750–2767 (2011).

28. Lehmann, B. D. *et al.* Refinement of Triple-Negative Breast Cancer Molecular Subtypes: Implications for Neoadjuvant Chemotherapy Selection. *PLOS ONE* **11**, e0157368 (2016).

29. Jiang, Y.-Z. *et al.* Genomic and Transcriptomic Landscape of Triple-Negative Breast Cancers: Subtypes and Treatment Strategies. *Cancer Cell* **35**, 428-440.e5 (2019).

30. Bareche, Y. *et al.* Unravelling triple-negative breast cancer molecular heterogeneity using an integrative multiomic analysis. *Ann Oncol* **29**, 895–902 (2018).

31. Cortazar, P. *et al.* Pathological complete response and long-term clinical benefit in breast cancer: the CTNeoBC pooled analysis. *The Lancet* **384**, 164–172 (2014).

32. Nedeljković, M. & Damjanović, A. Mechanisms of Chemotherapy Resistance in Triple-Negative Breast Cancer—How We Can Rise to the Challenge. *Cells* **8**, (2019).

33. Gluz, O. *et al.* Triple-negative breast cancer--current status and future directions. *Ann. Oncol.* **20**, 1913–1927 (2009).

34. Kassam, F. *et al.* Survival Outcomes for Patients with Metastatic Triple-Negative Breast Cancer: Implications for Clinical Practice and Trial Design. *Clinical Breast Cancer* **9**, 29–33 (2009).

35. Bardia, A. *et al.* Sacituzumab Govitecan-hziy in Refractory Metastatic Triple-Negative Breast Cancer. *New England Journal of Medicine* **380**, 741–751 (2019).

36. Bardia, A. *et al.* Sacituzumab Govitecan in Metastatic Triple-Negative Breast Cancer. *N Engl J Med* **384**, 1529–1541 (2021).

37. Bryant, H. E. *et al.* Specific killing of BRCA2-deficient tumours with inhibitors of poly(ADP-ribose) polymerase. *Nature* **434**, 913–917 (2005).

38. Farmer, H. *et al.* Targeting the DNA repair defect in BRCA mutant cells as a therapeutic strategy. *Nature* **434**, 917–921 (2005).

39. Schmid, P. *et al.* Atezolizumab plus nab-paclitaxel as first-line treatment for unresectable, locally advanced or metastatic triple-negative breast cancer (IMpassion130): updated efficacy results from a randomised, double-blind, placebo-controlled, phase 3 trial. *The Lancet Oncology* **21**, 44–59 (2020).

40. Emens, L. A. *et al.* First-line atezolizumab plus nab-paclitaxel for unresectable, locally advanced, or metastatic triple-negative breast cancer: IMpassion130 final overall survival analysis. *Ann Oncol* **32**, 983–993 (2021).

41. Cortes, J. *et al.* Pembrolizumab plus chemotherapy versus placebo plus chemotherapy for previously untreated locally recurrent inoperable or metastatic triple-negative breast cancer (KEYNOTE-355): a randomised, placebo-controlled, double-blind, phase 3 clinical trial. *Lancet* **396**, 1817–1828 (2020).

42. Rugo, H. S. *et al.* Abstract GS3-01: Additional efficacy endpoints from the phase 3 KEYNOTE-355 study of pembrolizumab plus chemotherapy vs placebo plus chemotherapy as first-line therapy for locally recurrent inoperable or metastatic triple-negative breast cancer. *Cancer Research* **81**, GS3-01 (2021).

43. Li, Y. *et al.* Recent advances in therapeutic strategies for triple-negative breast cancer. *Journal of Hematology & Oncology* **15**, 121 (2022).

44. Jin, J. *et al.* Incidence, pattern and prognosis of brain metastases in patients with metastatic triple negative breast cancer. *BMC Cancer* **18**, 446 (2018).

45. Martin, A. M. *et al.* Brain Metastases in Newly Diagnosed Breast Cancer. *JAMA Oncol* **3**, 1069–1077 (2017).

46. Giancotti, F. G. Mechanisms Governing Metastatic Dormancy and Reactivation. *Cell* **155**, 750–764 (2013).

47. Pantel, K. & Brakenhoff, R. H. Dissecting the metastatic cascade. *Nat Rev Cancer* **4**, 448–456 (2004).

48. Vanharanta, S. & Massagué, J. Origins of Metastatic Traits. *Cancer Cell* **24**, 410–421 (2013).

49. Luzzi, K. J. *et al.* Multistep Nature of Metastatic Inefficiency. *Am J Pathol* **153**, 865–873 (1998).

50. Insua-Rodríguez, J. & Oskarsson, T. The extracellular matrix in breast cancer. *Advanced Drug Delivery Reviews* **97**, 41–55 (2016).

51. Hynes, R. O. The extracellular matrix: not just pretty fibrils. *Science* **326**, 1216–1219 (2009).

52. Frantz, C., Stewart, K. M. & Weaver, V. M. The extracellular matrix at a glance. *J Cell Sci* **123**, 4195–4200 (2010).

53. Lu, P., Takai, K., Weaver, V. M. & Werb, Z. Extracellular matrix degradation and remodeling in development and disease. *Cold Spring Harb Perspect Biol* **3**, a005058 (2011).

54. Zolota, V. *et al.* Epigenetic Alterations in Triple-Negative Breast Cancer—The Critical Role of Extracellular Matrix. *Cancers (Basel)* **13**, 713 (2021).

55. Bhowmick, N. A. & Moses, H. L. Tumor-stroma interactions. *Curr Opin Genet Dev* **15**, 97–101 (2005).

56. Tlsty, T. D. & Coussens, L. M. Tumor stroma and regulation of cancer development. *Annu Rev Pathol* **1**, 119–150 (2006).

57. Kauppila, S., Stenbäck, F., Risteli, J., Jukkola, A. & Risteli, L. Aberrant type I and type III collagen gene expression in human breast cancer in vivo. *J Pathol* **186**, 262–268 (1998).

58. Kagan, H. M. & Li, W. Lysyl oxidase: properties, specificity, and biological roles inside and outside of the cell. *J Cell Biochem* **88**, 660–672 (2003).

59. Bondareva, A. *et al.* The Lysyl Oxidase Inhibitor, β-Aminopropionitrile, Diminishes the Metastatic Colonization Potential of Circulating Breast Cancer Cells. *PLoS One* **4**, e5620 (2009).

60. Erler, J. T. & Giaccia, A. J. Lysyl oxidase mediates hypoxic control of metastasis. *Cancer Res* **66**, 10238–10241 (2006).

61. Egeblad, M. & Werb, Z. New functions for the matrix metalloproteinases in cancer progression. *Nat Rev Cancer* **2**, 161–174 (2002).

62. Sternlicht, M. D. & Werb, Z. How matrix metalloproteinases regulate cell behavior. *Annu Rev Cell Dev Biol* **17**, 463–516 (2001).

63. Wu, W. *et al.* Drivers and suppressors of triple-negative breast cancer. *Proc Natl Acad Sci U S A* **118**, e2104162118 (2021).

64. Kang, Y. *et al.* A multigenic program mediating breast cancer metastasis to bone. *Cancer Cell* **3**, 537–549 (2003).

65. Bos, P. D. *et al.* Genes that mediate breast cancer metastasis to the brain. *Nature* **459**, 1005–1009 (2009).

66. Minn, A. J. *et al.* Genes that mediate breast cancer metastasis to lung. *Nature* **436**, 518–524 (2005).

67. Wang, Q.-M., Lv, L., Tang, Y., Zhang, L. & Wang, L.-F. MMP-1 is overexpressed in triple-negative breast cancer tissues and the knockdown of MMP-1 expression inhibits tumor cell malignant behaviors in vitro. *Oncol Lett* **17**, 1732–1740 (2019).

68. Zhang, B. *et al.* Tumor-derived matrix metalloproteinase-13 (MMP-13) correlates with poor prognosis of invasive breast cancer. *BMC Cancer* **8**, 83 (2008).

69. Ibaragi, S. *et al.* Induction of MMP-13 Expression in Bone-metastasizing Cancer Cells by Type I Collagen through Integrin α1β1 and α2β1-p38 MAPK Signaling. *Anticancer Research* **31**, 1307–1313 (2011).

70. Goepel, C., Buchmann, J., Schultka, R. & Koelbl, H. Tenascin-A marker for the malignant potential of preinvasive breast cancers. *Gynecol Oncol* **79**, 372–378 (2000).

71. Oskarsson, T. *et al.* Breast cancer cells produce tenascin C as a metastatic niche component to colonize the lungs. *Nat Med* **17**, 867–874 (2011).

72. Nagaharu, K. *et al.* Tenascin C Induces Epithelial-Mesenchymal Transition–Like Change Accompanied by SRC Activation and Focal Adhesion Kinase Phosphorylation in Human Breast Cancer Cells. *Am J Pathol* **178**, 754–763 (2011).

73. Zandberga, E. *et al.* Depletion of carbonic anhydrase IX abrogates hypoxia-induced overexpression of stanniocalcin-1 in triple negative breast cancer cells. *Cancer Biol Ther* **18**, 596–605 (2017).

74. Han, J., Jeon, M., Shin, I. & Kim, S. Elevated STC-1 augments the invasiveness of triple-negative breast cancer cells through activation of the JNK/c-Jun signaling pathway. *Oncology Reports* **36**, 1764–1771 (2016).

75. Jeon, M., Han, J., Nam, S. J., Lee, J. E. & Kim, S. STC-1 expression is upregulated through an Akt/NF-κB-dependent pathway in triple-negative breast cancer cells. *Oncol Rep* **36**, 1717–1722 (2016).

76. Chen, F., Zhang, Z. & Pu, F. Role of stanniocalcin-1 in breast cancer (Review). *Oncology Letters* **18**, 3946–3953 (2019).

77. Chang, A. C.-M. *et al.* STC1 expression is associated with tumor growth and metastasis in breast cancer. *Clin Exp Metastasis* **32**, 15–27 (2015).

78. Hanavadi, S., Martin, T. A., Watkins, G., Mansel, R. E. & Jiang, W. G. Expression of interleukin 11 and its receptor and their prognostic value in human breast cancer. *Ann Surg Oncol* **13**, 802–808 (2006).

79. Sotiriou, C. *et al.* Interleukins-6 and -11 expression in primary breast cancer and subsequent development of bone metastases. *Cancer Lett* **169**, 87–95 (2001).

80. Ren, L., Wang, X., Dong, Z., Liu, J. & Zhang, S. Bone metastasis from breast cancer involves elevated IL-11 expression and the gp130/STAT3 pathway. *Med Oncol* **30**, 634 (2013).

81. Liang, M. *et al.* IL-11 is essential in promoting osteolysis in breast cancer bone metastasis via RANKL-independent activation of osteoclastogenesis. *Cell Death Dis* **10**, 353 (2019).

82. Maroni, P., Bendinelli, P., Ferraretto, A. & Lombardi, G. Interleukin 11 (IL-11): Role(s) in Breast Cancer Bone Metastases. *Biomedicines* **9**, 659 (2021).

83. McCoy, E. M., Hong, H., Pruitt, H. C. & Feng, X. IL-11 produced by breast cancer cells augments osteoclastogenesis by sustaining the pool of osteoclast progenitor cells. *BMC Cancer* **13**, 16 (2013).

84. Cai, W.-L. *et al.* microRNA-124 inhibits bone metastasis of breast cancer by repressing Interleukin-11. *Mol Cancer* **17**, 9 (2018).

85. Viswanadhapalli, S. *et al.* EC359: A First-in-Class Small-Molecule Inhibitor for Targeting Oncogenic LIFR Signaling in Triple-Negative Breast Cancer. *Mol Cancer Ther* **18**, 1341–1354 (2019).

86. Dhingra, K., Sahin, A., Emami, K., Hortobagyi, G. N. & Estrov, Z. Expression of leukemia inhibitory factor and its receptor in breast cancer: a potential autocrine and paracrine growth regulatory mechanism. *Breast Cancer Res Treat* **48**, 165–174 (1998).

87. Yue, X. *et al.* Leukemia inhibitory factor promotes EMT through STAT3-dependent miR-21 induction. *Oncotarget* **7**, 3777–3790 (2016).

88. Li, X. *et al.* LIF promotes tumorigenesis and metastasis of breast cancer through the AKT-mTOR pathway. *Oncotarget* **5**, 788–801 (2014).

89. Bianchini, G., Balko, J. M., Mayer, I. A., Sanders, M. E. & Gianni, L. Triple-negative breast cancer: challenges and opportunities of a heterogeneous disease. *Nat Rev Clin Oncol* **13**, 674–690 (2016).

90. Hanahan, D. & Weinberg, R. A. The Hallmarks of Cancer. *Cell* **100**, 57–70 (2000).

91. McAllister, S. S. & Weinberg, R. A. The tumour-induced systemic environment as a critical regulator of cancer progression and metastasis. *Nat Cell Biol* **16**, 717–727 (2014).

92. Joyce, J. A. & Pollard, J. W. Microenvironmental regulation of metastasis. *Nat Rev Cancer* **9**, 239–252 (2009).

93. Bareche, Y. *et al.* Unraveling Triple-Negative Breast Cancer Tumor Microenvironment Heterogeneity: Towards an Optimized Treatment Approach. *J Natl Cancer Inst* **112**, 708–719 (2020).

94. Gruosso, T. *et al.* Spatially distinct tumor immune microenvironments stratify triple-negative breast cancers. *J Clin Invest* **129**, 1785–1800 (2019).

95. Solinas, G. *et al.* Tumor-conditioned macrophages secrete migration-stimulating factor: a new marker for M2-polarization, influencing tumor cell motility. *J Immunol* **185**, 642–652 (2010).

96. Chen, J. *et al.* CCL18 from Tumor-Associated Macrophages Promotes Breast Cancer Metastasis via PITPNM3. *Cancer cell* **19**, 541 (2011).

97. DeNardo, D. G. *et al.* CD4(+) T cells regulate pulmonary metastasis of mammary carcinomas by enhancing protumor properties of macrophages. *Cancer Cell* **16**, 91–102 (2009).

98. Martinez, F. O., Gordon, S., Locati, M. & Mantovani, A. Transcriptional Profiling of the Human Monocyte-to-Macrophage Differentiation and Polarization: New Molecules and Patterns of Gene Expression. *The Journal of Immunology* **177**, 7303–7311 (2006).

99. Richardsen, E., Uglehus, R. D., Johnsen, S. H. & Busund, L.-T. Macrophage-colony stimulating factor (CSF1) predicts breast cancer progression and mortality. *Anticancer Res* **35**, 865–874 (2015).

100. Patsialou, A. *et al.* Invasion of human breast cancer cells in vivo requires both paracrine and autocrine loops involving the colony-stimulating factor-1 receptor. *Cancer Res* **69**, 9498–9506 (2009).

101. Patsialou, A. *et al.* Autocrine CSF1R signaling mediates switching between invasion and proliferation downstream of TGFβ in claudin-low breast tumor cells. *Oncogene* **34**, 2721–2731 (2015).

102. Su, S. *et al.* A Positive Feedback Loop between Mesenchymal-like Cancer Cells and Macrophages Is Essential to Breast Cancer Metastasis. *Cancer Cell* **25**, 605–620 (2014).

103. Ghirelli, C. *et al.* Breast Cancer Cell-Derived GM-CSF Licenses Regulatory Th2 Induction by Plasmacytoid Predendritic Cells in Aggressive Disease Subtypes. *Cancer Res* **75**, 2775–2787 (2015).

104. Paltridge, J. L., Belle, L. & Khew-Goodall, Y. The secretome in cancer progression. *Biochimica et Biophysica Acta (BBA) - Proteins and Proteomics* **1834**, 2233–2241 (2013).

105. Feitelson, M. A. *et al.* Sustained proliferation in cancer: Mechanisms and novel therapeutic targets. *Seminars in Cancer Biology* **35**, S25–S54 (2015).

106. Giuli, M. V., Giuliani, E., Screpanti, I., Bellavia, D. & Checquolo, S. Notch Signaling Activation as a Hallmark for Triple-Negative Breast Cancer Subtype. *Journal of Oncology* vol. 2019 e8707053 https://www.hindawi.com/journals/jo/2019/8707053/ (2019).

107. Mathonnet, M. *et al.* Hallmarks in colorectal cancer: Angiogenesis and cancer stem-like cells. *World J Gastroenterol* **20**, 4189–4196 (2014).

108. Jin, K., Pandey, N. B. & Popel, A. S. Crosstalk between stromal components and tumor cells of TNBC via secreted factors enhances tumor growth and metastasis. *Oncotarget* **8**, 60210–60222 (2017).

109. Butcher, D. T., Alliston, T. & Weaver, V. M. A tense situation: forcing tumour progression. *Nat Rev Cancer* **9**, 108–122 (2009).

110. Yang, E. *et al.* Exosome-mediated metabolic reprogramming: the emerging role in tumor microenvironment remodeling and its influence on cancer progression. *Signal Transduct Target Ther* **5**, 242 (2020).

111. Farhan, H. & Rabouille, C. Signalling to and from the secretory pathway. *J Cell Sci* **124**, 171–180 (2011).

112. Skalnikova, H., Motlik, J., Gadher, S. J. & Kovarova, H. Mapping of the secretome of primary isolates of mammalian cells, stem cells and derived cell lines. *PROTEOMICS* **11**, 691–708 (2011).

113. Lodish, H. *et al.* Overview of the Secretory Pathway. *Molecular Cell Biology. 4th edition* (2000).

114. Mellman, I. & Warren, G. The Road Taken: Past and Future Foundations of Membrane Traffic. *Cell* **100**, 99–112 (2000).

115. Braakman, I. & Hebert, D. N. Protein folding in the endoplasmic reticulum. *Cold Spring Harb Perspect Biol* **5**, a013201 (2013).

116. Sakaguchi, M., Tomiyoshi, R., Kuroiwa, T., Mihara, K. & Omura, T. Functions of signal and signal-anchor sequences are determined by the balance between the hydrophobic segment and the N-terminal charge. *Proc Natl Acad Sci U S A* **89**, 16–19 (1992).

117. Orci, L. *et al.* Mammalian Sec23p homologue is restricted to the endoplasmic reticulum transitional cytoplasm. *Proc Natl Acad Sci U S A* **88**, 8611–8615 (1991).

118. Barlowe, C. *et al.* COPII: A membrane coat formed by Sec proteins that drive vesicle budding from the endoplasmic reticulum. *Cell* **77**, 895–907 (1994).

119. Lee, M. C. S., Miller, E. A., Goldberg, J., Orci, L. & Schekman, R. Bi-directional protein transport between the ER and Golgi. *Annu Rev Cell Dev Biol* **20**, 87–123 (2004).

120. Centonze, F. G. & Farhan, H. Crosstalk of endoplasmic reticulum exit sites and cellular signaling. *FEBS Letters* **593**, 2280–2288 (2019).

121. Klausner, R. D., Donaldson, J. G. & Lippincott-Schwartz, J. Brefeldin A: insights into the control of membrane traffic and organelle structure. *J Cell Biol* **116**, 1071–1080 (1992).

122. Roignot, J., Peng, X. & Mostov, K. Polarity in mammalian epithelial morphogenesis. *Cold Spring Harb Perspect Biol* **5**, a013789 (2013).

123. Bard, F. & Malhotra, V. The Formation of TGN-to-Plasma-Membrane Transport Carriers. *Annu. Rev. Cell Dev. Biol.* **22**, 439–455 (2006).

124. Royer, C. & Lu, X. Epithelial cell polarity: a major gatekeeper against cancer? *Cell Death Differ* **18**, 1470–1477 (2011).

125. Ferro-Novick, S. & Brose, N. Traffic control system within cells. *Nature* **504**, 98–98 (2013).

126. Nickel, W. & Rabouille, C. Mechanisms of regulated unconventional protein secretion. *Nat Rev Mol Cell Biol* **10**, 148–155 (2009).

127. Jacopo, M. Unconventional protein secretion (UPS): role in important diseases. *Mol Biomed* **4**, 2 (2023).

128. Goldenring, J. R. A central role for vesicle trafficking in epithelial neoplasia: intracellular highways to carcinogenesis. *Nat Rev Cancer* **13**, 813–820 (2013).

129. Olayioye, M. A., Noll, B. & Hausser, A. Spatiotemporal Control of Intracellular Membrane Trafficking by Rho GTPases. *Cells* **8**, 1478 (2019).

130. Van Aelst, L. & D'Souza-Schorey, C. Rho GTPases and signaling networks. *Genes Dev* **11**, 2295–2322 (1997).

131. Olson, M. F., Ashworth, A. & Hall, A. An Essential Role for Rho, Rac, and Cdc42 GTPases in Cell Cycle Progression Through G1. *Science* **269**, 1270–1272 (1995).

132. Lamaze, C., Chuang, T. H., Terlecky, L. J., Bokoch, G. M. & Schmid, S. L. Regulation of receptor-mediated endocytosis by Rho and Rac. *Nature* **382**, 177–179 (1996).

133. Ridley, A. J., Paterson, H. F., Johnston, C. L., Diekmann, D. & Hall, A. The small GTP-binding protein rac regulates growth factor-induced membrane ruffling. *Cell* **70**, 401–410 (1992).

134. Eisler, S. A. *et al.* A Rho signaling network links microtubules to PKD controlled carrier transport to focal adhesions. *eLife* **7**, e35907 (2018).

135. Arnette, C., Frye, K. & Kaverina, I. Microtubule and Actin Interplay Drive Intracellular c-Src Trafficking. *PLOS ONE* **11**, e0148996 (2016).

136. Vega, F. M., Colomba, A., Reymond, N., Thomas, M. & Ridley, A. J. RhoB regulates cell migration through altered focal adhesion dynamics. *Open Biol.* **2**, 120076 (2012).

137. Heck, J. N. *et al.* Microtubules regulate GEF-H1 in response to extracellular matrix stiffness. *MBoC* **23**, 2583–2592 (2012).

138. Makridakis, M. & Vlahou, A. Secretome proteomics for discovery of cancer biomarkers. *J Proteomics* **73**, 2291–2305 (2010).

139. Freitas, D. *et al.* O-glycans truncation modulates gastric cancer cell signaling and transcription leading to a more aggressive phenotype. *EBioMedicine* **40**, 349–362 (2019).

140. Del Giudice, S. *et al.* Endogenous and Exogenous Regulatory Signaling in the Secretory Pathway: Role of Golgi Signaling Molecules in Cancer. *Frontiers in Cell and Developmental Biology* **10**, (2022).

141. Myoui, A. *et al.* C-SRC tyrosine kinase activity is associated with tumor colonization in bone and lung in an animal model of human breast cancer metastasis. *Cancer Res* **63**, 5028–5033 (2003).

142. Halberg, N. *et al.* PITPNC1 recruits RAB1B to the Golgi network to drive malignant secretion. *Cancer Cell* **29**, 339–353 (2016).

143. Tokuda, E. *et al.* Phosphatidylinositol 4-phosphate in the Golgi apparatus regulates cell-cell adhesion and invasive cell migration in human breast cancer. *Cancer Res* **74**, 3054–3066 (2014).

144. Johannes, F. J., Prestle, J., Eis, S., Oberhagemann, P. & Pfizenmaier, K. PKCu is a novel, atypical member of the protein kinase C family. *J. Biol. Chem.* **269**, 6140–6148 (1994).

145. Sturany, S. *et al.* Molecular Cloning and Characterization of the Human Protein Kinase D2 A NOVEL MEMBER OF THE PROTEIN KINASE D FAMILY OF SERINE THREONINE KINASES. *J. Biol. Chem.* **276**, 3310–3318 (2001).

146. Hayashi, A., Seki, N., Hattori, A., Kozuma, S. & Saito, T. PKCnu, a new member of the protein kinase C family, composes a fourth subfamily with PKCmu. *Biochim Biophys Acta* **1450**, 99–106 (1999).

147. Rozengurt, E., Rey, O. & Waldron, R. T. Protein kinase D signaling. *J Biol Chem* **280**, 13205–13208 (2005).

148. Bossard, C., Bresson, D., Polishchuk, R. S. & Malhotra, V. Dimeric PKD regulates membrane fission to form transport carriers at the TGN. *J Cell Biol* **179**, 1123–1131 (2007).

149. Yeaman, C. *et al.* Protein kinase D regulates basolateral membrane protein exit from trans-Golgi network. *Nat Cell Biol* **6**, 106–112 (2004).

150. Eiseler, T., Schmid, M. A., Topbas, F., Pfizenmaier, K. & Hausser, A. PKD is recruited to sites of actin remodelling at the leading edge and negatively regulates cell migration. *FEBS Letters* **581**, 4279–4287 (2007).

151. Olayioye, M. A., Barisic, S. & Hausser, A. Multi-level control of actin dynamics by protein kinase D. *Cell Signal* **25**, 1739–1747 (2013).

152. Rykx, A. *et al.* Protein kinase D: a family affair. *FEBS Letters* **546**, 81–86 (2003).

153. Huck, B., Duss, S., Hausser, A. & Olayioye, M. A. Elevated protein kinase D3 (PKD3) expression supports proliferation of triple-negative breast cancer cells and contributes to mTORC1-S6K1 pathway activation. *J Biol Chem* **289**, 3138–3147 (2014).

154. Waldron, R. T., Iglesias, T. & Rozengurt, E. Phosphorylation-dependent protein kinase D activation. *Electrophoresis* **20**, 382–390 (1999).

155. Matthews, S. A., Rozengurt, E. & Cantrell, D. Protein kinase D. A selective target for antigen receptors and a downstream target for protein kinase C in lymphocytes. *J Exp Med* **191**, 2075–2082 (2000).

156. Newton, A. C. Protein kinase C: structural and spatial regulation by phosphorylation, cofactors, and macromolecular interactions. *Chem Rev* **101**, 2353–2364 (2001).

157. Iglesias, T. & Rozengurt, E. Protein kinase D activation by deletion of its cysteine-rich motifs. *FEBS Lett* **454**, 53–56 (1999).

158. Waldron, R. T. & Rozengurt, E. Protein Kinase C Phosphorylates Protein Kinase D Activation Loop Ser744 and Ser748 and Releases Autoinhibition by the Pleckstrin Homology Domain*. *Journal of Biological Chemistry* **278**, 154–163 (2003).

159. Wong, C. & Jin, Z.-G. Protein Kinase C-dependent Protein Kinase D Activation Modulates ERK Signal Pathway and Endothelial Cell Proliferation by Vascular Endothelial Growth Factor*. *Journal of Biological Chemistry* **280**, 33262–33269 (2005).

160. Hausser, A. *et al.* Phospho-specific binding of 14-3-3 proteins to phosphatidylinositol 4-kinase III beta protects from dephosphorylation and stabilizes lipid kinase activity. *J Cell Sci* **119**, 3613–3621 (2006).

161. Tóth, B. *et al.* Phosphatidylinositol 4-kinase IIIbeta regulates the transport of ceramide between the endoplasmic reticulum and Golgi. *J Biol Chem* **281**, 36369–36377 (2006).

162. Hanada, K., Kumagai, K., Tomishige, N. & Yamaji, T. CERT-mediated trafficking of ceramide. *Biochim Biophys Acta* **1791**, 684–691 (2009).

163. Fugmann, T. *et al.* Regulation of secretory transport by protein kinase D–mediated phosphorylation of the ceramide transfer protein. *Journal of Cell Biology* **178**, 15–22 (2007).

164. Gehart, H. *et al.* The BAR domain protein Arfaptin-1 controls secretory granule biogenesis at the trans-Golgi network. *Dev Cell* **23**, 756–768 (2012).

165. Cruz-Garcia, D. *et al.* Recruitment of arfaptins to the trans-Golgi network by PI(4)P and their involvement in cargo export. *EMBO J* **32**, 1717–1729 (2013).

166. Eiseler, T., Wille, C., Koehler, C., Illing, A. & Seufferlein, T. Protein Kinase D2 Assembles a Multiprotein Complex at the Trans-Golgi Network to Regulate Matrix Metalloproteinase Secretion *. *Journal of Biological Chemistry* **291**, 462–477 (2016).

167. Sheetz, M. P. Cell control by membrane-cytoskeleton adhesion. *Nat Rev Mol Cell Biol* **2**, 392–396 (2001).

168. Diz-Muñoz, A. *et al.* Control of Directed Cell Migration In Vivo by Membrane-to-Cortex Attachment. *PLoS Biol* **8**, e1000544 (2010).

169. Pollard, T. D. & Borisy, G. G. Cellular motility driven by assembly and disassembly of actin filaments. *Cell* **112**, 453–465 (2003).

170. Bernstein, B. W. & Bamburg, J. R. ADF/cofilin: a functional node in cell biology. *Trends Cell Biol* **20**, 187–195 (2010).

171. Kanellos, G. & Frame, M. C. Cellular functions of the ADF/cofilin family at a glance. *Journal of Cell Science* **129**, 3211–3218 (2016).

172. Marshall, T. W., Aloor, H. L. & Bear, J. E. Coronin 2A regulates a subset of focal-adhesion-turnover events through the cofilin pathway. *J Cell Sci* **122**, 3061–3069 (2009).

173. Barišić, S. *et al.* Phosphorylation of Ser 402 impedes phosphatase activity of slingshot 1. *EMBO reports* **12**, 527–533 (2011).

174. Spratley, S. J., Bastea, L. I., Döppler, H., Mizuno, K. & Storz, P. Protein Kinase D Regulates Cofilin Activity through p21-activated Kinase 4*. *Journal of Biological Chemistry* **286**, 34254–34261 (2011).

175. Döppler, H. *et al.* Protein Kinase D Isoforms Differentially Modulate Cofilin-Driven Directed Cell Migration. *PLOS ONE* **9**, e98090 (2014).

176. Eiseler, T., Hausser, A., De Kimpe, L., Van Lint, J. & Pfizenmaier, K. Protein Kinase D Controls Actin Polymerization and Cell Motility through Phosphorylation of Cortactin*. *Journal of Biological Chemistry* **285**, 18672–18683 (2010).

177. Weaver, A. M. Cortactin in tumor invasiveness. *Cancer Letters* **265**, 157–166 (2008).

178. Ziegler, S. *et al.* A novel protein kinase D phosphorylation site in the tumor suppressor Rab interactor 1 is critical for coordination of cell migration. *Mol Biol Cell* **22**, 570–580 (2011).

179. Borges, S. *et al.* Effective Targeting of Estrogen Receptor-Negative Breast Cancers with the Protein Kinase D Inhibitor CRT0066101. *Mol Cancer Ther* **14**, 1306–1316 (2015).

180. Hao, Q., McKenzie, R., Gan, H. & Tang, H. Protein kinases D2 and D3 are novel growth regulators in HCC1806 triple-negative breast cancer cells. *Anticancer Res* **33**, 393–399 (2013).

181. Eiseler, T., Döppler, H., Yan, I. K., Goodison, S. & Storz, P. Protein kinase D1 regulates matrix metalloproteinase expression and inhibits breast cancer cell invasion. *Breast Cancer Res* **11**, R13 (2009).

182. Du, C., Zhang, C., Hassan, S., Biswas, M. H. U. & Balaji, K. C. Protein kinase D1 suppresses epithelial-to-mesenchymal transition through phosphorylation of snail. *Cancer Res* **70**, 7810–7819 (2010).

183. Yang, Z.-F. *et al.* GABP transcription factor is required for development of chronic myelogenous leukemia via its control of PRKD2. *Proc Natl Acad Sci U S A* **110**, 2312–2317 (2013).

184. Harikumar, K. B. *et al.* A novel small molecule inhibitor of protein kinase D blocks pancreatic cancer growth in vitro and in vivo. *Mol Cancer Ther* **9**, 1136–1146 (2010).

185. Bernhart, E. *et al.* Protein kinase D2 regulates migration and invasion of U87MG glioblastoma cells in vitro. *Exp Cell Res* **319**, 2037–2048 (2013).

186. Wei, N., Chu, E., Wipf, P. & Schmitz, J. C. Protein kinase d as a potential chemotherapeutic target for colorectal cancer. *Mol Cancer Ther* **13**, 1130–1141 (2014).

187. Li, Q. Q. *et al.* Protein kinase D inhibitor CRT0066101 suppresses bladder cancer growth in vitro and xenografts via blockade of the cell cycle at G2/M. *Cell Mol Life Sci* **75**, 939–963 (2018).

188. Liu, Y. *et al.* The Role and Mechanism of CRT0066101 as an Effective Drug for Treatment of Triple-Negative Breast Cancer | Cell Physiol Biochem. *Cellular Physiology & Biochemistry* **52**, 382–396 (2019).

189. Sharom, F. J. The P-glycoprotein efflux pump: how does it transport drugs? *J Membr Biol* **160**, 161–175 (1997).

190. Chen, J. *et al.* PKD2 mediates multi-drug resistance in breast cancer cells through modulation of P-glycoprotein expression. *Cancer Lett* **300**, 48–56 (2011).

191. Lieb, W. S. *et al.* The GEF-H1/PKD3 signaling pathway promotes the maintenance of triple-negative breast cancer stem cells. *Int J Cancer* **146**, 3423–3434 (2020).

192. Durand, N., Borges, S. & Storz, P. Protein Kinase D Enzymes as Regulators of EMT and Cancer Cell Invasion. *J Clin Med* **5**, 20 (2016).

193. Gravdal, K., Halvorsen, O. J., Haukaas, S. A. & Akslen, L. A. A Switch from E-Cadherin to N-Cadherin Expression Indicates Epithelial to Mesenchymal Transition and Is of Strong and Independent Importance for the Progress of Prostate Cancer. *Clinical Cancer Research* **13**, 7003–7011 (2007).

194. Yang, J. & Weinberg, R. A. Epithelial-mesenchymal transition: at the crossroads of development and tumor metastasis. *Dev Cell* **14**, 818–829 (2008).

195. Alpsoy, A. & Gündüz, U. Protein kinase D2 silencing reduced motility of doxorubicin-resistant MCF7 cells. *Tumor Biol.* **36**, 4417–4426 (2015).

196. Hegedüs, L., Cho, H., Xie, X. & Eliceiri, G. L. Additional MDA-MB-231 breast cancer cell matrix metalloproteinases promote invasiveness. *J Cell Physiol* **216**, 480–485 (2008).

197. Roy, A. & Wang, Q. J. Protein Kinase D: A Potential Therapeutic Target in Prostate Cancer. *Molecular and cellular pharmacology* **9**, 1 (2017).

198. Yamamoto, H. *et al.* Wnt5a signaling is involved in the aggressiveness of prostate cancer and expression of metalloproteinase. *Oncogene* **29**, 2036–2046 (2010).

199. Wille, C. *et al.* Protein kinase D2 induces invasion of pancreatic cancer cells by regulating matrix metalloproteinases. *MBoC* **25**, 324–336 (2014).

200. LaValle, C. R., Zhang, L., Xu, S., Eiseman, J. L. & Wang, Q. J. Inducible silencing of protein kinase D3 inhibits secretion of tumor-promoting factors in prostate cancer. *Mol Cancer Ther* **11**, 1389–1399 (2012).

201. Zou, Z. *et al.* PKD2 and PKD3 promote prostate cancer cell invasion by modulating NF-κB- and HDAC1-mediated expression and activation of uPA. *J Cell Sci* **125**, 4800–4811 (2012).

202. Mehner, C. *et al.* Tumor cell-produced matrix metalloproteinase 9 (MMP-9) drives malignant progression and metastasis of basal-like triple negative breast cancer. *Oncotarget* **5**, 2736–2749 (2014).

203. Harbeck, N. *et al.* Urokinase-type plasminogen activator (uPA) and its inhibitor PAI-I: novel tumor-derived factors with a high prognostic and predictive impact in breast cancer. *Thromb Haemost* **91**, 450–456 (2004).

204. Xu, W. *et al.* Protein kinase Ds promote tumor angiogenesis through mast cell recruitment and expression of angiogenic factors in prostate cancer microenvironment. *Journal of Experimental & Clinical Cancer Research* **38**, 114 (2019).

205. Aebersold, R. & Mann, M. Mass spectrometry-based proteomics. *Nature* **422**, 198–207 (2003).

206. Pham, T. V., Piersma, S. R., Oudgenoeg, G. & Jimenez, C. R. Label-free mass spectrometry-based proteomics for biomarker discovery and validation. *Expert Review of Molecular Diagnostics* **12**, 343–359 (2012).

207. Deeb, S. J., D'Souza, R. C. J., Cox, J., Schmidt-Supprian, M. & Mann, M. Super-SILAC allows classification of diffuse large B-cell lymphoma subtypes by their protein expression profiles. *Mol Cell Proteomics* **11**, 77–89 (2012).

208. Geiger, T., Wehner, A., Schaab, C., Cox, J. & Mann, M. Comparative proteomic analysis of eleven common cell lines reveals ubiquitous but varying expression of most proteins. *Mol Cell Proteomics* **11**, M111.014050 (2012).

209. Cmielová, J. & Rezáčová, M. p21Cip1/Waf1 protein and its function based on a subcellular localization [corrected]. *J Cell Biochem* **112**, 3502–3506 (2011).

210. Domon, B. & Aebersold, R. Mass spectrometry and protein analysis. *Science* **312**, 212–217 (2006).

211. Neilson, K. A. *et al.* Less label, more free: approaches in label-free quantitative mass spectrometry. *Proteomics* **11**, 535–553 (2011).

212. Elshal, M. F. & McCoy, J. P. Multiplex Bead Array Assays: Performance Evaluation and Comparison of Sensitivity to ELISA. *Methods* **38**, 317–323 (2006).

213. Vignali, D. A. Multiplexed particle-based flow cytometric assays. *J Immunol Methods* **243**, 243–255 (2000).

214. de Jager, W. & Rijkers, G. T. Solid-phase and bead-based cytokine immunoassay: a comparison. *Methods* **38**, 294–303 (2006).

215. duPont, N. C., Wang, K., Wadhwa, P. D., Culhane, J. F. & Nelson, E. L. Validation and comparison of luminex multiplex cytokine analysis kits with ELISA: Determinations of a panel of nine cytokines in clinical sample culture supernatants. *Journal of reproductive immunology* **66**, 175 (2005).

216. Linkov, F. *et al.* Early detection of head and neck cancer: development of a novel screening tool using multiplexed immunobead-based biomarker profiling. *Cancer Epidemiol Biomarkers Prev* **16**, 102–107 (2007).

217. Birse, C. E. *et al.* Blood-based lung cancer biomarkers identified through proteomic discovery in cancer tissues, cell lines and conditioned medium. *Clinical Proteomics* **12**, 18 (2015).

218. Birse, C. E., Tomic, J. L., Pass, H. I., Rom, W. N. & Lagier, R. J. Clinical validation of a blood-based classifier for diagnostic evaluation of asymptomatic individuals with pulmonary nodules. *Clinical Proteomics* **14**, 25 (2017).

219. Ziegler, Y. S., Moresco, J. J., Yates, J. R. & Nardulli, A. M. Integration of Breast Cancer Secretomes with Clinical Data Elucidates Potential Serum Markers for Disease Detection, Diagnosis, and Prognosis. *PLoS One* **11**, e0158296 (2016).

220. Läubli, H. *et al.* Lectin Galactoside-binding Soluble 3 Binding Protein (LGALS3BP) Is a Tumor-associated Immunomodulatory Ligand for CD33-related Siglecs. *J Biol Chem* **289**, 33481–33491 (2014).

221. Yee, K. O. *et al.* The effect of thrombospondin-1 on breast cancer metastasis. *Breast Cancer Res Treat* **114**, 85–96 (2009).

222. Fontana, A. *et al.* Human breast tumors override the antiangiogenic effect of stromal thrombospondin-1 in vivo. *Int J Cancer* **116**, 686–691 (2005).

223. Wu, Q.-W. *et al.* Expression and clinical significance of extracellular matrix protein 1 and vascular endothelial growth factor-C in lymphatic metastasis of human breast cancer. *BMC Cancer* **12**, 47 (2012).

224. Boersema, P. J., Geiger, T., Wiśniewski, J. R. & Mann, M. Quantification of the N-glycosylated Secretome by Super-SILAC During Breast Cancer Progression and in Human Blood Samples *. *Molecular & Cellular Proteomics* **12**, 158–171 (2013).

225. Neufeld, G. & Kessler, O. The semaphorins: versatile regulators of tumour progression and tumour angiogenesis. *Nat Rev Cancer* **8**, 632–645 (2008).

226. Shin, J. *et al.* Identification of ganglioside GM2 activator playing a role in cancer cell migration through proteomic analysis of breast cancer secretomes. *Cancer Sci* **107**, 828–835 (2016).

227. Zhao, K., Wang, M. & Wu, A. ATP6AP2 is Overexpressed in Breast Cancer and Promotes Breast Cancer Progression. *Cancer Manag Res* **12**, 10449–10459 (2020).

228. Tkach, M. *et al.* Extracellular vesicles from triple negative breast cancer promote pro-inflammatory macrophages associated with better clinical outcome. *Proceedings of the National Academy of Sciences* **119**, e2107394119 (2022).

229. Hamester, F. *et al.* Insights into the Steps of Breast Cancer–Brain Metastases Development: Tumor Cell Interactions with the Blood–Brain Barrier. *International Journal of Molecular Sciences* **23**, 1900 (2022).

230. Piersma, S. R. *et al.* Workflow Comparison for Label-Free, Quantitative Secretome Proteomics for Cancer Biomarker Discovery: Method Evaluation, Differential Analysis, and Verification in Serum. *J. Proteome Res.* **9**, 1913–1922 (2010).

231. Piersma, S. R. *et al.* Feasibility of label-free phosphoproteomics and application to base-line signaling of colorectal cancer cell lines. *J Proteomics* **127**, 247–258 (2015).

232. Cox, J. & Mann, M. MaxQuant enables high peptide identification rates, individualized p.p.b.-range mass accuracies and proteome-wide protein quantification. *Nat Biotechnol* **26**, 1367–1372 (2008).

233. Perez-Riverol, Y. *et al.* The PRIDE database resources in 2022: a hub for mass spectrometry-based proteomics evidences. *Nucleic Acids Res* **50**, D543–D552 (2021).

234. Liu, H., Sadygov, R. G. & Yates, J. R. A model for random sampling and estimation of relative protein abundance in shotgun proteomics. *Anal Chem* **76**, 4193–4201 (2004).

235. Pham, T. V. & Jimenez, C. R. An accurate paired sample test for count data. *Bioinformatics* **28**, i596–i602 (2012).

236. Raudvere, U. *et al.* g:Profiler: a web server for functional enrichment analysis and conversions of gene lists (2019 update). *Nucleic Acids Research* **47**, W191–W198 (2019).

237. Kuleshov, M. V. *et al.* Enrichr: a comprehensive gene set enrichment analysis web server 2016 update. *Nucleic Acids Research* **44**, W90–W97 (2016).

238. Zhao, L. *et al.* OutCyte: a novel tool for predicting unconventional protein secretion. *Sci Rep* **9**, 19448 (2019).

239. Szklarczyk, D. *et al.* The STRING database in 2023: protein–protein association networks and functional enrichment analyses for any sequenced genome of interest. *Nucleic Acids Research* **51**, D638–D646 (2023).

240. Borges, S. *et al.* Pharmacologic reversion of epigenetic silencing of the PRKD1promoter blocks breast tumor cell invasion and metastasis. *Breast Cancer Research* **15**, R66 (2013).

241. Kunkel, M. T. & Newton, A. C. Protein Kinase D inhibitors uncouple phosphorylation from activity by promoting agonist-dependent activation loop phosphorylation. *Chem Biol* **22**, 98–106 (2015).

242. Canzler, S. *et al.* Prospects and challenges of multi-omics data integration in toxicology. *Arch Toxicol* **94**, 371–388 (2020).

243. Piersma, S. R. *et al.* Whole gel processing procedure for GeLC-MS/MS based proteomics. *Proteome Science* **11**, 17 (2013).

244. Ashburner, M. *et al.* Gene Ontology: tool for the unification of biology. *Nat Genet* **25**, 25–29 (2000).

245. Bernstein, K. A., Gallagher, J. E. G., Mitchell, B. M., Granneman, S. & Baserga, S. J. The Small-Subunit Processome Is a Ribosome Assembly Intermediate. *Eukaryot Cell* **3**, 1619–1626 (2004).

246. Kater, L. *et al.* Visualizing the Assembly Pathway of Nucleolar Pre-60S Ribosomes. *Cell* **171**, 1599-1610.e14 (2017).

247. Morello, L. G. *et al.* The Human Nucleolar Protein FTSJ3 Associates with NIP7 and Functions in Pre-rRNA Processing. *PLoS One* **6**, e29174 (2011).

248. Tseng, T.-L. *et al.* The RNA helicase Ddx52 functions as a growth switch in juvenile zebrafish. *Development* **148**, dev199578 (2021).

249. Quiroga-Artigas, G., Jong, D. de & Schnitzler, C. E. GNL3 is an evolutionarily conserved stem cell gene influencing cell proliferation, animal growth and regeneration in the hydrozoan Hydractinia. *Open Biology* **12**, (2022).

250. Rössler, I. *et al.* The C-terminal tail of ribosomal protein Rps15 is engaged in cytoplasmic pre-40S maturation. *RNA Biol* **19**, 560–574.

251. Zhao, S. *et al.* Sas10 controls ribosome biogenesis by stabilizing Mpp10 and delivering the Mpp10-Imp3-Imp4 complex to nucleolus. *Nucleic Acids Res* **47**, 2996–3012 (2019).

252. Damianov, A., Kann, M., Lane, W. S. & Bindereif, A. Human RBM28 protein is a specific nucleolar component of the spliceosomal snRNPs. **387**, 1455–1460 (2006).

253. Tafforeau, L. *et al.* The Complexity of Human Ribosome Biogenesis Revealed by Systematic Nucleolar Screening of Pre-rRNA Processing Factors. *Molecular Cell* **51**, 539–551 (2013).

254. Hirai, Y. *et al.* Nucleolar scaffold protein, WDR46, determines the granular compartmental localization of nucleolin and DDX21. *Genes Cells* **18**, 780–797 (2013).

255. Liljedahl, M. *et al.* Protein Kinase D Regulates the Fission of Cell Surface Destined Transport Carriers from the Trans-Golgi Network. *Cell* **104**, 409–420 (2001).

256. Naba, A., Clauser, K. R., Lamar, J. M., Carr, S. A. & Hynes, R. O. Extracellular matrix signatures of human mammary carcinoma identify novel metastasis promoters. *eLife* **3**, e01308 (2014).

257. Naba, A. *et al.* The extracellular matrix: Tools and insights for the 'omics' era. *Matrix Biol* **49**, 10–24 (2016).

258. Wang, J. *et al.* Matrix metalloproteinase-1 expression in breast carcinoma: a marker for unfavorable prognosis. *Oncotarget* **8**, 91379–91390 (2017).

259. Gupta, G. P. *et al.* Mediators of vascular remodelling co-opted for sequential steps in lung metastasis. *Nature* **446**, 765–770 (2007).

260. Martinson, H. A., Jindal, S., Durand-Rougely, C., Borges, V. F. & Schedin, P. Wound healing-like immune program facilitates postpartum mammary gland involution and tumor progression. *Int J Cancer* **136**, 1803–1813 (2015).

261. Hancox, R. A. *et al.* Tumour-associated tenascin-C isoforms promote breast cancer cell invasion and growth by matrix metalloproteinase-dependent and independent mechanisms. *Breast Cancer Res* **11**, R24 (2009).

262. Ioachim, E. *et al.* Immunohistochemical expression of extracellular matrix components tenascin, fibronectin, collagen type IV and laminin in breast cancer: their prognostic value and role in tumour invasion and progression. *Eur J Cancer* **38**, 2362–2370 (2002).

263. Joensuu, K., Heikkilä, P. & Andersson, L. C. Tumor dormancy: Elevated expression of stanniocalcins in late relapsing breast cancer. *Cancer Letters* **265**, 76–83 (2008).

264. Murai, R. *et al.* Stanniocalcin-1 promotes metastasis in a human breast cancer cell line through activation of PI3K. *Clin Exp Metastasis* **31**, 787–794 (2014).

265. Nannuru, K. C. *et al.* Matrix Metalloproteinase (MMP)-13 Regulates Mammary Tumor–Induced Osteolysis by Activating MMP9 and Transforming Growth Factor-β Signaling at the Tumor-Bone Interface. *Cancer Research* **70**, 3494–3504 (2010).

266. Manolagas, S. C. & Jilka, R. L. Bone marrow, cytokines, and bone remodeling. Emerging insights into the pathophysiology of osteoporosis. *N Engl J Med* **332**, 305–311 (1995).

267. Guedán, A. *et al.* Investigation of the Role of Protein Kinase D in Human Rhinovirus Replication. *J Virol* **91**, e00217-17 (2017).

268. Neve, R. M. *et al.* A collection of breast cancer cell lines for the study of functionally distinct cancer subtypes. *Cancer Cell* **10**, 515–527 (2006).

269. Prat, A. *et al.* Characterization of cell lines derived from breast cancers and normal mammary tissues for the study of the intrinsic molecular subtypes. *Breast Cancer Res Treat* **142**, 237–255 (2013).

270. Hollestelle, A. *et al.* Distinct gene mutation profiles among luminal-type and basal-type breast cancer cell lines. *Breast Cancer Res Treat* **121**, 53–64 (2010).

271. Kao, J. *et al.* Molecular Profiling of Breast Cancer Cell Lines Defines Relevant Tumor Models and Provides a Resource for Cancer Gene Discovery. *PLOS ONE* **4**, e6146 (2009).

272. Riaz, M. *et al.* miRNA expression profiling of 51 human breast cancer cell lines reveals subtype and driver mutation-specific miRNAs. *Breast Cancer Res* **15**, R33 (2013).

273. Fu, Y. & Rubin, C. S. Protein kinase D: coupling extracellular stimuli to the regulation of cell physiology. *EMBO Rep* **12**, 785–796 (2011).

274. Angel, P., Hattori, K., Smeal, T. & Karin, M. The jun proto-oncogene is positively autoregulated by its product, Jun/AP-1. *Cell* **55**, 875–885 (1988).

275. Kovary, K. & Bravo, R. Expression of different Jun and Fos proteins during the G0-to-G1 transition in mouse fibroblasts: in vitro and in vivo associations. *Mol Cell Biol* **11**, 2451–2459 (1991).

276. Kalluri, R. & LeBleu, V. S. The biology, function, and biomedical applications of exosomes. *Science* **367**, eaau6977 (2020).

277. *Emerging Concepts of Tumor Exosome–Mediated Cell-Cell Communication*. (Springer, 2013). doi:10.1007/978-1-4614-3697-3.

278. Kessenbrock, K., Plaks, V. & Werb, Z. Matrix Metalloproteinases: Regulators of the Tumor Microenvironment. *Cell* **141**, 52–67 (2010).

279. Suarez-Carmona, M., Lesage, J., Cataldo, D. & Gilles, C. EMT and inflammation: inseparable actors of cancer progression. *Mol Oncol* **11**, 805–823 (2017).

280. Bahcecioglu, G., Basara, G., Ellis, B. W., Ren, X. & Zorlutuna, P. Breast cancer models: Engineering the tumor microenvironment. *Acta Biomater* **106**, 1–21 (2020).

281. Durand, N., Bastea, L. I., Döppler, H., Eiseler, T. & Storz, P. Src-mediated tyrosine phosphorylation of Protein Kinase D2 at focal adhesions regulates cell adhesion. *Sci Rep* **7**, 9524 (2017).

282. Manolagas, S. C. Role of cytokines in bone resorption. *Bone* **17**, S63–S67 (1995).

283. Roy, A. *et al.* Protein Kinase D2 and D3 Promote Prostate Cancer Cell Bone Metastasis by Positively Regulating Runx2 in a MEK/ERK1/2–Dependent Manner. *The American Journal of Pathology* (2023) doi:10.1016/j.ajpath.2023.01.004.

284. Ohshiba, T., Miyaura, C., Inada, M. & Ito, A. Role of RANKL-induced osteoclast formation and MMP-dependent matrix degradation in bone destruction by breast cancer metastasis. *Br J Cancer* **88**, 1318–1326 (2003).

285. Weiss, W. A., Taylor, S. S. & Shokat, K. M. Recognizing and exploiting differences between RNAi and small-molecule inhibitors. *Nat Chem Biol* **3**, 739–744 (2007).

286. Huck, B. *et al.* GIT1 Phosphorylation on Serine 46 by PKD3 Regulates Paxillin Trafficking and Cellular Protrusive Activity. *J Biol Chem* **287**, 34604–34613 (2012).

287. Zhang, X., Klamer, B., Li, J., Fernandez, S. & Li, L. A pan-cancer study of class-3 semaphorins as therapeutic targets in cancer. *BMC Medical Genomics* **13**, 45 (2020).

288. Cole-Healy, Z. *et al.* The relationship between semaphorin 3C and microvessel density in the progression of breast and oral neoplasia. *Exp Mol Pathol* **99**, 19–24 (2015).

289. Toosi, B. M. *et al.* EPHB6 augments both development and drug sensitivity of triple-negative breast cancer tumours. *Oncogene* **37**, 4073–4093 (2018).

290. Fukai, J. *et al.* EphA4 promotes cell proliferation and migration through a novel EphA4-FGFR1 signaling pathway in the human glioma U251 cell line. *Molecular Cancer Therapeutics* **7**, 2768–2778 (2008).

291. Schmucker, D. & Zipursky, S. L. Signaling downstream of Eph receptors and ephrin ligands. *Cell* **105**, 701–704 (2001).

292. Chukkapalli, S. *et al.* Role of the EphB2 receptor in autophagy, apoptosis and invasion in human breast cancer cells. *Experimental Cell Research* **320**, 233–246 (2014).

293. Chaillou, T., Kirby, T. J. & McCarthy, J. J. Ribosome biogenesis: emerging evidence for a central role in the regulation of skeletal muscle mass. *J Cell Physiol* **229**, 1584–1594 (2014).

294. Iadevaia, V., Huo, Y., Zhang, Z., Foster, L. J. & Proud, C. G. Roles of the mammalian target of rapamycin, mTOR, in controlling ribosome biogenesis and protein synthesis. *Biochem Soc Trans* **40**, 168–172 (2012).

295. Shaulian, E. & Karin, M. AP-1 in cell proliferation and survival. *Oncogene* **20**, 2390–2400 (2001).

296. Vleugel, M. M., Greijer, A. E., Bos, R., van der Wall, E. & van Diest, P. J. c-Jun activation is associated with proliferation and angiogenesis in invasive breast cancer. *Hum Pathol* **37**, 668–674 (2006).

297. Jiao, X. *et al.* c-Jun Induces Mammary Epithelial Cellular Invasion and Breast Cancer Stem Cell Expansion*. *Journal of Biological Chemistry* **285**, 8218–8226 (2010).

Alexia Gali

Cholargos, 15562, Athens, Greece
galia@tcd.ie | agali

Professional Experience

Protavio Ltd — *Athens, Greece*
PhD fellow (Industrial PhD) — *May, 2020 – exp. May, 2023*

- Led PhD research project on breast cancer, demonstrating project management skills such as design of experiments, results analysis, and ensuring study deliverables.
- Effectively communicated scientific findings to diverse audiences.
- Developed strong analytical skills through the analysis of complex datasets using R programming.
- Collaborated with Amsterdam University Medical Centre (Mar. 2021 - May 2021) and University of Stuttgart (Oct. 2022 - Nov. 2022), to conduct PhD research.
- Successfully managed analytical projects for academic clients of Protavio, ensuring high-quality deliverables and maintaining strong client relationships.

UCL Cancer Institute — *London, UK*
GCLP Facility Analyst — *Jun., 2017 – Feb, 2020*

- Analysed clinical trial samples and produced data in accordance with GCLP standards to support early phase oncology trials of University College London hospital.
- Deputy Analytical Project Manager for UCL-sponsored clinical trial, oversaw conduct of trial deliverables.
- Collaborated with physicians of CAR-T trials and delivered presentations on scientific results.
- Contributed to facility's Quality Management System documentation (SOPs, CAPAs etc.) and adhered to it.
- Reported in a timely manner the generated clinical sample data to trial sponsors.

University of Southampton — *Southampton, UK*
Research Assistant — *Jan., 2017 – May, 2017*

- Employed the CRISPR/Cas9 system to generate novel genome edited cell lines that were used to study how signalling lipids impact on nuclear functions.

Academic Education

Ph.D. in Cancer Biology — *Athens, Greece*
National Technical University of Athens (NTUA) — *May, 2020 – May, 2023*

- Marie Skłodowska-Curie PhD fellow in the "SECRET" Innovative Training Network (ITN)
- Topic: Triple Negative Breast Cancer research with focus on the secretory pathway

M.Sc. in Translational Oncology — *Dublin, Ireland*
Trinity College Dublin — *Sept., 2015 – Jul., 2016*

- Graduated with Distinction, Final Result: 70%

B.Sc. in Biology — *Thessaloniki, Greece*
Aristotle University of Thessaloniki — *Sept., 2010 – Mar., 2015*

- Major: General Biology, Final Result: 75%

Qualifications

Certifications Good Clinical Laboratory Practise (GCLP), Good Clinical Practise (GCP), Human Tissue Act (HTA)

Quality Assurance Generation of SOPs, Deviations, CAPAs, Analytical Plans, Validation Plans and Reports

IT Skills Programming with R (R Project for Statistical Computing) for data analysis and visualisation.
Use of Microsoft Office for creating documents (Word), spreadsheets (Excel) and presentations (Powerpoint).

Research Articles

- **Gali, A.**, Bijnsdorp, I.V., Piersma, S.R., Pham, T.V., Gutiérrez-Galindo, E., Tsolakos, N., Jimenez, C., Hausser, A. and Alexopoulos, L.G., Protein Kinase D Drives the Secretion of Invasion Mediators in Triple-Negative Breast Cancer Cell Lines. Preprint Available at SSRN: http://dx.doi.org/10.2139/ssrn.4439712

- Roddie, C., O'Reilly, M., Marzolini, M., Wood, L., Dias Alves Pinto, J., Abbasian, M., Vispute, K., Lowdell, M.W., Wheeler, G., Olejnik, J., Popova, B., Champion, K., **Gali, A.,** et al. AUTO1, a Novel Fast Off CD19CAR Delivers Durable Remissions and Prolonged CAR T Cell Persistence with Low CRS or Neurotoxicity in Adult ALL. ***Blood*** 134, 226 (2019) DOI: 10.1182/blood-2019-131086

- Roddie, C., O'Reilly, M., Marzolini, M., Wood, L., Dias Alves Pinto, J., Abbasian, M., Vispute, Bosshard, L., Lowdell, M. W., Wheeler, G., Day, A., Popova, B., Champion, K., Pathak, Y., **Gali, A.** et al. Automated Manufacture of Matched Donor-Derived Allogeneic CD19 CAR T-Cells for Relapsed/Refractory B-ALL Following Allogeneic Stem Cell Transplantation: Toxicity, Efficacy and the Important Role of Lymphodepletion. ***Blood*** 134, 776 (2019) DOI: 10.1182/blood-2019-129640

Additional Research Experience

Trinity College Dublin — *Dublin, Ireland*

POSTGRADUATE DISSERTATION — *Apr., 2016 – Jul., 2016*

- Analyzed the potential of exosomes released under hypoxic and normoxic conditions from different HER2-positive drug-sensitive and drug-resistant breast cancer cell lines.

The Institute of Cancer Research, Chester Beatty Laboratories — *London, UK*

ERASMUS INTERNSHIP — *Oct., 2014 – Dec., 2014*

- Performed a set of siRNA viability assays in a panel of breast and prostate cancer cell lines in order to identify new possible targetable proteins.

'Demokritos' National Center for Scientific Research — *Athens, Greece*

UNDERGRADUATE INTERNSHIP — *Jun., 2014 – Jul., 2014*

- Created a set of plasmids that expressed mutated forms of human apolipoprotein E and the proteins were subsequently purified and analyzed.

Papageorgiou Hospital — *Thessaloniki, Greece*

UNDERGRADUATE DISSERTATION — *Sept., 2013 – May, 2014*

- Performed a set of RFLP-PCRs to study the potential contribution of the E167D and T267I mutations and R202Q polymorphism in the manifestation of Familial Mediterranean Fever.